

5-2022

# Optimizing Virus Prefiltration for Biopharmaceutical Manufacturing

Solomon Isu  
*University of Arkansas, Fayetteville*

Follow this and additional works at: <https://scholarworks.uark.edu/etd>



Part of the [Catalysis and Reaction Engineering Commons](#), [Membrane Science Commons](#), and the [Process Control and Systems Commons](#)

---

## Citation

Isu, S. (2022). Optimizing Virus Prefiltration for Biopharmaceutical Manufacturing. *Graduate Theses and Dissertations* Retrieved from <https://scholarworks.uark.edu/etd/4501>

This Dissertation is brought to you for free and open access by ScholarWorks@UARK. It has been accepted for inclusion in Graduate Theses and Dissertations by an authorized administrator of ScholarWorks@UARK. For more information, please contact [scholar@uark.edu](mailto:scholar@uark.edu).

# Optimizing Virus Prefiltration for Biopharmaceutical Manufacturing

A dissertation submitted in partial fulfillment  
of the requirements for the degree of  
Doctor of Philosophy in Chemical Engineering

by

Solomon Ogbonnia Isu  
Federal University of Technology, Owerri  
Bachelor of Engineering in Chemical Engineering, 2007  
University of Arkansas  
Master of Science in Chemical Engineering, 2020

May 2022  
University of Arkansas

This dissertation is approved for recommendation to the Graduate Council.

---

Ranil Wickramasinghe, Ph.D.  
Dissertation Director

---

Xianghong Qian, Ph.D.  
Committee Member

---

Andrew Zydney, Ph.D.  
Committee Member

---

David Ford, Ph.D.  
Committee Member

---

Jorge Almodovar, Ph.D.  
Committee Member

## **Abstract**

Virus filters are single-use devices that use a size-based separation process. In virus filters, contaminating virus particles are retained while the therapeutic molecules pass through the membrane pores. Virus filters are an essential component of the overall virus clearance strategy. Sections 1 and 2 of this dissertation provide an introduction and extensive review of monoclonal antibody (mAb) process development, where virus filtration is pivotal.

In section 3, prefiltration studies were performed with an industrially relevant IgG1 type mAb using adsorptive and size-exclusion-based prefilters with different mechanisms of action. This mAb has an isoelectric point range of 7.1 to 8.0 and a molecular weight (MW) of 148 kDa. Decoupled prefiltration and virus filtration studies were conducted. We attempted to elute bound species from the membrane to identify them. Permeate fractions from the prefilters were introduced as feed fractions to a Planova BioEX (Asahi Kasei Medical, Tokyo, Japan) commercial virus filter for flux decay studies. Prefiltration and virus filtration studies were performed at different pH and ionic strength buffer conditions. By adjusting buffer conditions, and choosing prefilters with an appropriate mechanism of action, increased selectivity for foulant capture resulting in improved flux behavior during virus filtration could be achieved. Extensive characterization was also performed for the various filtration fractions to determine molecular species that increase fouling propensity in the virus filter and the efficacy of the different prefilters at removing these species.

In section 4, prefiltration and flux decay studies on a Viresolve Pro (MilliporeSigma, Billerica, MA) as well as the Planova BioEX virus filter was performed with another industrially relevant mAb with an isoelectric point range of 5.95 - 6.55. The impact of excipients on mAb fouling behavior was determined. The impact of buffer pH was also evaluated with one pH

condition below the isoelectric point (pI) of the mAb and another pH condition above the mAb pI. Decoupled prefiltration was performed to evaluate the impact of different types of prefilters on the filterability of this mAb. The pharmaceutical analysis system PA800 plus (SCIEX, Redwood City, CA) was also used to characterize the various mAb fractions from prefiltration and virus filtration. Dynamic light scattering (particle size analysis), size exclusion chromatography, SDS PAGE, capillary electrophoresis, and MALDI mass spectrometry were used for characterization.

In section 5, a new technique of fractionating close molecular weight biomolecules was evaluated for virus clearance. The technique is known as internally staged ultrafiltration (ISUF), where layers of ultrafiltration membranes operate in stages to fractionate biomolecules based on differences in isoelectric points. The membranes of interest were the Pall Omega PES 300 kDa molecular weight cutoff (MWCO) flat sheet membrane, Pall Omega PES 100 kDa MWCO membrane, Millipore Ultracel 100kDa MWCO, and the Millipore Ultracel 30kDa MWCO. Virus clearance studies were performed using internally staged ultrafiltration membranes in skin and backing configurations.

Section 6 is an overall conclusion for this work showing major findings and identifying areas for future study.

©2022 by Solomon Ogonnia Isu  
All Rights Reserved

## **Acknowledgments**

I would first like to thank my advisors, Prof. Ranil Wickramasinghe and Prof. Xianghong Qian, whose mentorship, expertise, and direction enabled me to complete this degree successfully. The steady and motivating leadership empowered me to thrive throughout graduate school. I want to thank the Ph.D. committee members, Prof. Jorge Almodovar, Prof. David Ford, and Prof. Andrew Zydney, for their guidance throughout my Ph.D. I would also like to thank Dr. Rohana Liyanage for the numerous characterization consultations and research insight.

I want to thank the industry advisory board of the MAST Center for funding my Ph.D. research and providing astute mentors to guide my research. I remain grateful to my industry mentors, particularly Dr. Christina Carbrello of MilliporeSigma, Dr. Daniel Strauss of Asahi Kasei Bioprocess, Yik Lam of Biogen, and Xiaosong Wu of Pall Corporation. To my fellow lab members, I thank you all for the assistance and encouragement that you gave. It was a fulfilling experience working alongside all of you.

I would like to thank my family for their support during graduate school, especially my wife, Oma, my children, Ethan and Anita, and my siblings, Christiana, Maxwell, Frances, and Gilbert. You have all been a source of strength and a pillar of support.

## **Dedication**

This work is dedicated to the memory of my mother.  
Christiana Ojii Isu (M.Ed., PGDE, B.Sc. Ed) July 19, 1959 - February 15, 2005.

## Contents

1.0 General Introduction .....	1
1.1 Aim and Outline.....	1
1.2 Downstream Purification .....	1
1.3 Optimization of Batch Processes in Downstream Purification.....	3
1.4 Monoclonal Antibodies and Emerging Biologics.....	4
References.....	6
2.0 Process- and Product-Related Foulants in Virus Filtration.....	9
2.1 Introduction.....	10
2.2 Downstream Processing.....	14
2.2.1 Platform Processes .....	14
2.2.2 Viruses, Virus Clearance, and Virus Filters.....	16
2.3 Virus Filter Foulants .....	20
2.3.1 Monoclonal Antibody Aggregates .....	20
2.3.1.1 Reversible Aggregates .....	22
2.3.1.2 Irreversible Aggregates .....	22
2.3.2 Host Cell Proteins (HCP), Proteases, and Nucleic Acids .....	23
2.3.3 Endotoxins .....	24
2.3.4 Product-Mediated Foulants .....	25
2.4 Mitigation of virus filter fouling.....	30
2.4.1 Prefiltration before virus filtration.....	30
2.4.2 Mitigation of virus filter fouling using process parameters.....	33
2.5 Outlook .....	34
References.....	35
3.0 Impact of Prefilter Mechanisms of Action on Virus Filtration of A mAb.....	44
3.1 Introduction.....	44



3.2 Materials and Methods.....	47
3.2.1 Materials.....	47
3.2.2 Monoclonal Antibody Sample Preparation and Buffer Conditions.....	48
3.2.3 Hydrophobic Interaction Chromatography Based Prefiltration.....	54
3.2.4 Cation Exchange Chromatography-Based Prefiltration.....	55
3.2.5 Anion Exchange Chromatography-Based Prefiltration.....	57
3.2.6 Capillary Electrophoresis (CE) Characterization.....	59
3.2.7 Dynamic Light Scattering (Particle Size Analysis).....	61
3.2.8 Size Exclusion Analysis.....	62
3.2.9 MALDI Mass Spectrometry.....	63
3.3 Virus Filtration and Prefiltration Results.....	64
3.3.1 BioEX Filtration of mAb B without Prefiltration.....	64
3.3.2 Size Exclusion-Based Prefiltration of mAb B.....	68
3.3.3 HIC Prefiltration of mAb B.....	68
3.3.4 IEX-S Prefiltration of mAb B.....	69
3.3.5 IEX-Q Prefiltration of mAb B.....	70
3.3.6 Composite BioEX flux data for mAb B in different buffer conditions with IEX-Q, IEX-S, HIC, and Size-Based Prefilters.....	71
3.4 Dynamic Light Scattering (DLS) of mAb B Fractions in pH 5 Sodium Acetate with Salt .....	76
3.5 Size Exclusion Chromatography Analysis of mAb B BioEX Filtration Fractions.....	77
3.6 Capillary Electrophoresis Characterization of mAb B Fractions.....	78
3.6.1 Capillary Isoelectric Focusing (cIEF) Of mAb B Samples.....	78
3.6.2 Capillary Electrophoresis CE-SDS Analysis of mAb B Fractions Constituted in DI water after Desalting using Centrifugal Filters.....	79
3.6.3 Capillary Zone Electrophoresis (Charge Variant Analysis) of mAb B Fractions.....	80
3.6.4 Glycan Analysis of mAb B Fractions.....	82
3.7 MALDI MS Analysis of mAb B Fractions.....	84
3.8 Sodium dodecyl sulfate (SDS) polyacrylamide gel electrophoresis (PAGE) analysis.....	90
3.9 Conclusion.....	93

References.....	95
4.0 Impact of Buffer Conditions on Filterability of Monoclonal Antibodies .....	98
4.1 Introduction.....	98
4.2 Materials and Methods.....	100
4.2.1 Materials.....	100
4.2.2 Monoclonal Antibody Sample Preparation and Buffer Conditions.....	102
4.2.3 Capillary Electrophoresis (CE) Characterization.....	108
4.2.4 Dynamic Light Scattering (Particle Size Analysis) .....	108
4.2.5 Size Exclusion Analysis.....	109
4.2.6 MALDI Mass Spectrometry.....	110
4.3 mAb M Filtration Results .....	110
4.3.1 BioEX Virus Filtration of mAb M In Sodium Acetate Buffer without Prefiltration	110
4.3.2 BioEX Filtration of mAb M in Sodium Acetate Buffer with HIC Prefiltration .....	114
4.3.3 Virus Filtration of mAb M in 20 mM Histidine Plus 150 mM Arginine Buffer Without Prefiltration .....	116
4.3.4 Virus Filtration of mAb M in 20 mM Histidine (Only) Buffer Without Prefiltration .....	118
4.3.5 Virus Filtration of mAb M in pH 6.7, 20 mM Histidine Buffer with Adsorptive Prefiltration (Sartobind S, Sartobind Phenyl, and Viresolve Prefilter).....	121
4.4 mAb M Characterization.....	123
4.4.1 Dynamic Light Scattering (DLS) Characterization of mAb M Fractions.....	123
4.4.2. Size Exclusion Chromatography Analysis of mAb M Filtration Fractions .....	128
4.4.3 Capillary Electrophoresis Characterization of mAb M Fractions.....	130
4.4.4 Sodium Dodecyl Sulfate (SDS) Polyacrylamide Gel Electrophoresis (PAGE) Analysis.....	135
4.4.5. MALDI MS Characterization of mAb M Fractions.....	138
4.5 Conclusion .....	140
References.....	141
5.0 Ultrafiltration based fractionation of biotherapeutics .....	144
5.1 Introduction.....	144

5.2 Materials and Methods.....	147
5.2.1 Materials.....	147
5.2.2 Methods.....	148
5.3 Results.....	150
5.3.1 Partitioning of Proteins using Internally Staged Ultrafiltration (ISUF).....	150
5.3.2 MVM Clearance using Internally Staged Ultrafiltration .....	153
Conclusion .....	155
References.....	156
6.0 Conclusion and Future Directions .....	158
Appendix A: Supplementary Chromatograms for Adsorptive Prefiltration of mAb B .....	160
Appendix B: Supplementary Characterization for mAb B Bind-and-Elute Fractionation .....	163
Appendix C: mAb B partitioning using cation exchange columns in bind-and-elute mode ....	164
Appendix D: Glycan Profiles of mAb B Determined using Capillary Electrophoresis.....	166
Appendix E: SEC data for mAb B prefiltration and virus filtration fractions .....	168
Appendix F: DLS data for mAb B prefiltration and virus filtration fractions .....	170

## List of Figures

Figure 2.1: Downstream Purification of Mammalian Cell-derived Biotherapeutics.....	15
Figure 2.2: Fouling of Virus Filtration Membranes Induced by Product-related Foulants (mAb Variants).....	26
Figure 3.1: Flow Chart of a Monoclonal Antibody Production System.....	44
Figure 3.2: Decoupled Prefiltration and Virus Filtration Workflow (Prefiltration was not Inline) .....	50
Figure 3.3: Workflow for BioEX Filtration in Series for mAb B without Prefiltration .....	52
Figure 3.4: Specification of Prefilters and Buffer Conditions used for mAb B Study .....	53
Figure 3.5: Cross-sectional Area of a Sartobind Phenyl (HIC) Membrane Adsorber .....	55
Figure 3.6: Sartobind-S Matrix-Ligand Structure.....	56
Figure 3.7: Sartobind-Q Matrix-Ligand Structure .....	57
Figure 3.8: Typical Ligands used to Functionalize Anion Exchange Membranes .....	58
Figure 3.9: BioEX Filtration of 5 g/L mAb B in 20 mM Sodium Acetate, pH 5 with Salt, pH 7.5 without Salt, and pH 8.6 with Salt. ....	66
Figure 3.10: Chromatogram for HIC Prefiltration of mAb B at pH 5 with 200mM NaCl.....	69
Figure 3.11: Chromatogram for IEX-S Prefiltration of mAb B at pH 5 with 200 mM NaCl.....	70
Figure 3.12: Chromatogram for IEX-Q Prefiltration of mAb B at pH 7.5 without Salt.....	71
Figure 3.13: mAb B Flux through a BioEX Filter after Prefiltration (pH 5 with 200mM NaCl).....	72
Figure 3.14: mAb B Flux through BioEX Filter after Prefiltration (pH 7.5 no Salt, Except for HIC where 200 mM NaCl is Required for Hydrophobic Interaction Chromatography).....	73
Figure 3.15: mAb B Flux through the BioEX Filter after Prefiltration with Different Prefilters (pH 8.6 Buffer with 200 mM NaCl) .....	74
Figure 3.16: Composite Figure for mAb B Flux at pH 5 with Salt, pH 7.5 without Salt, and pH 8.6 with Salt through the BioEX Filter According to Prefilter Mechanisms (A) HIC. (B) IEX-S. (C) IEX-Q. (D) No Prefiltration. ....	75
Figure 3.17: SEC Spectra of mAb B BioEX Filtration Fractions.....	77
Figure 3.18: Quantification of Peak Areas for cIEF Electropherogram of mAb B Feed at pH 7.5	

without Salt .....	79
Figure 3.19: CE-SDS for mAb B Purity Analysis from Capillary Electrophoresis (PA800 Plus) .....	80
Figure 3.20: Glycan Analysis for Quantification of G0F and G1F Glycoforms per Filtration Fraction of mAb B (pH 7.5, 20 mM Sodium Acetate Buffer, without Salt) .....	84
Figure 3.21: MALDI MS Spectra of mAb B BioEX Fractions without Prefiltration.....	84
Figure 3.22: Zoomed-in MALDI Spectra for Monomeric mAb B Peaks in BioEX Fractions...	86
Figure 3.23: MALDI-MS Spectra for mAb B IEX-S Prefiltration Fractions (Inset at 150 kDa)	87
Figure 3.24: MALDI MS of HIC Prefiltration Fractions and mAb B Feed at Different pH .....	88
Figure 3.25: MALDI MS Spectra of DTT-reduced mAb B BioEX Filtration Fractions .....	89
Figure 3.26: SDS PAGE of mAb B BioEX Filtration Fractions without Prefiltration.....	90
Figure 3.27: SDS PAGE of mAb B Feed Titrated to Different pH Values .....	91
Figure 3.28: SDS PAGE of mAb B BioEX (No Prefiltration), HIC, and IEX-S Filtration Fractions.....	92
Figure 3.29: 2D PAGE of mAb B Feed in a Non-reducing Buffer Condition .....	93
Figure 4.1: Charge and Hydrophobicity Asymmetry of IgG2a mAb. (RBSB Protein Databank). Positively Charged Residues in Blue, Negatively Charged Residues in Red, and Hydrophobic Residues in Yellow. ....	99
Figure 4.2: Decoupled Prefiltration / Virus Filtration Workflow and Filtration Conditions....	104
Figure 4.3: Virus Filtration Mechanism of the Planova BioEX .....	106
Figure 4.4: mAb Monomers Passing Through the 20 nm Capillary of the Planova BioEX.....	107
Figure 4.5: BioEX Filtration of mAb M in pH 5 Sodium Acetate Buffer, with and without Salt. .....	111
Figure 4.6: Run 1 and 2 BioEX Filtration of 5 g/L mAb M in pH 5, 20 mM Sodium Acetate Buffer with 200 mM NaCl, 0.2- $\mu$ m Prefiltration.....	113
Figure 4.7: Chromatogram for HIC Prefiltration of mAb M at pH 5 with 200 mM NaCl.....	115
Figure 4.8: BioEX Filtration of mAb M in pH 5 Sodium Acetate Buffer after HIC Prefiltration .....	115

Figure 4.9: BioEX Filtration of 5 g/L mAb M in pH 5.11, 20 mM Histidine plus 150 mM Arginine Buffer without Prefiltration .....	116
Figure 4.10: BioEX Filtration of 10 g/L mAb M in pH 5.11, 20 mM Histidine Plus 150 mM Arginine Buffer without Prefiltration .....	117
Figure 4.11: BioEX Filtration of 10 g/L mAb M in 20 mM Histidine Buffer (without Salt) at pH 5.11 without Prefiltration .....	119
Figure 4.12: VPro Filtration of 5 g/l mAb M in pH 5.11, 20 mM Histidine Buffer with and without VPF Prefiltration.....	119
Figure 4.13: VPro Filtration of 5 g/L mAb M in 20 mM Histidine Buffer (Only) at pH 6.7 without Prefiltration .....	120
Figure 4.14: (A) HIC Prefiltration of 10 g/l mAb M in pH 6.7, 20 mM Histidine Buffer. (B) IEX-S Prefiltration of 10 g/l mAb M in pH 6.7, 20 mM Histidine Buffer. ....	121
Figure 4.15: (A) VPro Filtration of 10 g/l mAb M in pH 6.7, 20 mM Histidine Buffer after HIC Prefiltration. (B) VPro Filtration of 10 g/l mAb M in pH 6.7, 20 mM Histidine Buffer after IEX-S Prefiltration. ....	122
Figure 4.16: (A) DLS of mAb M Fractions in Sodium Acetate Buffer with/without Salt and in DI Water. (B) DLS of mAb M in 20 mM Histidine pH 5.11, pH 6.7, and 20 mM Histidine Plus 150 mM Arginine Buffer Formulations for Stability Studies. ....	123
Figure 4.17: (A) Differential Intensity for mAb M in Original Buffer. (B) Differential Intensity for mAb M in pH 5 Sodium Acetate Buffer with Salt after Desalting in DI Water .....	124
Figure 4.18: Differential Intensity for mAb M in 20 mM Histidine Buffer, pH 6.3 at Different Ionic Strengths .....	125
Figure 4.19: (A) DLS Size Analysis of mAb M in 20 mM Histidine Buffer, pH 6.3, at Different Concentrations. (B) DLS Size Analysis of mAb M in 20 mM Histidine Buffer, pH 6.7, at Different Concentrations.....	126
Figure 4.20: Plot of Diffusion Coefficient Versus Concentration of mAb M in 20 mM Histidine Buffer at (A) pH 6.3. (B) pH 6.7.....	127
Figure 4.21: HPLC SEC of mAb M in 20 mM Histidine Buffer, pH 6.3, at Different mAb M Concentrations .....	128
Figure 4.22: HPLC SEC of 2.5 g/L mAb M in 20mM Histidine Buffer, pH 6.3, at Different Buffer Salt Concentrations (1 M NaCl, 1.88 M NaCl, 2.5 M NaCl, and 3.75 M NaCl). .	129
Figure 4.23: (A) c-IEF of mAb M in pH 5.11, 20 mM Histidine, 150 mM Arginine Buffer. (B) Isoform Distribution of mAb M in pH 5.11, 20 mM Histidine, 150 mM Arginine Buffer. ....	130

Figure 4.24: CE-SDS Purity Analysis of mAb M Fractions using PA800 Plus. (A) mAb M in pH 5.11 Histidine plus Arginine Buffer, pH 5.11 and pH 6.7 Histidine Only Buffers, respectively. (B) CE-SDS of mAb M in 20 mM Histidine Buffer, pH 5.11 for VPF and VPro Fractions (C) CE SDS of mAb M BioEX Fractions without Prefiltration (pH 5.11, 200mM NaCl).....	133
Figure 4.25: (A) CE SDS Electropherogram of mAb M HIC and VPro Fractions in pH 6.7, 20mM Histidine Buffer (B) CE SDS Electropherogram of mAb M IEX-S and VPro Fractions in pH 6.7, 20 mM Histidine buffer.....	134
Figure 4.26: SDS PAGE of mAb M Samples in Original Buffer and when in DI Water .....	136
Figure 4.27: SDS PAGE of mAb M Feed Titrated to Different pH Values .....	137
Figure 4.28: SDS PAGE of BioEX Fractions (No Prefiltration) for mAb M in 20 mM Sodium Acetate Buffer, No Salt.....	138
Figure 4.29: MALDI MS Spectra for VPro Feed (A) and VPro Permeate (B) Fractions in 20 mM Histidine Buffer, pH 5.11 .....	139
Figure 5.1: Layout of an Internally Staged Ultrafiltration System. ....	146
Figure 5.2: Workflow for an Amicon UF Cell in Series Experiment.....	149
Figure 5.3: SEM Images for Skin Side of 30 kDa MWCO RC Ultracel Membrane.....	150
Figure 5.4: SEM Images for the Backing Side of 30 kDa MWCO RC Ultracel Membrane....	151
Figure 5.5: Ultrafiltration using a Single 30 kDa Ultracel RC Membrane to Evaluate BSA Rejection with (A) Skin Side as Feed-Facing. (B) Backing Side as Feed-Facing.....	152
Figure 5.6: Ultrafiltration of MVM-spiked, pH 4.8 Acetate Buffer using Double Pall Omega 300 kDa + Pall Omega 100 kDa MWCO Membranes at 3 psi (Backing Sides were Feed-Facing). ....	153
Figure A1: Chromatograms for HIC Prefiltration of mAb B in 20 mM Sodium Acetate Buffer at (i) pH 7.5 with 200 mM NaCl. (ii) pH 8.6 with 200 mM NaCl.....	160
Figure A2: Chromatograms for IEX-S Prefiltration of mAb B in 20 mM Sodium Acetate Buffer at (i) pH 7.5 without Salt. (ii) pH 8.6 with 200 mM NaCl.....	161
Figure A3: Chromatograms for IEX-Q Prefiltration of mAb B in 20 mM Sodium Acetate Buffer at (i) pH 5 with 200 mM NaCl. (ii) pH 8.6 with 200 mM NaCl.....	162
Figure B1: Capillary Zone Electrophoresis of mAb B Fractionated by Gradient Elution using a Capto S Cation Exchange Column (Buffer A: 20 mM Sodium Acetate, pH 6.5, No Salt. Buffer B: pH 8.6, 20 mM Sodium Acetate with 200 mM NaCl). (i) Composite Plot for Fractions 2 - 6. (ii) Plot of Capto S Eluate Fractions 2 and 3 Only. ....	163

Figure C1: IEX-S Bind-and-Elute Chromatograms for Charge Variant Partitioning of mAb B in 20 mM Sodium Acetate Buffer (i) pH 5 without Salt. (ii) pH 6.5 without Salt. ....	164
Figure C2: Capto-S Bind-and-Elute Chromatograms for Charge Variant Partitioning of 0.5 g/L mAb B in 20 mM Sodium Acetate Buffer at pH 6.5 without Salt. ....	165
Figure D1: Fast Glycan Analysis Characterization of mAb B BioEX Filtration fractions in DI Water after PNGase Deglycosylation and Glycan Purification by Solid-Phase Extraction. ....	166
Figure E1: 220 nm Absorbance Spectra for TSKgel HPLC SEC Characterization of (i) mAb B Feed in 20 mM Sodium Acetate Buffer (pH 5 with 200 mM NaCl), BioEX Buffer Chase (pH 5 with 200 mM NaCl), BioEX Eluate Fractions (pH 4 and pH 9 without Salt), HIC Wash (pH 5 with 200 mM NaCl), and IEX-S Eluate Fraction (pH 5 with 1 M NaCl). (ii) HIC pH 4 Backwash. ....	168
Figure E2: Dimer Quantitation from TSKgel HPLC SEC Characterization of mAb B BioEX Feed, Permeate and Buffer Chase in 20 mM Sodium Acetate Buffer without Salt, pH 7.5. ....	169
Figure F1: DLS Spectra of mAb B HIC, IEX-S, and BioEX Filtration Fractions.....	170



## List of Tables

Table 2.1: Examples of Approved Chinese Hamster Ovary (CHO) Cell-derived Biotherapeutics. (Non-exhaustive List Compiled from Publicly Available Resources, <a href="https://www.accessdata.fda.gov/scripts/cder/daf/index.cfm?event=BasicSearch.process">https://www.accessdata.fda.gov/scripts/cder/daf/index.cfm?event=BasicSearch.process</a> ), US Food and Drug Administration, European Medicines Agency [16].	11
Table 2.1 (continued): Examples of Approved Chinese Hamster Ovary (CHO) Cell-derived Biotherapeutics. (Non-exhaustive List Compiled from Publicly Available Resources, <a href="https://www.accessdata.fda.gov/scripts/cder/daf/index.cfm?event=BasicSearch.process">https://www.accessdata.fda.gov/scripts/cder/daf/index.cfm?event=BasicSearch.process</a> ), US Food and Drug Administration, European Medicines Agency [16].	12
Table 2.2: Some Common Viruses Used for Validation Studies in Biomanufacturing [20].	17
Table 2.3: Commercially Available Virus Filters [1, 24, 26]. Asahi Kasei Bioprocess is a Part of the Asahi Kasei Group; MilliporeSigma is a Subsidiary of Merck KGaA.	19
Table 2.4: Commercially Available Prefilters, Modes of Action, and Manufacturers	31
Table 3.1: Structure and Potency of some Anion Exchange Ligands	58
Table 3.2: Mass Balance/Protein Content for BioEX Filtration of mAb B without Prefiltration in 20 mM Sodium Acetate Buffer, pH 5 with Salt, pH 7.5 without Salt, and pH 8.6 with Salt	65
Table 3.3: mAb B Filtration Parameters for BioEX Runs 1 and 2 without Prefiltration.	67
Table 3.4: Net Charge of mAb Variants at pH 5, 7.5, and 8.6 and Suggested Membrane Adsorbers Based on Virus Filtration and Prefiltration Studies	76
Table 3.5: Capillary Zone Electrophoresis Peak Analysis for Capto S Fractions of mAb B	81
Table 3.6: Characteristics of Glycans Identified in mAb B Fractions	83
Table 4.1: Changing Charge States of Arginine at Different Buffer pH Values.	100
Table 4.2: Mass Balance of mAb M in pH 5 Sodium Acetate (with and without Salt)	112
Table 4.3: Mass Balance for BioEX Run 1 and 2 Fractions of mAb M in pH 5 Sodium Acetate	114
Table 4.4: Mass Balance for BioEX Fractions of 10 g/L mAb M in pH 5.11, 20 mM Histidine Plus 150 mM Arginine Buffer	118
Table 5.1: Summary of Virus Clearance Experiments for Multiple Configurations of UF Membranes in Ultrafiltration Stirred Cells.	154

## **List of published papers**

### Section 2.0: Process- and Product-Related Foulants in Virus Filtration (Published)

Isu, S., Qian, X., Zydney, A. L., & Wickramasinghe, S. R. (2022). Process- and Product-Related Foulants in Virus Filtration. *Bioengineering*, 9(4), 155. doi:10.3390/bioengineering9040155

## **1.0 General Introduction**

### **1.1 Aim and Outline**

This research aims to fill a significant knowledge gap: understanding virus prefiltration to select an appropriate virus prefilter for a given biological drug substance. Today, virus prefilters are tested in an arbitrary manner. Sterilizing grade filters such as 0.2- $\mu\text{m}$  or 0.1- $\mu\text{m}$  filters are routinely used. When a significant flux decline of the virus filter is observed, prefilters with other mechanisms of action such as ion exchange and hydrophobic interaction are investigated. This research also explores virus clearance using a parvovirus known as Minute virus of mice (MVM) and ultrafiltration membranes in the internally staged ultrafiltration (ISUF) mode.

The primary research methodology involved virus filtration of different monoclonal antibodies (mAbs) in different buffer conditions and with multiple brands of virus filters and prefilters. Virus filter parameters that play a role in filter fouling include filter chemistry, membrane orientation, pore size distribution, and pore size gradient [1-5]. These experiments yielded a large data set for predicting filterability and fouling propensity of mAbs under different parameters. The impact of different formulation excipients on fouling behavior was explored.

Next, a molecular level characterization of the fouling species was performed to optimize filtration conditions that enhance prefiltration performance. Finally, these results were used to implement optimized prefiltration and virus filtration processes by leveraging the biophysical properties of mAb feed streams.

### **1.2 Downstream Purification**

Downstream purification of mammalian cell-derived therapeutic proteins involves platform processes typically operated in a batch mode [6, 7]. The core role of downstream

purification is to purify the biological drug substance (biologic) and remove any pathogens that could endanger the patient's life. Some unit operations involved in downstream purification are affinity chromatography, chromatographic polishing steps, virus filtration, and ultrafiltration/diafiltration (UF/DF). Downstream purification typically makes up 50-70 percent of monoclonal antibody manufacturing costs. Virus filtration makes up about ten percent of manufacturing costs [8].

Monoclonal antibody (mAb) downstream purification unit operations typically begin with a capture step. The capture step consists of a resin-based affinity chromatography step such as protein A. Protein A purification mechanism involves hydrophobic interactions between the protein A ligand and the crystallizable fragment region of the antibody's heavy chain [9]. Other factors, such as ionic interactions and hydrogen bonds, play a part in affinity chromatography [10].

Two additional chromatography polishing steps are typically included, e.g., ion exchange or hydrophobic interaction chromatography. One of these polishing steps could use a membrane adsorber in place of a packed resin column. Chromatographic polishing steps purify the mAb and eliminate non-desirables such as DNA, monomeric variants, host cell proteins, and oligomers of the mAb [11].

Two unit operations (most commonly low pH hold and virus filtration) are targeted to validate virus clearance [11]. Validation of adequate virus clearance is essential to obtain approval for a manufacturing process [11, 12]. Other operations performed to exclude or inactivate viruses, virus-like particles, and disease vectors include solvent/detergent treatment, heat treatment, and UV/gamma irradiation [13-15].

### 1.3 Optimization of Batch Processes in Downstream Purification

In the context of reducing manufacturing costs, each of the individual unit operations can be optimized to minimize waste, mitigate fouling of single-use membranes, and reduce process downtime. Virus filtration occurs downstream of protein A chromatography, usually after one or more of the chromatographic polishing steps. Virus filtration typically involves highly purified biologics. The virus filtration process is the final defense against adventitious virus contamination of biologics. Virus filters are costly and can sometimes foul rapidly. The use of prefilters to remove virus filter foulants before virus filtration extends the run-time and productivity of the virus filter, thereby reducing manufacturing costs.

Batch processes have typically been the mainstay of the industrial-scale manufacture of therapeutic proteins. There is a cascade of sequential unit operations in downstream processing with a hold step between each operation. Process optimization of batch processes involves evaluating unit operations in isolation and optimizing them. Nevertheless, batch processes ensure the real-time availability of product quality parameters and critical quality attributes between unit operations [16].

Interest in optimized bioprocessing that focuses on continuous processing is necessary because of economic pressure to reduce the cost burden of paying patients who rely on life-saving therapeutic proteins [16]. Economic competition is also a result of companies in emerging economies using less overhead costs to produce biosimilars [16]. Continuous operations would increase the manufacturer's productivity and mass availability of these biologics.

Several approaches have been explored for optimized process development, including experimental approaches, expert knowledge, and empirical modeling (in-silico methods) [17, 18]. Approaches adopted to explore continuous operations in downstream processing include

multiple modular (disposable or regenerating) units programmed to switch from one bank to another. At the same time, the cartridges are replaced or regenerated. Continuous chromatographic separations have also been and are still being developed based on multi-column systems [16]. Adaptations of continuous anion exchange chromatography for optimized processes include periodic countercurrent chromatography [19], simulated moving bed chromatography (SMB) [20], and multi-column countercurrent solvent gradient purification (MCGSP) [21].

#### **1.4 Monoclonal Antibodies and Emerging Biologics**

Biologics have become an indispensable drug in the healthcare toolkit in the last few decades. mAbs have particularly revolutionized the healthcare industry. The first mAb to be approved by the Food and Drug Administration (FDA) for human use was a murine mAb called Muromonab-CD3, which prevents transplanted organ rejection [22, 23]. Muromonab is an IgG-2 isotype mAb approved in 1986 [24]. Nebacumab which is an IgM isotype is indicated for the treatment of sepsis by targeting endotoxins and was the first mAb to be approved by the European regulatory agency [24].

Since 2016, about ten mAbs have received regulatory approval in the USA, Europe, and Japan annually [25]. More than 570 antibody therapeutics were undergoing clinical trial phases in 2019 [26]. Antibody-related therapeutics include bispecific antibodies (bsAbs), Fc-fusion proteins, and antibody-drug conjugates (ADCs) [24]. mAbs are invaluable in oncology, treatment of autoimmune disorders, transplanted organ rejection, nervous system disorders, COVID-19, and other indications. Commercial-scale mAb production has provided relief to sick patients globally; however, the cost of care is still a cause of concern. An anti-SARS COV-2 mAb cocktail regimen by Regeneron costs over \$3000 per dose.

The mAb industry grossed over \$154 billion in 2020 [27, 28]. Some blockbuster mAbs like Humira (Adalimumab), Herceptin (Trastuzumab), Keytruda (Pembrolizumab), and Rituxan (Rituximab) each generate over \$6 billion in annual sales [29]. The high cost of these mAbs can be attributed to the extensive research and clinical trials required for their development, among other factors. Due to the rise of generic biologics or biosimilars in emerging economies, industrial demand for reduced production costs is pertinent [30, 31]. The biosimilar industry is angling for a share of the profitable market as older, successful mAbs face patent expirations [30]. For the established brand name mAb manufacturers to ward off competition from generics, much research is needed to optimize the upstream and downstream production process. Companies have also adapted by researching new therapeutic indications for their blockbuster mAbs or application as antibody-drug conjugates [31].

## References

1. Bieberbach, M., et al., Investigation of fouling mechanisms of virus filters during the filtration of protein solutions using a high throughput filtration screening device. *Biotechnol Prog*, 2019. 35(4): p. e2776.
2. Kosiol, P., et al., Determination of pore size gradients of virus filtration membranes using gold nanoparticles and their relation to fouling with protein containing feed streams. *Journal of Membrane Science*, 2018. 548: p. 598-608.
3. Langdon, B.B., et al., Single-molecule resolution of protein dynamics on polymeric membrane surfaces: the roles of spatial and population heterogeneity. *ACS Appl Mater Interfaces*, 2015. 7(6): p. 3607-17.
4. Marques, B.F., D.J. Roush, and K.E. Göklen, Virus filtration of high-concentration monoclonal antibody solutions. *Biotechnology Progress*, 2009. 25(2): p. 483-491.
5. Syedain, Z.H., D.M. Bohonak, and A.L. Zydney, Protein Fouling of Virus Filtration Membranes: Effects of Membrane Orientation and Operating Conditions. *Biotechnology Progress*, 2006. 22(4): p. 1163-1169.
6. Kornecki, et al., Accelerating Biomanufacturing by Modeling of Continuous Bioprocessing—Piloting Case Study of Monoclonal Antibody Manufacturing. *Processes*, 2019. 7(8).
7. Konstantinov, K.B. and C.L. Cooney, White Paper on Continuous Bioprocessing May 20–21 2014 Continuous Manufacturing Symposium. *Journal of Pharmaceutical Sciences*, 2015. 104(3): p. 813-820.
8. Rayfield, W.J., et al., Prediction of viral filtration performance of monoclonal antibodies based on biophysical properties of feed. *Biotechnology Progress*, 2015. 31(3): p. 765-774.
9. Vunnum, S., G. Vedantham, and B. Hubbard, Protein A-Based Affinity Chromatography. *Process Scale Purification of Antibodies*, 2017: p. 113-133.
10. Bramer, C., et al., Membrane Adsorber for the Fast Purification of a Monoclonal Antibody Using Protein A Chromatography. *Membranes (Basel)*, 2019. 9(12).
11. Wickramasinghe, S.R., et al., Virus Removal and Virus Purification, in *Current Trends and Future Developments on (Bio-) Membranes*. 2019. p. 69-96.
12. Wieser, A., et al., The evolution of down-scale virus filtration equipment for virus clearance studies. *Biotechnology and Bioengineering*, 2015. 112(3): p. 633-637.
13. Li, Y., et al., Emerging biomaterials for downstream manufacturing of therapeutic proteins. *Acta Biomater*, 2019. 95: p. 73-90.



14. Weaver, J., et al., Anion exchange membrane adsorbers for flow-through polishing steps: Part I. Clearance of minute virus of mice. *Biotechnol Bioeng*, 2013. 110(2): p. 491-9.
15. Shukla, A., M. Etzel, and S. Gadam, *Process Scale Bioseparations for the Biopharmaceutical Industry*. CRC Press: Boca Raton, Florida, 2007: p. 449-462.
16. Zydney, A.L., Perspectives on integrated continuous bioprocessing—opportunities and challenges. *Current Opinion in Chemical Engineering*, 2015. 10: p. 8-13.
17. Baumann, P. and J. Hubbuch, Downstream process development strategies for effective bioprocesses: Trends, progress, and combinatorial approaches. *Engineering in Life Sciences*, 2017. 17(11): p. 1142-1158.
18. Kroner, F., et al., Analytical characterization of complex, biotechnological feedstocks by pH gradient ion exchange chromatography for purification process development. *J Chromatogr A*, 2013. 1311: p. 55-64.
19. Godawat, R., et al., Periodic counter-current chromatography -- design and operational considerations for integrated and continuous purification of proteins. *Biotechnol J*, 2012. 7(12): p. 1496-508.
20. Aniceto, J.P.S. and C.M. Silva, *Simulated Moving Bed Strategies and Designs: From Established Systems to the Latest Developments*. *Separation & Purification Reviews*, 2015. 44(1): p. 41-73.
21. Aumann, L. and M. Morbidelli, A continuous multicolumn countercurrent solvent gradient purification (MCSGP) process. *Biotechnol Bioeng*, 2007. 98(5): p. 1043-55.
22. Surjit, S., et al., Monoclonal Antibodies: A Review. *Current Clinical Pharmacology*, 2018. 13(2): p. 85-99.
23. Todd, P.A. and R.N. Brogden, Muromonab CD3. A review of its pharmacology and therapeutic potential. *Drugs*, 1989. 37(6): p. 871-99.
24. Goswami, S., et al., Developments and Challenges for mAb-Based Therapeutics. *Antibodies*, 2013. 2(4): p. 452-500.
25. Reichert, J.M., Antibodies to watch in 2017. *MAbs*, 2017. 9(2): p. 167-181.
26. Kaplon, H. and J.M. Reichert, Antibodies to watch in 2019. *MAbs*, 2019. 11(2): p. 219-238.
27. Dhara, V.G., et al., Recombinant Antibody Production in CHO and NS0 Cells: Differences and Similarities. *BioDrugs*, 2018. 32(6): p. 571-584.

28. Global Market Insights, G. Monoclonal Antibodies Market Size by Type (Fully Human, Humanized, Chimeric), By Application (Oncology, Autoimmune Diseases, Infectious Diseases), By End-use (Hospitals, Clinics), COVID19 Impact Analysis, Regional Outlook, Application Potential, Competitive Market Share & Forecast, 2021 - 2027. 2021 [cited 2022 March 19, 2022]; GMI5065: [Available from: <https://www.gminsights.com/industry-analysis/monoclonal-antibodies-market>].
29. Kang, H.-N., et al., The regulatory landscape of biosimilars: WHO efforts and progress made from 2009 to 2019. *Biologicals: journal of the International Association of Biological Standardization*, 2020. 65: p. 1-9.
30. São Pedro, M.N., et al., Process analytical technique (PAT) miniaturization for monoclonal antibody aggregate detection in continuous downstream processing. *Journal of Chemical Technology & Biotechnology*, 2021.
31. Grilo, A.L. and A. Mantalaris, The Increasingly Human and Profitable Monoclonal Antibody Market. *Trends Biotechnol*, 2019. 37(1): p. 9-16.

## **2.0 Process- and Product-Related Foulants in Virus Filtration**

\* This chapter is adapted from a published paper: Isu, S., Qian, X., Zydney, A. L., & Wickramasinghe, S. R. (2022). Process- and Product-Related Foulants in Virus Filtration. *Bioengineering*, 9(4), 155. doi:10.3390/bioengineering9040155.

### **Abstract**

Regulatory authorities place stringent guidelines on the removal of contaminants during the manufacture of biopharmaceutical products. Monoclonal antibodies, Fc-fusion proteins, and other mammalian cell-derived biotherapeutics are heterogeneous molecules that are validated based on the production process and not on molecular homogeneity. Validation of clearance of potential contamination by viruses is a major challenge during the downstream purification of these therapeutics. Virus filtration is a single-use, size-based separation process in which the contaminating virus particles are retained while the therapeutic molecules pass through the membrane pores. Virus filtration is routinely used as part of the overall virus clearance strategy.

Compromised performance of virus filters due to membrane fouling, low throughput, and reduced viral clearance is of considerable industrial significance and is frequently a major challenge. This review shows how components generated during cell culture, contaminants, and product variants can affect virus filtration of mammalian cell-derived biologics. Cell culture-derived foulants include host cell proteins, proteases, and endotoxins. We also provide mitigation measures for each potential foulant.

## 2.1 Introduction

A virus filtration step is frequently included to provide a robust size-based clearance of both enveloped and non-enveloped viruses during the manufacture of mammalian cell-derived biotherapeutics, such as monoclonal antibodies (mAbs) and Fc-fusion proteins [1, 2]. Before approval of new therapeutics, regulatory agencies such as the US Food and Drug Administration (FDA) require validation of adequate virus clearance [3]. Consequently, unit operations are added to the purification train to ensure high levels of virus clearance [4].

Virus filtration uses large pore size ultrafiltration membranes to retain any contaminating virus particles while recovering the virus-free product in the permeate. Unlike ultrafiltration operations, the performance criteria for virus filters are far stricter [5]. Typically, around 95% product recovery is required while maintaining at least 1000-fold virus clearance [1].

Virus filtration is different from typical pressure-driven membrane filtration processes as the filter is designed to obtain high levels of removal of potential virus contaminants. Further, as it is impractical to validate that there is zero carryover of any trapped virus particles, reuse of the virus filter is impossible. Consequently, these are single-use devices. Virus filters are typically run in normal flow (dead end) mode rather than tangential flow mode used for protein ultrafiltration since normal flow is less complex and requires only a single pump.

Table 2.1 lists a range of mammalian cell-derived biotherapeutics that have been approved by the food and drug administration in the last three decades. This is a non-exhaustive list showing the various classes and drug names. Mammalian cells used for the expression of recent FDA-approved monoclonal antibodies include Chinese hamster ovary (CHO) cells and murine myeloma cells (Sp2/0, NS0), among others [6, 7].

Table 2.1: Examples of Approved Chinese Hamster Ovary (CHO) Cell-derived Biotherapeutics. (Non-exhaustive List Compiled from Publicly Available Resources, <https://www.accessdata.fda.gov/scripts/cder/daf/index.cfm?event=BasicSearch.process>), US Food and Drug Administration, European Medicines Agency [16].

<b>Drug classification</b>	<b>Examples</b>	<b>First approval by FDA</b>	<b>Manufacturer</b>
Monoclonal antibodies	Pembrolizumab	2014	Merck
	Nivolumab	2014	Bristol-Myers Squibb
	Aducanumab	2021	Biogen
	Avelumab	2017	EMD Serono
	Omalizumab	2003	Genentech
	Adalimumab	2002	Abbvie
	Tezepelumab-ekko	2021	Amgen / AstraZeneca
Fc-fusion proteins	Abatacept	2021	Bristol-Myers Squibb
	Aflibercept	2011	Regeneron
	Alefacept	2003	Biogen
	Etanercept	1998	Amgen
	Rilonacept	2008	Regeneron
Cytokines	Darbepoetin alfa	2011	Amgen
	Interferon beta-1a	2003	Biogen
	Epoetin alfa	2011	Amgen

Table 2.1 (continued): Examples of Approved Chinese Hamster Ovary (CHO) Cell-derived Biotherapeutics. (Non-exhaustive List Compiled from Publicly Available Resources, <https://www.accessdata.fda.gov/scripts/cder/daf/index.cfm?event=BasicSearch.process>), US Food and Drug Administration, European Medicines Agency [16].

<b>Drug classification</b>	<b>Examples</b>	<b>First approval by FDA</b>	<b>Manufacturer</b>
Enzymes	Agalsidase beta	2003	Genzyme
	Human DNase	1993	Genentech
	Laronidase	2003	BioMarin
	Tenecteplase	2000	Genentech
Hormones	Choriogonadotropin alfa	2000	EMD Serono
	Follitropin alfa	2004	EMD Serono
	Osteogenic protein-1	2001	Stryker Biotech
	Thyrotropin alfa	1998	Genzyme

The performance of virus filters is measured in terms of product recovery, log reduction value (LRV) of the virus (defined as the logarithm base 10 of the ratio of the virus concentration in the feed to that in the permeate), and the productivity of the filter. Productivity is typically expressed as the volume of feed that can be processed per membrane area ( $L/m^2$ ) before the filtrate flux has decreased to unacceptably low levels (for operation at constant transmembrane pressure). Since biopharmaceutical manufacturing operations are still essentially batch processes, the virus filter is often sized such that the entire batch can be processed in one shift.

Frequently, identifying a virus filter that meets the three performance requirements: product recovery, LRV, and productivity is challenging and highly dependent on the feed stream and membrane properties. As the virus filtration step is located towards the end of the purification train, the product is highly purified and moderately concentrated [1]. Membrane fouling, which leads to compromised performance, is typically due to the product- and process-related foulants rather than any rejected virus particles [1]. The concentration of virus particles in any process will be orders of magnitude less than that for the product.

Virus filtration membranes are sometimes designed with a reverse asymmetric structure to improve the removal of impurities and foulants [9]. In this case, the barrier layer faces away (downstream) while the more open support layer faces towards the feed stream [10]. The support layer can act as an inline prefilter that traps larger foulants and protects the tight barrier layer [11]. However, essentially symmetric membranes are also used industrially. The unique requirements of virus filtration are different from typical pressure-driven membrane separation processes such as ultrafiltration. Identifying and sizing an appropriate virus filter is often particularly challenging.

This review describes a typical ‘platform process’ for the downstream purification of biopharmaceutical products. First, the location of the virus filtration step in the downstream processing workflow is identified. Next, the major commercially available virus filters are summarized. The remaining sections of this review highlight various impurities and foulants that could lead to fouling and compromised performance during virus filtration of mammalian cell-derived biologics. Inline virus prefilters that are frequently used to remove product-related aggregates are also discussed. The review ends with a discussion of future trends in the development of virus filters.

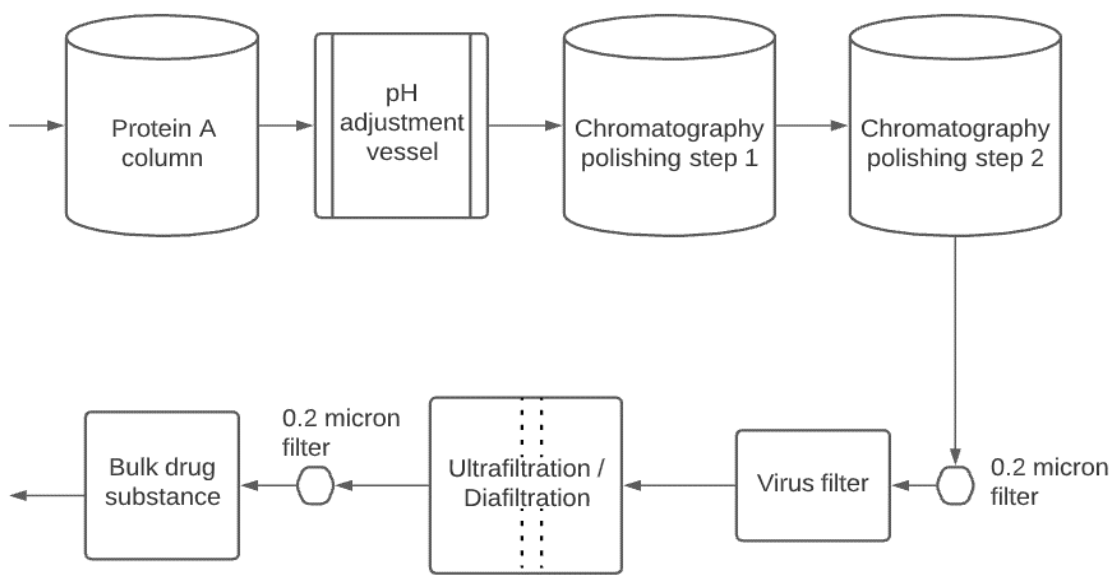
## 2.2 Downstream Processing

### 2.2.1 Platform Processes

Biopharmaceutical manufacturing processes can be divided into two main processing trains: upstream cell culture operations and downstream purification processes. Various bioreactor configurations are used to produce the cells that express the product of interest (mAbs, enzymes, Fc-fusion proteins, or hormones). Removing particulate matter such as cells and cell debris occurs at the interface between upstream and downstream unit operations. These bioreactor clarification operations are sometimes referred to as midstream processes [12, 13].

Figure 2.1 is a typical 'platform' process for the downstream purification of monoclonal antibodies. The first unit operation is typically an affinity chromatography capture step using protein A (resin-based chromatography) [14]. Affinity interaction is a specific interaction based on both the topological fit and a combination of electrostatic, hydrophobic, and hydrogen-bonding interactions [15]. Antibody elution from the protein A column is done at low pH, making it convenient to include a low pH hold for virus inactivation.





**Figure 2.1:** Downstream Purification of Mammalian Cell-derived Biotherapeutics.

Frequently two polishing steps are used to remove the remaining impurities and product variants/aggregates [16]. Resin- or membrane-based chromatography (ion exchange or hydrophobic interaction chromatography) is frequently used. The polishing steps remove impurities such as DNA, host cell proteins (HCP), and product aggregates [1]. Typically, all streams and buffers which enter the purification process are passed through sterilizing grade (0.2- $\mu\text{m}$  pore size) filters to reduce bioburden.

As shown in Figure 2.1, the virus filtration step is typically located near the end of the purification train. The product is relatively concentrated and highly purified. High product concentrations can lead to compromised performance due to product aggregation and increased adsorption to the virus filter membrane. A final ultrafiltration /diafiltration step is used to concentrate the product and place it in the formulation buffer needed for stability during

shipping/storage and delivery to the patient. The final 0.2- $\mu\text{m}$  pore size filter is used to ensure sterility of the product and is often done as part of the final fill-finish operation.

### **2.2.2 Viruses, Virus Clearance, and Virus Filters**

Many mammalian cell lines produce endogenous retrovirus-like particles [1]. These particles are typically around 80-100 nm in size. Clearance can be achieved by inactivation and physical removal from the process stream [11, 17, 18]. During purification, manufacturers of mammalian cell-derived biotherapeutics must demonstrate that the process will yield a final product containing no more than one virus particle in a million doses. Estimates of the number of virus particles in a single dose equivalent from the bioreactor could be as high as  $10^{10}$ - $10^{15}$  retrovirus-like particles per mL [1].

Removal of adventitious viruses such as parvovirus is also required. These much smaller viruses are around 20 nm in size. In the past, filters targeted for retrovirus and parvovirus removal were included in the purification train [3]. Recent studies show that virus clearance filters designed to provide clearance of smaller parvovirus can be used to clear much larger retroviruses simultaneously [19].

Table 2.2 shows some viruses that are employed for validation studies in biomanufacturing. The enveloped viruses are typically bigger than the non-enveloped viruses. Virus filters constitute the last line of defense to guarantee the safety of intravenously-delivered biologics and, therefore, these must be validated with the smallest possible viruses (non-enveloped viruses). Parvoviruses are commonly used.

**Table 2.2:** Some Common Viruses Used for Validation Studies in Biomanufacturing [20].

Name of Virus	Diameter (nm)
Animal parvoviruses (non-enveloped DNA viruses, bovine, canine, or porcine)	18–24
Poliovirus (picornavirus, non-enveloped RNA virus)	25–30
Encephalomyocarditis virus (EMC, picornavirus, non-enveloped RNA virus)	25–30
Feline calicivirus (calicivirus, non-enveloped RNA virus)	35–39
Bovine viral diarrhea virus (BVDV, flavivirus, enveloped RNA virus)	40–60
SV40 (simian vacuolating virus 40, polyomavirus, non-enveloped DNA virus)	45–55
Sindbis virus (togavirus, enveloped RNA virus)	60–70
Reovirus (non-enveloped RNA virus)	60–80
Herpes simplex virus (HSV, herpesviridae, enveloped DNA virus)	150
Pseudorabies virus (PRV, herpesviridae, enveloped DNA virus)	120–200

Adventitious virus contamination is a concern in the manufacture of biologics. Validation of virus clearance is shown by conducting scale-down testing [21]. The feed is spiked with model virus particles, and clearance in the product stream is determined. Minute virus of mice (MVM, mouse parvovirus) is often used to validate adventitious virus clearance. The FDA requires at least two orthogonal steps with different mechanisms of action for validation of viral clearance with the required level of virus clearance for the process, determined by summing the clearances obtained from the individual unit operations [1].

Virus filtration uses porous polymeric membranes in normal flow mode [11, 22, 23]. The predominant mechanism of action for virus filters is size exclusion [11]. The difference in

hydrodynamic diameter between a protein product and MVM is often less than two-fold [5]. Today, virus filters are a critical component of the overall virus clearance strategy [11].

Virus filter materials are typically hydrophilic [24], preventing hydrophobic biomolecules from significantly fouling the membrane through adsorptive mechanisms. As shown in Table 2.3, virus filter membrane materials include hydrophilic cuprammonium regenerated cellulose, hydrophilic / surface-modified polyethersulfone, and hydrophilic acrylate-modified polyvinylidene difluoride [24].

The latter two materials are hydrophilized to minimize fouling by adsorption and maximize flux during virus filtration. While the membrane should be biocompatible, non-fouling, and minimize adsorption on the membrane surface, it is also essential that the membrane is robust and dimensionally stable to ensure the required level of virus clearance.

These virus filters are typically designed to ensure that only monomeric biomolecules with a hydrodynamic diameter less than 20 nm can pass through the size cutoff pores. Much research is needed to understand how a multidomain, anisotropic mAb with varied surface moieties interacts with virus filtration membranes, prefilters, and other product monomers [25].

**Table 2.3:** Commercially Available Virus Filters [1, 24, 26]. Asahi Kasei Bioprocess is a Part of the Asahi Kasei Group; MilliporeSigma is a Subsidiary of Merck KGaA.

<b>Filter</b>	<b>Manufacturer</b>	<b>Membrane material</b>	<b>Configuration</b>	<b>Comments</b>
Planova 15N, 20N	Asahi Kasei	Regenerated cellulose	Asymmetric single-layer hollow fibers	Parvovirus filter
Planova 35N	Asahi Kasei	Regenerated cellulose	Asymmetric single-layer hollow fibers	Retrovirus filter
Planova BioEX	Asahi Kasei	Hydrophilized PVDF	Asymmetric single-layer hollow fibers	Parvovirus filter
Viresolve NFR	MilliporeSigma	Polyethersulfone	Asymmetric triple-layer pleated sheets	Retrovirus filter
Viresolve Pro	MilliporeSigma	Polyethersulfone	Asymmetric double-layer flat sheets	Parvovirus filter
Pegasus SV4	Pall Corporation	Hydrophilized PVDF	Symmetric double-layer pleated sheets	Parvovirus filter
Ultipor VF DV20	Pall Corporation	Hydrophilized PVDF	Symmetric double-layer pleated sheets	Parvovirus filter
Ultipor VF DV50	Pall Corporation	Hydrophilized PVDF	Symmetric double-layer pleated sheets	Retrovirus filter
Virosart HC	Sartorius AG	Polyethersulfone	Asymmetric double-layer pleated sheets	Parvovirus filter
Virosart HF	Sartorius AG	Modified polyethersulfone	Asymmetric single-layer hollow fibers	Parvovirus filter

Table 2.3 is a non-exhaustive list showing commercially available virus filters and material configurations.

Virus filter membrane fouling is a significant challenge [23, 27, 28]. Fouling can compromise virus clearance and reduce membrane productivity (product recovered per membrane surface area) [29]. Fouling is often due to product variants because of the high product purity before virus filtration and the high product concentration compared to the spiked virus concentration [1, 30].

Recent studies focusing on virus filtration of mAbs showed that membrane performance depends on the mAb properties (pI, hydrophobicity, net charge, dipole moment, oligomericity), buffer conditions, membrane material, and operating pressure [23, 31, 32]. Buffer excipients such as arginine and lysine can stabilize mAbs and reduce fouling propensities [33]. Excipients such as histidine, arginine, and lysine can reduce reversible self-association of mAbs to varying degrees [34]. Reversible self-association is often concentration-dependent [23, 34, 35].

## **2.3 Virus Filter Foulants**

This section describes the major classes of foulants in virus filtration. This includes irreversible and reversible product aggregates and minor product variants that differ in their charge or hydrophobicity. Product variants arise because mammalian cell-derived biotherapeutics are heterogeneous. The product is defined based on the production process and not on a single molecular species. Product variants with different post-translational modifications can have different hydrophobicity, charge, and conformations. If present, HCP, proteases, and nucleic acids can also foul the virus filter.

### **2.3.1 Monoclonal Antibody Aggregates**

Aggregation is a typical occurrence with mAbs and other therapeutic proteins. Several pathways have been proposed to describe the aggregation of proteins. They include

agglomeration of monomers in their native states, aggregation of conformationally altered or chemically modified monomers, nucleation, and surface-induced aggregation [36-38].

Significant attention has been placed on non-native monomer aggregation since exposed hydrophobic moieties tend to self-associate [36]. Some surfactants, osmolytes, and chaotropes induce aggregation because they denature the monomeric product, exposing more of the hydrophobic core and distorting the surface charge distribution [39]. Physical and biochemical events can also induce product degradation through enzymatic and non-enzymatic processes such as shock, light, and oxidation [40].

Physical or chemical perturbations that put a strain on the native conformation of biotherapeutic proteins such as mAbs can result in clipping or aggregation [41]. Such conditions include the presence of chaotropic chemical species, pH swings [42], shock, mechanical stress, increased concentration, and large temperature fluctuation [36, 43, 44]. The size, surface charge, and hydrophobicity of a mAb multimer will differ from that of the native monomer.

Interfacial damage can also affect the stability of a product monomer, especially at the air-liquid interface, which induces nucleation and aggregation [45]. Surface tension and physical adsorption on solid surfaces also lead to conformational changes [36, 46, 47]. Freezing and thawing of the product induce more aggressive fouling of virus filters [1, 22, 48]. Freeze-thaw-induced aggregation is due to conformational changes at the ice-liquid interface and by freeze concentration [36, 46, 49].

Reversible aggregates are usually a precursor to nucleation [50], followed by irreversible aggregation as the aggregates increase in size [51, 52]. As buffer ionic strength increases, electrostatic repulsion between the mAbs decreases, whereas hydrophobic attraction between the mAb increases, often leading to product aggregation [46]. Aggregation and precipitation occur

most easily at the product's isoelectric point (pI) due to reduced electrostatic repulsion between individual product molecules [53, 54].

### **2.3.1.1 Reversible Aggregates**

Aggregation can occur through different pathways resulting in aggregates that are reversible or non-reversible [36, 39]. mAb oligomers such as dimers, trimers, and tetramers are typically reversible [36, 37]. Reversible aggregates are known as soluble aggregates, and the associated product monomers are not significantly denatured. Soluble aggregates are caused by interactions between product molecules via hydrogen bonding, electrostatic, or van der Waals forces [39, 55]. These soluble aggregates could foul virus filters if their size exceeds the 20 nm size cutoff of most parvovirus filters.

Rayfield et al. [27] investigated the impact of mAb properties on virus filter filterability and showed that aggregates bigger than 17 nm were correlated to the flux decline during virus filtration [1, 27]. Monoclonal antibodies typically have a hydrodynamic diameter of 9-12 nm; thus, the small oligomers can be 20 nm to as much as 50 nm in diameter. Other studies have shown that freeze-thawing of mAbs may not cause aggregation in significant amounts detectable by size exclusion chromatography due to the relatively small diameters of potential aggregates formed [48, 56, 57].

### **2.3.1.2 Irreversible Aggregates**

When product dimers and trimers undergo further aggregation, they attain a critical mass where the aggregate can no longer remain soluble. These large aggregates then precipitate out of the solution [36]. The precipitates become visible and show increased turbidity and cloudiness. These large aggregates are known as irreversible aggregates. Large, insoluble aggregates have an



increased propensity to foul the separation-active layer during virus filtration. Barnard et al. investigated the principal foulant of freeze-thawed mAb solutions and found that the freeze-thaw process could induce the formation of large aggregates ( $>1 \mu\text{m}$ ) [48]. The use of 0.1 or 0.2  $\mu\text{m}$  pore size prefilters can marginally reduce virus filter fouling by removing large aggregates.

Irreversible aggregation is prevalent with denatured product monomers [37, 39]. Chemical degradation, such as oxidation and deamidation, alters the surface charge of product monomers and affects colloidal stability [37]. Irreversible aggregation of mAbs results in product loss, although low levels of aggregation ( $<1\%$ ) can cause a significant increase in filter fouling. Hawe et al. studied mAb aggregates formed during freeze-thaw and heat-induced thermal stress [47]. Other studies show that heat denatures mAbs and leads to irreversible mAb aggregation [37, 39].

### **2.3.2 Host Cell Proteins (HCP), Proteases, and Nucleic Acids**

HCP features significantly in the downstream processing of protein-based therapeutics [31]. HCP includes proteins, enzymes, and co-enzymes which emanate from the host cell used for product expression [58]. It is essential to remove HCP from therapeutic proteins because they can elicit an immune response. There are regulatory requirements for robust HCP removal before clinical trials of drug candidates to prevent the development of anti-CHO antibodies by volunteers [59, 60]. Some HCP can coelute with the mAbs through polishing and purification steps either due to binding to the resin or association with the mAb product [58, 61-63]. Zhang et al. identified over 500 HCP in a cell culture sample and tracked their fate through downstream processing unit operations [64]. After studying nine different mAbs, they determined that actin and clusterin were most abundant in protein A eluates [64].

Enzymatic HCP (host cell proteases) can clip or denature product monomers, expose hydrophobic residues, and charged moieties, and alter the product's biophysical properties. Denatured product monomers with exposed residues induce virus filter fouling by adsorptive processes in addition to mAb-mAb and mAb-HCP association. Host cell proteases have been reported to result in the fragmentation of mAb products, with increased susceptibility to nucleation and aggregation [65]. However, proteases themselves are probably not principal foulants of virus filters since virus filtration occurs towards the end of downstream processing, where only trace amounts of non-mAb impurities may be detected [18, 66].

HCP diminishes the biotherapeutic quality of biotherapeutic products and increases downstream processing costs. If HCP is not sufficiently removed, it could potentially induce flux decay during virus filtration. HCP has a range of biophysical properties, such as pI (2-11) and mass (10-200 kDa) which can be used to separate the HCP from the biotherapeutic [67, 68]. Protein A chromatography significantly reduces HCP in the mAb product due to high selectivity for the Fc region of mAbs [61]. Several studies reported that the propensity of different HCPs to bind and coelute with mAbs from protein A columns vary from mAb to mAb [62, 69]. Problematic HCP are many and include lipoprotein lipase, nidogen-1, clusterin, histones, keratins, phospholipases, ribosomal proteins, and serine proteases [67].

### **2.3.3 Endotoxins**

Endotoxins or lipopolysaccharides (LPS) are contaminants that can enter the process through growth media or other cell culture additives used in mammalian cell cultures. LPS are produced by gram-negative bacteria, commonly used in recombinant DNA production [70-72]. Endotoxins are commonly found as contaminants in mammalian cell-derived therapeutics [73]. LPS are complex molecular conjugates of an amphiphilic component (lipid A) and a polar

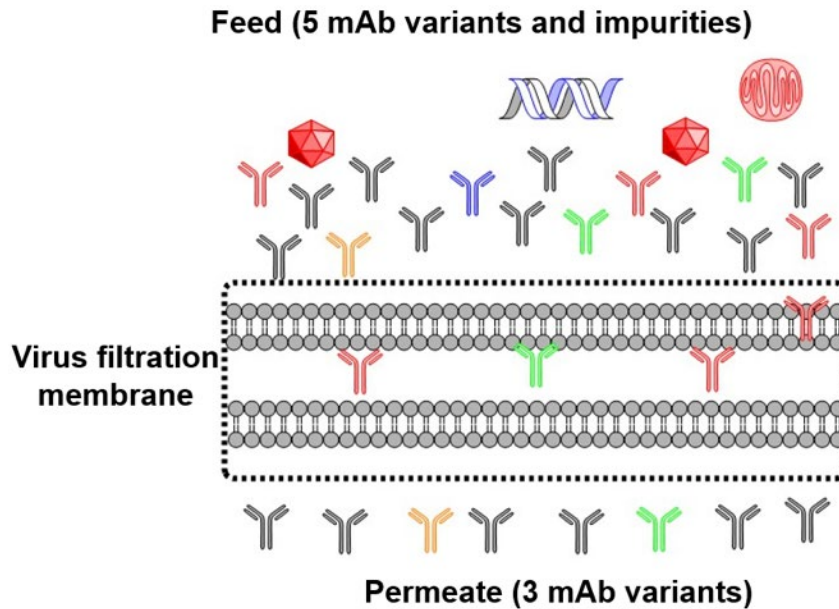
polysaccharide component [71, 72]. The isoelectric point of LPS ranges from 1 to 4 [68]. LPS removal techniques that have been reported include two-phase extraction, affinity chromatography, and ion-exchange chromatography [72].

LPS has been reported to have a high affinity for some biotherapeutic proteins [73]. LPS and therapeutic proteins can form micellar aggregates, complicating the removal process and potentially carrying over into the virus filtration step [72, 74]. Phosphorylated moieties of LPS electrostatically bind with the carboxyl moieties of amino acids in the biologic of interest [72, 74]. Solutions of 0.5 M arginine have been shown to promote LPS clearance during polishing steps [74].

LPS have molecular masses ranging from 3 - 40 kDa, which varies due to their polysaccharide chain lengths [68, 72]. Endotoxins can coelute with mAbs and Fc-fusion proteins from protein A resins by molecular conjugation through hydrophobic and electrostatic interactions, ultimately causing problems during virus filtration. Endotoxin-contaminated mAb streams have an increased propensity to cause virus filter fouling. Removal of endotoxins through ion exchange polishing steps increases the virus filtration capacity of virus filters.

#### **2.3.4 Product-Mediated Foulants**

Product-mediated foulants are mAb species that have a higher propensity to induce fouling of the virus filter, as shown by the illustration in Figure 2.2 below.



**Figure 2.2:** Fouling of Virus Filtration Membranes Induced by Product-related Foulants (mAb Variants)

Figure 2.2 shows five variants of the mAb present in the feed and color-coded red, grey, blue, green, and yellow. The red and green color-coded foulants induce fouling on the virus filter. In contrast, the black, yellow, and green mAb variants are collected in the permeate.

### 2.3.4.1 Charge Variants

The charge variant profile is a critical quality attribute of mAbs,[75] and Fc-fusion proteins. Charge variants in mAbs can result from post-translational modifications (PTMs), such as deamidation of asparagine, C-terminal lysine variants, and glycosylation [76-79]. Glycans are mostly polar, hydrophilic oligosaccharides that can induce micro-differences in the surface charge of a glycoprotein [80]. Negatively charged glycans incorporating phosphorylated mannose and sialic acid can introduce micro-heterogeneities [80]. Charge heterogeneity is observed in isoelectric focusing electropherograms of most glycoproteins [76]. Acidic and basic

variants of glycoproteins such as mAbs and Fc-fusion proteins can have different glycan profiles [81, 82]. Meyer et al.<sup>72</sup> reported that specific charge variants of a mAb candidate were aggregation-prone. Acidic variants of this mAb showed increased hydrophobicity [80].

The net charge and surface charge distribution of glycoproteins change with buffer pH [78, 83, 84]. The pI of a protein is the pH value at which the net charge is zero [53]. For most mAbs, the pI ranges from 6.5 to 9.5 [53]. There is more biochemical variability with Fc-fusion proteins. A protein will be net negatively charged when the buffer pH is above the pI and positively charged when the buffer pH is below the pI [85]. Exposed surface residues on a glycoprotein can become protonated or deprotonated depending on the buffer pH, thereby inducing localized charged groups [86]. Charged moieties due to glycosylation, phosphorylation, and other PTMs affect the net charge of glycoproteins and their interactions with other product monomers and virus filtration membranes [85].

#### **2.3.4.2 Denatured variants**

Hydrophobic interaction is the preferential association of non-polar residues in aqueous media [87]. Amino acids with non-polar side chains are typically hydrophobic, e.g., valine, leucine, proline, and tryptophan. Polar amino acids such as arginine impart hydrophilic attributes to glycoproteins [88]. When hydrophobic amino acids are surface-exposed on a glycoprotein, hydrophobicity increases. Hydrophobic amino acids tend to be buried in the globular core of most glycoproteins. The hydrophobicity of a protein is also affected by the buffer pH and the protein's charge state [89]. When the buffer pH is close to the pI of the protein, the protein is the most hydrophobic [87]. Denaturation and unfolding of glycoproteins can lead to variants with a higher fouling propensity on virus filters.

The glycan appendages of glycoproteins also contribute to the final stable conformation, and glycan variation can introduce minor hydrophobicity variations. Careful handling and mild changes in formulation conditions will reduce the formation of conformational variants, which could foul virus filters or induce product aggregation.

#### **2.3.4.3 Sequence Variants**

Monoclonal antibodies and Fc-fusion proteins consist of amino acids in specific sequences that form secondary, tertiary, and quaternary structures. Sequence variants arise due to genetically unprogrammed amino acid substitutions, omissions, or insertions during biosynthesis [90]. Sequence variants result in macro-heterogeneities with biomolecular differences from the desired product [90]. Sequence variants possess different affinities to substrates [91] due to surface charge and hydrophobicity dissimilarities. The amino acid sequence of a glycoprotein determines its hydrophobicity, conformation, and charge, amongst other properties [90].

The primary structure (amino acid sequence) of a glycoprotein can determine intermolecular, monomeric association, and multimerization propensity [51]. Even minor sequence differences can cause conformational differences leading to product variants with different biophysical attributes and virus filter fouling propensity. Inadvertent substitution of hydrophilic amino acids with hydrophobic amino acids or vice versa in the polypeptide sequence amplifies sequence variants.

#### **2.3.4.4 Microheterogeneity-Induced Product Variants**

mAbs, antibody fragments, bispecific antibodies, and Fc-fusion proteins are expressed in mammalian cells like Chinese Hamster Ovary (CHO) cells for pharmaceutically relevant glycosylation profiles [15]. Flynn et al. reported that a typical CHO cell culture batch of mAbs

has three major glycan species present, and they are G0F, G1F, and G2F [92]. These three dominant glycan structures are dependent on cell lineage and culture parameters [93]. *E. coli* expresses mostly insoluble, non-glycosylated variants [77]. Hybridomas offer a rapid expression template for initial product manufacture [15, 94, 95].

During cell culture and harvesting operations, expressed glycoproteins are usually not uniformly glycosylated [40, 96, 97]. Glycoproteins are expressed with a range of glycosylation profiles depending on cell culture conditions [98-103]. Micro-heterogeneity of glycoproteins can occur as a result of differences in glycosylation and other post-translational modifications. Variations in appended glycans introduce charge heterogeneity to the product monomer and determine the glycoprotein's native fold state, aggregate susceptibility, and stability [104-107]. These product variants can affect the performance of virus filters.

Glycans are hydrophilic oligosaccharide moieties typically appended to glycoproteins in the cell during glycoprotein synthesis [108]. Glycans assist in the proper folding of the polypeptide chain before product secretion [76, 96, 109]. Most therapeutic proteins are glycoproteins. Glycoforms of protein products introduce structural heterogeneity, which affects their affinity to substrates, their stability, and other physicochemical characteristics of these therapeutic proteins [108, 110, 111]. Even in the same cell culture batch, a range of glycoforms occurs [108, 112, 113]. Glycoforms occur due to skipped glycosylation sites on the glycoprotein or differences in the structure of appended glycans [96].

Glycan type and abundance can alter the product's biophysical properties. Several studies have looked at the stability of different mAb glycoforms. These results show that aggregation is more prevalent in unglycosylated mAbs since glycans modulate aggregation [108, 114].

Furthermore, a study showed that in terms of physical stability between pH 4 - 6, di-

glycosylated IgG1 type mAbs were the most stable, and mono-glycosylated IgG1 was the least stable [115]. Post-translational modification can strongly affect the pI of a glycoprotein [76, 108]. Variations in the pIs of product variants would affect hydrophobic and electrostatic interactions.

## **2.4 Mitigation of virus filter fouling**

### **2.4.1 Prefiltration before virus filtration**

Even though the support structure of the virus filter can function as an inline prefilter, significant fouling is often observed due to the product and process-related foulants listed above that could be present in the feed stream. Standard practice involves the inclusion of a virus prefilter to remove these contaminants. Virus prefilters may rely on one or more mechanisms of action for the removal of foulants. The use of prefilters upstream of a virus filter increases permeate flux to the degree allowed by the biotherapeutic product properties, prefilter material, and buffer conditions [1]. The mechanisms and conditions for foulant capture are different for different prefilters [1].



**Table 2.4:** Commercially Available Prefilters, Modes of Action, and Manufacturers [24]

<b>Prefilter</b>	<b>Material</b>	<b>Mechanism of action</b>	<b>Manufacturer</b>
Planova 75N	Regenerated cellulose	Size exclusion, removal of small aggregates	Asahi Kasei
Bottle top 0.1 / 0.2 $\mu\text{m}$	Polyethersulfone	Size exclusion, removal of large aggregates	ThermoFisher Scientific
Pegasus Protect	Nylon	Size exclusion, removal of large aggregates	Pall
Sartobind Q	Quaternary ammonium ligands	Anion exchange	Sartorius AG
Sartobind S	Sulfonic acid ligands	Cation exchange	Sartorius AG
Sartobind phenyl	Phenyl ligands	Hydrophobic interaction	Sartorius AG
Viresolve Pro Shield	Surface modified PES	Size exclusion, ion exchange (cation)	MilliporeSigma
Viresolve Pro Shield H	Surface modified PES	Size exclusion, hydrophobic interaction	MilliporeSigma
Viresolve Prefilter	Diatomaceous earth, cellulose fibers, and a cationic imine binder	Cation exchange, size exclusion, hydrophobic interaction, ion exchange,	MilliporeSigma

Table 2.4 above shows a non-exhaustive list of common prefilters used to capture foulants and mitigate fouling during downstream virus filtration. Size exclusion prefilters such as the 0.1 and 0.2-micron filters remove aggregates large than the respective size cutoff of the prefilters. Ion exchange prefilters are more effective at low conductivity due to the reduction in electrostatic shielding when the solution pH is close to the pI of the biologic. If the solution pH is 1-2 units away from the pI of the biomolecules, then an ionic strength increase is required to enable operation in the flowthrough mode

The Sartobind S membrane is typically used as a prefilter before virus filtration. Sulfonic acid ligands are negatively charged in aqueous solutions and preferentially bind more positively charged species in the feed stream. Process development teams typically optimize buffer parameters to ensure the biotherapeutic flows through cation exchange membranes while aggregates and the most basic molecular variants are captured by the cation exchange prefilter [116]. The Sartobind Q membrane is an anion exchange membrane with positively charged quaternary ammonium ligands. Ion exchange membranes are used as adsorptive prefilters that remove aggregates and aggregation-prone charged variants of a biotherapeutic product [80].

Wickramasinghe et al. opined that trace amounts of aggregates that have a diameter less than 50 nm play a significant role in virus filtration membrane fouling [1]. These small aggregates with diameters less than 50 nm cannot be removed by 0.1- $\mu\text{m}$  or 0.2- $\mu\text{m}$  size exclusion filters but can block the virus filter pores. Virus filtration membranes typically have a pore size around 20 nm at the separation-active layer.

Soluble aggregates (20 – 50 nm) can be removed using adsorptive prefilters (cation exchange, anion exchange, multimodal) to prevent fouling of virus filters. Adsorptive prefilters have been shown to bind aggregates, thereby reducing subsequent fouling of virus filters. Adsorptive prefilters work well for product oligomers in the 600 - 1500 kDa range, which cannot be removed by 0.2- $\mu\text{m}$  size-exclusion prefilters. Ion-exchange prefilters have shown great potential in clearing aggregates for effective downstream processing operations [117].

Endotoxins can be removed using hydrophobic prefilters, which bind the phosphorylated lipid moiety, or using anion exchange prefilters to capture the polysaccharide moiety [71, 74, 118]. Anion exchange membranes work well for endotoxin removal due to the positively charged ligands binding with the negatively charged endotoxin (isoelectric point = 1 - 4).

Hydrophobic prefilters require a moderate/high salt content (ionic strength) to reduce the product's solvation layer enabling exposed hydrophobic patches to adsorb on the hydrophobic prefilter. Hydrophobic interaction prefilters can be effective in removing product variants with different hydrophobicity as well as some of the more hydrophobic product aggregates.

Ion exchange prefilters are helpful in the downstream removal of HCPs due to the pI difference between mAbs and most HCPs. DNA is strongly negatively charged in an aqueous solution and can be effectively removed using anion exchange membranes during polishing operations [19, 118].

Multimodal prefilters are helpful for filtering out foulants that cannot be removed by ion exchange, size exclusion, or hydrophobic interaction-based prefilters alone. These multimodal prefilters include the three prefilters from MilliporeSigma, as shown in Table 2.4.

#### **2.4.2 Mitigation of virus filter fouling using process parameters**

MAb properties are highly dependent on the buffer conditions and excipients that are part of the formulation. Excipients are non-drug substance components of the formulation. During high throughput screening of mAbs for optimum buffer conditions, a specific buffer type and composition may be found to inhibit aggregation and mitigate fouling of virus filters. Phosphate, acetate, and tris buffers may work for some biomolecules, while viscosity inhibiting buffers may be preferred for highly concentrated mAbs. Arginine reduces mAb monomeric self-association, nonspecific membrane interactions, and mAb aggregation [119]. Excipients such as histidine and arginine marginally improve the stability of monomeric species during formulation [37, 120]. These excipients can result in cost reduction for virus filter consumables but may require further removal before drug substance delivery to the patient.

## 2.5 Outlook

Achieving the high levels of virus clearance for mammalian cell-derived biotherapeutics will continue to be a challenge. There is a continuing need for better virus filters that maximize productivity, flux, and LRV for batch processes. As biomanufacturing moves towards continuous manufacturing platforms, there will be a need to develop new virus filters. Unlike current virus filters, which are designed to process a product batch in one shift, in continuous biomanufacturing, the virus filter will be run for much longer times and likely at much lower filtrate flux/transmembrane pressure. Further development of virus filters for continuous operations will be needed.

There is a growing demand for virus particles and virus-like particle-based vectors to deliver gene therapies and vaccines. Virus particle-based delivery systems such as attenuated, recombinant, infectious, and inactivated virus particles, as well as virus-like particles and even subunits of virus particles, are highly effective therapeutics. However, downstream purification of these new therapeutics is challenging [121]. Future virus filter designs will need to be optimized for these emerging therapeutics.

## References

1. Wickramasinghe, S.R., et al., Virus Removal and Virus Purification, in Current Trends and Future Developments on (Bio-) Membranes. 2019. p. 69-96.
2. Troccoli, N.M., et al., Removal of viruses from human intravenous immune globulin by 35 nm nanofiltration. *Biologicals*, 1998. 26(4): p. 321-9.
3. FDA, Points to Consider in the Manufacture and Testing of Monoclonal Antibody Products for Human Use. 1997: Bethesda, Maryland.
4. Han, B., et al., Enhanced virus removal by flocculation and microfiltration. *Biotechnology and Bioprocess Engineering*, 2002. 7(1): p. 6-9.
5. Billups, M., et al., Antibody retention by virus filtration membranes: Polarization and sieving effects. *Journal of Membrane Science*, 2021. 620.
6. Wagner, E., et al., Determination of size variants by CE-SDS for approved therapeutic antibodies: Key implications of subclasses and light chain specificities. *J Pharm Biomed Anal*, 2020. 184: p. 113166.
7. Dhara, V.G., et al., Recombinant Antibody Production in CHO and NS0 Cells: Differences and Similarities. *BioDrugs*, 2018. 32(6): p. 571-584.
8. Dumont, J., et al., Human cell lines for biopharmaceutical manufacturing: history, status, and future perspectives. *Crit Rev Biotechnol*, 2016. 36(6): p. 1110-1122.
9. Zhang, D., et al., Modeling flux in tangential flow filtration using a reverse asymmetric membrane for Chinese hamster ovary cell clarification. *Biotechnol Prog*, 2021. 37(3): p. e3115.
10. Hoffmann, D., et al., Chapter 5 - Purification of New Biologicals Using Membrane-Based Processes, in Current Trends and Future Developments on (Bio-) Membranes, A. Basile and C. Charcosset, Editors. 2019, Elsevier. p. 123-150.
11. Wickramasinghe, S.R., et al., Understanding virus filtration membrane performance. *Journal of Membrane Science*, 2010. 365(1-2): p. 160-169.
12. Zalai, D., et al., Microbial technologies for biotherapeutics production: Key tools for advanced biopharmaceutical process development and control. *Drug Discovery Today: Technologies*, 2021.
13. DePalma, A., Continuity Promotes Bioprocessing Intensity. *Genetic Engineering & Biotechnology News*, 2016. 36(7): p. 1, 24, 26.
14. Vunnum, S., G. Vedantham, and B. Hubbard, Protein A-Based Affinity Chromatography. *Process Scale Purification of Antibodies*, 2017: p. 113-133.

15. Bramer, C., et al., Membrane Adsorber for the Fast Purification of a Monoclonal Antibody Using Protein A Chromatography. *Membranes (Basel)*, 2019. 9(12).
16. Chollangi, S., et al., Development of robust antibody purification by optimizing protein-A chromatography in combination with precipitation methodologies. *Biotechnol Bioeng*, 2015. 112(11): p. 2292-304.
17. Huang, P.Y. and J. Peterson, Scaleup and virus clearance studies on virus filtration in monoclonal antibody manufacture, in *Membrane Separations in Biotechnology*. 2001, Marcel Dekker: New York.
18. Bolton, G.R., S. Spector, and D. LaCasse, Increasing the capacity of parvovirus-retentive membranes: performance of the Viresolve™ Prefilter. *Biotechnology and Applied Biochemistry*, 2006. 43(1): p. 55-63.
19. Miesegaes, G.R., et al., Viral clearance by flow-through mode ion exchange columns and membrane adsorbers. *Biotechnol Prog*, 2014. 30(1): p. 124-31.
20. Burnouf, T. and M. Radosevich, Nanofiltration of plasma-derived biopharmaceutical products. *Haemophilia*, 2003. 9(1): p. 24-37.
21. Wieser, A., et al., The evolution of down-scale virus filtration equipment for virus clearance studies. *Biotechnology and Bioengineering*, 2015. 112(3): p. 633-637.
22. Kern, G. and M. Krishnan, Virus Removal by Filtration: Points to Consider. *BioPharm International*, 2006. 19.
23. Bieberbach, M., et al., Investigation of fouling mechanisms of virus filters during the filtration of protein solutions using a high throughput filtration screening device. *Biotechnol Prog*, 2019. 35(4): p. e2776.
24. Johnson, S.A., et al., Virus filtration: A review of current and future practices in bioprocessing. *Biotechnol Bioeng*, 2021.
25. Robinson, J., D. Roush, and S. Cramer, Domain contributions to antibody retention in multimodal chromatography systems. *J Chromatogr A*, 2018. 1563: p. 89-98.
26. Gefroh, E., et al., Use of MMV as a Single Worst-Case Model Virus in Viral Filter Validation Studies. *PDA Journal of Pharmaceutical Science and Technology*, 2014. 68(3): p. 297.
27. Rayfield, W.J., et al., Prediction of viral filtration performance of monoclonal antibodies based on biophysical properties of feed. *Biotechnology Progress*, 2015. 31(3): p. 765-774.
28. Bolton, G.R., J. Basha, and D.P. Lacasse, Achieving high mass-throughput of therapeutic proteins through parvovirus retentive filters. *Biotechnol Prog*, 2010. 26(6): p. 1671-7.

29. Kosiol, P., et al., Investigation of virus retention by size exclusion membranes under different flow regimes. *Biotechnol Prog*, 2019. 35(2): p. e2747.
30. Syedain, Z.H., D.M. Bohonak, and A.L. Zydney, Protein Fouling of Virus Filtration Membranes: Effects of Membrane Orientation and Operating Conditions. *Biotechnology Progress*, 2006. 22(4): p. 1163-1169.
31. Namila, F.N.U., et al., The effects of buffer condition on the fouling behavior of MVM virus filtration of an Fc-fusion protein. *Biotechnology and Bioengineering*, 2019. 116(10): p. 2621-2631.
32. Marques, B.F., D.J. Roush, and K.E. Göklen, Virus filtration of high-concentration monoclonal antibody solutions. *Biotechnology Progress*, 2009. 25(2): p. 483-491.
33. Rodrigues, D., et al., Product-Specific Impact of Viscosity Modulating Formulation Excipients During Ultra-High Concentration Biotherapeutics Drug Product Development. *J Pharm Sci*, 2021. 110(3): p. 1077-1082.
34. Hu, Y., et al., Characterization of Excipient Effects on Reversible Self-Association, Backbone Flexibility, and Solution Properties of an IgG1 Monoclonal Antibody at High Concentrations: Part 1. *J Pharm Sci*, 2020. 109(1): p. 340-352.
35. Kosiol, P., Membranes for virus removal by size exclusion, in Department of Chemistry. 2018, University of Duisburg-Essen: Germany.
36. Manning, M.C., et al., Stability of protein pharmaceuticals: an update. *Pharm Res*, 2010. 27(4): p. 544-75.
37. Philo, J.S. and T. Arakawa, Mechanisms of protein aggregation. *Curr Pharm Biotechnol*, 2009. 10(4): p. 348-51.
38. Chakroun, N., et al., Mapping the Aggregation Kinetics of a Therapeutic Antibody Fragment. *Mol Pharm*, 2016. 13(2): p. 307-19.
39. Woll, A.K. and J. Hubbuch, Investigation of the reversibility of freeze/thaw stress-induced protein instability using heat cycling as a function of different cryoprotectants. *Bioprocess Biosyst Eng*, 2020. 43(7): p. 1309-1327.
40. Dorai, H. and S. Ganguly, Mammalian cell-produced therapeutic proteins: heterogeneity derived from protein degradation. *Current Opinion in Biotechnology*, 2014. 30: p. 198-204.
41. Diaz-Villanueva, J.F., R. Diaz-Molina, and V. Garcia-Gonzalez, Protein Folding and Mechanisms of Proteostasis. *Int J Mol Sci*, 2015. 16(8): p. 17193-230.
42. Sule, S.V., et al., Solution pH that minimizes self-association of three monoclonal antibodies is strongly dependent on ionic strength. *Mol Pharm*, 2012. 9(4): p. 744-51.

43. Zheng, J.Y. and L.J. Janis, Influence of pH, buffer species, and storage temperature on physicochemical stability of a humanized monoclonal antibody LA298. *International Journal of Pharmaceutics*, 2006. 308(1): p. 46-51.
44. Salinas, B.A., et al., Buffer-Dependent Fragmentation of a Humanized Full-Length Monoclonal Antibody. *Journal of Pharmaceutical Sciences*, 2010. 99(7): p. 2962-2974.
45. Shieh, I.C. and A.R. Patel, Predicting the Agitation-Induced Aggregation of Monoclonal Antibodies Using Surface Tensiometry. *Mol Pharm*, 2015. 12(9): p. 3184-93.
46. Kuelzo, L.A., et al., Effects of solution conditions, processing parameters, and container materials on aggregation of a monoclonal antibody during freeze-thawing. *J Pharm Sci*, 2008. 97(5): p. 1801-12.
47. Hawe, A., et al., Structural properties of monoclonal antibody aggregates induced by freeze-thawing and thermal stress. *European Journal of Pharmaceutical Sciences*, 2009. 38(2): p. 79-87.
48. Barnard, J.G., et al., Investigations into the fouling mechanism of parvovirus filters during filtration of freeze-thawed mAb drug substance solutions. *J Pharm Sci*, 2014. 103(3): p. 890-9.
49. Barnett, G.V., et al., Structural Changes and Aggregation Mechanisms for Anti-Streptavidin IgG1 at Elevated Concentration. *J Phys Chem B*, 2015. 119(49): p. 15150-63.
50. Li, W., et al., Antibody Aggregation: Insights from Sequence and Structure. *Antibodies (Basel)*, 2016. 5(3).
51. Wang, W., Protein aggregation and its inhibition in biopharmaceutics. *Int J Pharm*, 2005. 289(1-2): p. 1-30.
52. Vazquez-Rey, M. and D.A. Lang, Aggregates in monoclonal antibody manufacturing processes. *Biotechnol Bioeng*, 2011. 108(7): p. 1494-508.
53. Novák, P. and V. Havlíček, Protein Extraction and Precipitation, in *Proteomic Profiling and Analytical Chemistry*. 2016. p. 51-62.
54. Franco, R., et al., Influence of osmolarity and pH increase to achieve a reduction of monoclonal antibodies aggregates in a production process. *Cytotechnology*, 1999. 29(1): p. 11-25.
55. Leckband, D. and J. Israelachvili, Intermolecular forces in biology. *Quarterly Reviews of Biophysics*, 2001. 34(2): p. 105-267.



56. Barnard, J.G. et al., Subvisible particle counting provides a sensitive method of detecting and quantifying aggregation of monoclonal antibody caused by freeze-thawing: insights into the roles of particles in the protein aggregation pathway. *J Pharm Sci*, 2011. 100(2): p. 492-503.
57. Bria, C.R., et al., Probing Submicron Aggregation Kinetics of an IgG Protein by Asymmetrical Flow Field-Flow Fractionation. *J Pharm Sci*, 2016. 105(1): p. 31-9.
58. Aboulaich, N., et al., A novel approach to monitor clearance of host cell proteins associated with monoclonal antibodies. *Biotechnol Prog*, 2014. 30(5): p. 1114-24.
59. Gutierrez, A.H., L. Moise, and A.S. De Groot, Of [Hamsters] and men: a new perspective on host cell proteins. *Hum Vaccin Immunother*, 2012. 8(9): p. 1172-4.
60. Doneanu, C.E., et al., Analysis of host-cell proteins in biotherapeutic proteins by comprehensive online two-dimensional liquid chromatography/mass spectrometry. *MAbs*, 2012. 4(1): p. 24-44.
61. Shukla, A.A. and P. Hinckley, Host cell protein clearance during protein a chromatography: Development of an improved column wash step. *Biotechnology Progress*, 2008. 24(5): p. 1115-1121.
62. Nogal, B., K. Chiba, and J.C. Emery, Select host cell proteins coelute with monoclonal antibodies in protein A chromatography. *Biotechnol Prog*, 2012. 28(2): p. 454-8.
63. Ahluwalia, D., et al., Identification of a host cell protein impurity in therapeutic protein, P1. *J Pharm Biomed Anal*, 2017. 141: p. 32-38.
64. Zhang, Q., et al., Comprehensive tracking of host cell proteins during monoclonal antibody purifications using mass spectrometry. *MAbs*, 2014. 6(3): p. 659-70.
65. Gao, S.X., et al., Fragmentation of a highly purified monoclonal antibody attributed to residual CHO cell protease activity. *Biotechnol Bioeng*, 2011. 108(4): p. 977-82.
66. Charcosset, C., 4 - Virus filtration, in *Membrane Processes in Biotechnology and Pharmaceutics*, C. Charcosset, Editor. 2012, Elsevier: Amsterdam. p. 143-167.
67. Gilgunn, S., et al., Identification and tracking of problematic host cell proteins removed by a synthetic, highly functionalized nonwoven media in downstream bioprocessing of monoclonal antibodies. *J Chromatogr A*, 2019. 1595: p. 28-38.
68. Kornecki, M., et al., Host Cell Proteins in Biologics Manufacturing: The Good, the Bad, and the Ugly. *Antibodies (Basel)*, 2017. 6(3).
69. Luhrs, K.A., et al., Evicting hitchhiker antigens from purified antibodies. *J Chromatogr B Analyt Technol Biomed Life Sci*, 2009. 877(14-15): p. 1543-52.

70. Chen, R.H., et al., Factors affecting endotoxin removal from recombinant therapeutic proteins by anion exchange chromatography. *Protein Expr Purif*, 2009. 64(1): p. 76-81.
71. Zhang, M., et al., Extracorporeal endotoxin removal by novel l-serine grafted PVDF membrane modules. *Journal of Membrane Science*, 2012. 405-406: p. 104-112.
72. Ongkudon, C.M., et al., Chromatographic Removal of Endotoxins: A Bioprocess Engineer's Perspective. *ISRN Chromatography*, 2012. 2012: p. 649746.
73. Petsch, D. and F.B. Anspach, Endotoxin removal from protein solutions. *Journal of Biotechnology*, 2000. 76(2): p. 97-119.
74. Ritzén, U., et al., Endotoxin reduction in monoclonal antibody preparations using arginine. *Journal of Chromatography B*, 2007. 856(1): p. 343-347.
75. Kahle, J. and H. Watzig, Determination of protein charge variants with (imaged) capillary isoelectric focusing and capillary zone electrophoresis. *Electrophoresis*, 2018. 39(20): p. 2492-2511.
76. Zhou, Q., et al., N-linked oligosaccharide analysis of glycoprotein bands from isoelectric focusing gels. *Analytical Biochemistry*, 2004. 335(1): p. 10-16.
77. Wingfield, P.T., Overview of the purification of recombinant proteins. *Curr Protoc Protein Sci*, 2015. 80: p. 6 1 1-6 1 35.
78. Vlasak, J. and R. Ionescu, Heterogeneity of monoclonal antibodies revealed by charge-sensitive methods. *Curr Pharm Biotechnol*, 2008. 9(6): p. 468-81.
79. Kahle, J., et al., Comparative charge-based separation study with various capillary electrophoresis (CE) modes and cation exchange chromatography (CEX) for the analysis of monoclonal antibodies. *J Pharm Biomed Anal*, 2019. 174: p. 460-470.
80. Meyer, R.M., et al., Identification of Monoclonal Antibody Variants Involved in Aggregate Formation - Part 1: Charge Variants. *Eur J Pharm Biopharm*, 2020.
81. Dai, J., et al., Capillary Isoelectric Focusing-Mass Spectrometry Method for the Separation and Online Characterization of Intact Monoclonal Antibody Charge Variants. *Anal Chem*, 2018. 90(3): p. 2246-2254.
82. Liu, H., et al., Characterization of recombinant monoclonal antibody charge variants using WCX chromatography, icIEF and LC-MS/MS. *Anal Biochem*, 2019. 564-565: p. 1-12.
83. Rohani, M.M. and A.L. Zydney, Role of electrostatic interactions during protein ultrafiltration. *Adv Colloid Interface Sci*, 2010. 160(1-2): p. 40-8.

84. Robinson, J., D. Roush, and S.M. Cramer, The effect of pH on antibody retention in multimodal cation exchange chromatographic systems. *J Chromatogr A*, 2020. 1617: p. 460838.
85. Snyder, L.R., J.J. Kirkland, and J.W. Dolan, *Introduction to Modern Liquid Chromatography*. Third ed. 2010, Hoboken: Wiley-VCH. 584-618.
86. Lehermayr, C., et al., Assessment of net charge and protein-protein interactions of different monoclonal antibodies. *J Pharm Sci*, 2011. 100(7): p. 2551-62.
87. Fekete, S., et al., Hydrophobic interaction chromatography for the characterization of monoclonal antibodies and related products. *J Pharm Biomed Anal*, 2016. 130: p. 3-18.
88. Burns, A., P. Olszowy, and P. Ciborowski, Biomolecules, in *Proteomic Profiling and Analytical Chemistry*. 2016. p. 7-24.
89. Fekete, S., et al., Chromatographic, Electrophoretic, and Mass Spectrometric Methods for the Analytical Characterization of Protein Biopharmaceuticals. *Anal Chem*, 2016. 88(1): p. 480-507.
90. Borisov, O.V., et al., Sequence Variants and Sequence Variant Analysis in Biotherapeutic Proteins, in *State-of-the-Art and Emerging Technologies for Therapeutic Monoclonal Antibody Characterization Volume 2. Biopharmaceutical Characterization: The NISTmAb Case Study*. 2015, American Chemical Society. p. 63-117.
91. Hinkle, J.D., et al., Unambiguous Sequence Characterization of a Monoclonal Antibody in a Single Analysis Using a Nonspecific Immobilized Enzyme Reactor. *Anal Chem*, 2019. 91(21): p. 13547-13554.
92. Flynn, G.C., et al., Naturally occurring glycan forms of human immunoglobulins G1 and G2. *Mol Immunol*, 2010. 47(11-12): p. 2074-82.
93. Srebalus Barnes, C.A. and A. Lim, Applications of mass spectrometry for the structural characterization of recombinant protein pharmaceuticals. *Mass Spectrometry Reviews*, 2007. 26(3): p. 370-388.
94. Herschel, T., A. El-Armouche, and S. Weber, Monoclonal antibodies, overview and outlook of a promising therapeutic option. *Dtsch med Wochenschr*, 2016. 141: p. 1390-1394.
95. Ribatti, D., Edelman's view on the discovery of antibodies. *Immunol Lett*, 2015. 164(2): p. 72-5.
96. Dicker, M. and R. Strasser, Using glyco-engineering to produce therapeutic proteins. *Expert Opin Biol Ther*, 2015. 15(10): p. 1501-16.
97. Zydney, A.L., Perspectives on integrated continuous bioprocessing—opportunities and challenges. *Current Opinion in Chemical Engineering*, 2015. 10: p. 8-13.

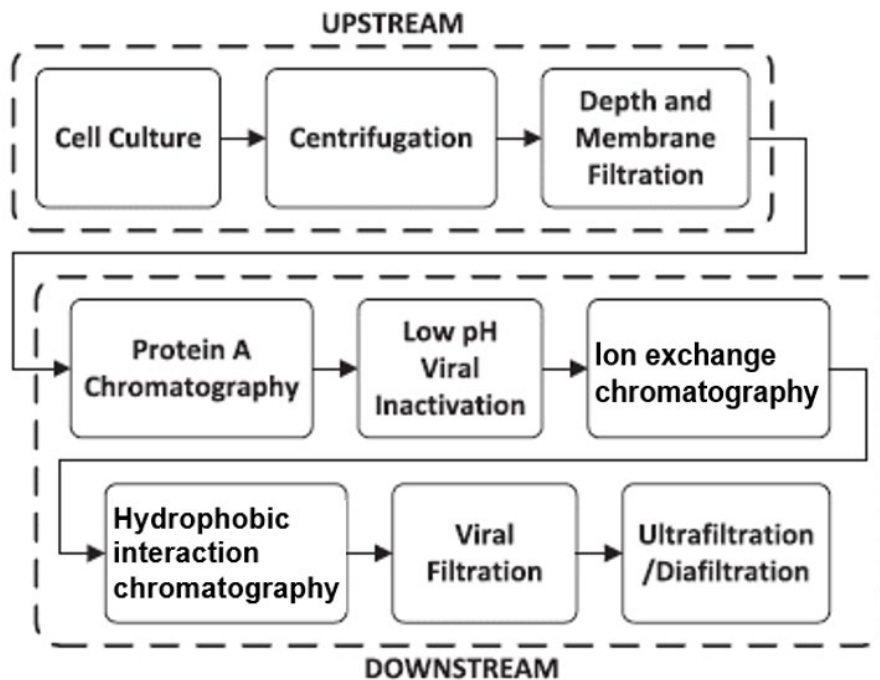
98. Rowe, L., G. El Khoury, and C.R. Lowe, Affinity Chromatography: Historical and Prospective Overview. *Biopharmaceutical Production Technology*, 2012: p. 223-282.
99. Wang, Y., et al., Simultaneous monitoring of oxidation, deamidation, isomerization, and glycosylation of monoclonal antibodies by liquid chromatography-mass spectrometry method with ultrafast tryptic digestion. *MAbs*, 2016. 8(8): p. 1477-1486.
100. Yang, X., et al., Ultrafast and high-throughput N-glycan analysis for monoclonal antibodies. *MAbs*, 2016. 8(4): p. 706-17.
101. Strohl, W.R. and L.M. Strohl, *Therapeutic Antibody Engineering : Current and Future Advances Driving the Strongest Growth Area in the Pharmaceutical Industry*. Vol. 11. 2012, Cambridge: Elsevier Science & Technology.
102. Radhakrishnan, D., A.S. Robinson, and B.A. Ogunnaike, Controlling the Glycosylation Profile in mAbs Using Time-Dependent Media Supplementation. *Antibodies (Basel)*, 2017. 7(1).
103. Ivarsson, M., et al., Evaluating the impact of cell culture process parameters on monoclonal antibody N-glycosylation. *J Biotechnol*, 2014. 188: p. 88-96.
104. Wu, W., et al., *Characterization of Protein Therapeutics by Mass Spectrometry: Accelerating Protein Biotherapeutics from Lab to Patient*. 2017. p. 221-249.
105. Gagneux, P. and A. Varki, Evolutionary considerations in relating oligosaccharide diversity to biological function. *Glycobiology*, 1999. 9(8): p. 747-755.
106. Barinka, C., et al., Identification of the N-glycosylation sites on glutamate carboxypeptidase II necessary for proteolytic activity. *Protein Sci*, 2004. 13(6): p. 1627-35.
107. Mrázek, H., et al., Carbohydrate synthesis and biosynthesis technologies for cracking of the glycan code: Recent advances. *Biotechnology advances*, 2012. 31.
108. Zhou, Q. and H. Qiu, The Mechanistic Impact of N-Glycosylation on Stability, Pharmacokinetics, and Immunogenicity of Therapeutic Proteins. *Journal of Pharmaceutical Sciences*, 2019. 108(4): p. 1366-1377.
109. Wada, R., M. Matsui, and N. Kawasaki, Influence of N-glycosylation on effector functions and thermal stability of glycoengineered IgG1 monoclonal antibody with homogeneous glycoforms. *MAbs*, 2019. 11(2): p. 350-372.
110. Planinc, A., et al., Glycan characterization of biopharmaceuticals: Updates and perspectives. *Anal Chim Acta*, 2016. 921: p. 13-27.
111. Sola, R.J. and K. Griebenow, Effects of glycosylation on the stability of protein pharmaceuticals. *J Pharm Sci*, 2009. 98(4): p. 1223-45.

112. Wang, Z., J. Zhu, and H. Lu, Antibody glycosylation: impact on antibody drug characteristics and quality control. *Appl Microbiol Biotechnol*, 2020. 104(5): p. 1905-1914.
113. Liu, H., et al., Heterogeneity of Monoclonal Antibodies. *Journal of Pharmaceutical Sciences*, 2008. 97(7): p. 2426-2447.
114. Hari, S.B., et al., Acid-induced aggregation of human monoclonal IgG1 and IgG2: molecular mechanism and the effect of solution composition. *Biochemistry*, 2010. 49(43): p. 9328-38.
115. Alsenaidy, M.A., et al., Physical stability comparisons of IgG1-Fc variants: effects of N-glycosylation site occupancy and Asp/Gln residues at site Asn 297. *J Pharm Sci*, 2014. 103(6): p. 1613-1627.
116. Stone, M.T., K.A. Cotoni, and J.L. Stoner, Cation exchange frontal chromatography for the removal of monoclonal antibody aggregates. *J Chromatogr A*, 2019. 1599: p. 152-160.
117. Yigzaw, Y., et al., Ion exchange chromatography of proteins and clearance of aggregates. *Curr Pharm Biotechnol*, 2009. 10(4): p. 421-6.
118. Saraswat, M., et al., Preparative purification of recombinant proteins: current status and future trends. *Biomed Res Int*, 2013. 2013: p. 312709.
119. Arakawa, T., et al., The effects of arginine on protein binding and elution in hydrophobic interaction and ion-exchange chromatography. *Protein Expr Purif*, 2007. 54(1): p. 110-6.
120. Jabra, M.G., et al., pH and excipient profiles during formulation of highly concentrated biotherapeutics using bufferless media. *Biotechnol Bioeng*, 2020. 117(11): p. 3390-3399.
121. Kroner, F., et al., Analytical characterization of complex, biotechnological feedstocks by pH gradient ion exchange chromatography for purification process development. *J Chromatogr A*, 2013. 1311: p. 55-64.

### 3.0 Impact of Prefilter Mechanisms of Action on Virus Filtration of A mAb

#### 3.1 Introduction

Biopharmaceutical manufacturing often consists of a 'standard' sequence of unit operations (platform processes). These unit operations are grouped into two major categories: upstream and downstream, as shown in Figure 3.1 below. The upstream unit operations include the cell culture and bioreactor clarification steps [1]. At the same time, downstream purification processes comprise sequential steps of chromatography, virus filtration, and ultrafiltration/diafiltration (UF/DF) [1].



**Figure 3.1:** Flow Chart of a Monoclonal Antibody Production System

Typically, the bioreactor is operated in a batch mode; however, perfusion bioreactors have become mainstream in recent times. Clarification processes are used to separate extracellular products (mAbs) and proteins from bulk cellular materials, while protein A columns

are used to separate the mAbs from the HCP. Polishing and downstream purification processes are predominantly batch processes with large industrial and cost footprints and significant residence times [2, 3].

Polishing steps are mandated by regulatory bodies after protein A affinity chromatography to eliminate remaining impurities [1]. Impurities can be structural and biophysical variants of the mAb, such as oligomers, denatured mAbs, and host cell proteins. Cation exchange, anion exchange, and hydrophobic interaction chromatography (HIC) are typically used as chromatographic polishing steps that further purify the mAb before virus filtration.

Two polishing steps are shown in Figure 3.1, Hydrophobic interaction chromatography (HIC) and ion-exchange chromatography (comprising cation exchange chromatography and anion exchange chromatography). HIC polishing removes aggregates and denatured proteins from the feedstream based on a difference in hydrophobicity in the presence of buffer salts. Ion exchange membrane adsorbers remove contaminants and aggregates by an adsorptive process driven by electrostatic interactions in low salt buffers. Polishing with the anion exchange membranes can also remove viruses due to the pI difference between viruses and mAbs. Ion exchange membranes generally ensure HCP removal by pI differences between the mAb and HCP.

The polished product passes to a virus filter before the final formulation. Virus filtration is mandated for the robust removal of adventitious virus contamination. These single-use virus filters are typically the most expensive component needed in downstream purification [4]. Protein A columns are expensive but are reusable. Virus filtration works on the size exclusion principle, where particles 20 nm or larger do not pass the virus filter [5].

Less expensive mAb biosimilars have resulted in process intensification efforts for cost-competitiveness [6]. Continuous bioprocessing efforts have led to moving bed systems and counter-current chromatography systems [7]. Pall, GE Healthcare, Semba, Chromacon, and Novasep are developing continuous downstream processing unit operations [8]. Integrating new technologies into existing downstream platform processes remains a central challenge [9].

Biologics are mainly produced from mammalian cell cultures [10]. There is always a likelihood of product contamination by DNA, HCP, proteases, endotoxins, and viruses. mAb and protein stability are governed by amino acid sequence and post-translational modifications [11], which influence pI and hydrophobicity and affinity to polishing membranes.

Therapeutic proteins require process validation for safety reasons, including the absence of virus contaminants from the host cell. Virus removal strategies are robustly implemented and begin with rigorous quality control testing of source materials and finished products coupled with multiple virus inactivation/removal unit operations [7, 12]. The manufacture of mAbs includes several harvesting and orthogonal purification/sterilization steps. Environmental factors such as pH, temperature, ionic strength, protein concentration, oxygen, and shear forces can affect filtration performance [13-15].

Ion exchange chromatography is viewed as the gold standard in protein partitioning due to its excellent robustness and resolution [16]. Ion exchange membranes are most effective when there is less competition between the biomolecules and buffer ions. This is the case when low ionic strength buffers are used to constitute the mAb. The pI of mAbs is usually higher than the pI of HCPs, thereby enabling mAb purification by electrostatic partitioning. Charge heterogeneity of biologics is a valuable partitioning parameter for anion and cation exchange membranes or resins [17]. HIC membranes require a moderate/high salt content (ionic strength)



to reduce the mAb solvation layer enabling exposed hydrophobic patches on foulant species to adsorb on the HIC ligands.

Prefiltration of mAbs before virus filtration aims to reduce flux decay during virus filtration by capturing fouling species before virus filtration. Such foulants may include multimers and denatured mAbs with a high multimerization tendency. Denatured mAbs with more surface-exposed hydrophobic residues present as monomeric variants to the native-state mAb monomers and increase fouling tendency through an increased tendency to aggregate. Aggregates can be categorized as soluble when they are bound by non-covalent forces with a small number of proteins involved; and insoluble otherwise [18]. Small reversible aggregates have been largely identified as the principal foulant of virus filters [18-20]. In this work, we seek to understand the impact of different prefilter types, buffer pH, salt content, and excipients on the fouling of virus filters.

## **3.2 Materials and Methods**

### **3.2.1 Materials**

Reagents used include tris(hydroxymethyl)aminomethane (biotechnology grade, 99% purity), Ammonium sulfate (proteomics grade, > 99.5% purity), and Sodium dodecyl sulfate (biotechnology grade, > 99% purity) sourced from VWR Life Science (Radnor, PA). Sodium chloride (molecular biology grade > 98% purity), Sodium phosphate monobasic monohydrate (ACS reagent, > 98% purity), Sodium phosphate dibasic (reagent plus, >99% purity), OmniPur sodium acetate trihydrate (molecular biology grade, > 99% purity), Glycine (for electrophoresis, > 99% purity), Acrylamide for synthesis (79-06-1), Acetonitrile (liquid  $\geq$ 99.8% purity), and Glacial acetic acid (100% purity) were sourced from MilliporeSigma (Billerica, MA).

Ultrapure water with a resistivity of 18.2 M $\Omega$  was used for buffer formulation. Recombinant glycosidase (PNGase F, 500 units with 10 u/ $\mu$ l) was sourced from Promega (Madison, WI). Precision protein plus MW standard and Bromophenol blue indicator, Supelco (115-39-9) were sourced from Bio-Rad laboratories (Hercules, CA). Dithiothreitol (molecular biology grade, >99% purity) was sourced from Gold Biotechnology (St. Louis, MO).

10 kDa molecular weight cutoff (MWCO) PES centrifugal filters were sourced from VWR Life Science (Radnor, PA). Nalgene™ rapid-flow™ sterile single-use bottle top filters (0.2 $\mu$ m and 0.1 $\mu$ m) were sourced from ThermoFisher Scientific (Waltham, MA). Other selected prefilters were Planova 75N provided by Asahi Kasei Medical (Tokyo, Japan), Sartobind® Phenyl nano 3 mL, Sartobind® Q nano 3 mL, 8 mm bed height, and Sartobind® S nano 3 mL, 8 mm bed height provided by Sartorius (Göttingen, Germany). The selected virus filter was Planova BioEX (membrane surface area 0.0003m<sup>2</sup>) provided by Asahi Kasei Medical (Tokyo, Japan).

HiTrap Capto S Impact column (5 ml) was sourced from Cytiva (Marlborough, MA). TangenX Sius PDn Cassette (30 kDa MWCO, mPES, 0.1 m<sup>2</sup>) was sourced from Repligen (Marlborough, MA). SDS MW analysis kit (PN: 390953), Fast glycan labeling and analysis kit (PN: B94499), CZE rapid charge variant analysis kit (PN: C44790), and Advanced cIEF starter kit (PN: A80976) were sourced from SCIEX (Redwood City, CA).

### **3.2.2 Monoclonal Antibody Sample Preparation and Buffer Conditions**

mAb B was provided by a biopharmaceutical company and had been processed through two chromatography polishing steps prior to receipt. The isoelectric point (pI) of mAb B was initially given as 8.0; pI determination by cIEF on receipt showed a pI range of 7.1 to 8.0. 250

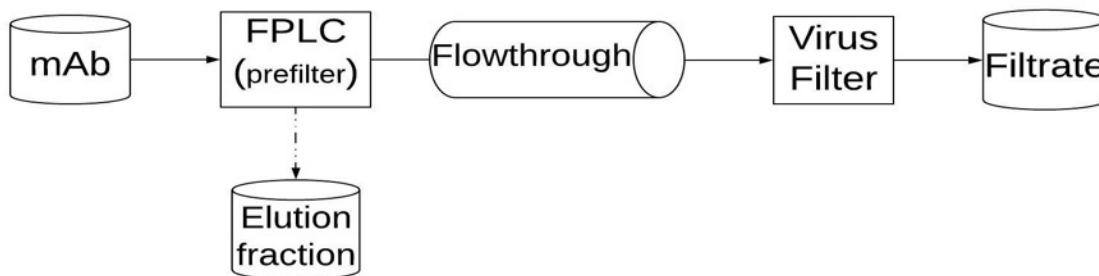
ml batches of mAb B (5.4 g/L) were ultrafiltered and diafiltered from the original buffer to a final formulation of 5 g/L mAb B in 20 mM sodium acetate buffer, 200 mM NaCl (pH 5) with the same final volume as the initial volume (250 ml). Other portions of mAb B were buffer exchanged into 20 mM sodium acetate buffer, 200 mM NaCl (pH 8.6 titrated with tris base) at 5 g/L, and 20 mM sodium acetate buffer, with no salt (pH 7.5, titrated with tris base) at 5 g/L. All mAb B filtration studies were performed at 5 g/L. TangenX Sius PDn Cassette (30 kDa MWCO, mPES, 0.1 m<sup>2</sup>) was used for UF/DF.

The mAb stock concentration was measured by UV spectrophotometric analysis at 280 nm using Genesys10 UV Scanning System (Waltham, MA) with VWR quartz spectrophotometer cell (path length 1 cm; West Chester, PA). mAb concentration and turbidity were determined by measuring the absorbance at 280 and 340 nm, respectively. Mass balance on the UF/DF mAb feed and final product resulted in over 95% mAb recovery, with the feed concentration dropping from 5.4 g/L to 5 g/L in the retentate.

Buffer exchange was performed by ultrafiltration and diafiltration (UF/DF) of 5 g/L mAb B in five diafiltration volumes using a TangenX Sius™ PDn HyStream 30kDa tangential flow filtration (TFF) Cassette (Shrewsbury, MA). Buffer pH and conductivity were measured using Orion Star™ A215 pH/conductivity benchtop multiparameter meter from ThermoFisher Scientific (Waltham, MA). mAb fractions were immediately used for prefiltration or virus filtration following buffer exchange or stored at 4°C for one week. mAbs were stored for extended periods at -80°C.

Sartobind membrane adsorbers are typically used for mAb polishing; however, we adopted them as adsorptive prefilters post mAb polishing. HIC prefiltration was performed using the Sartobind phenyl 3 ml membrane. At the same time, anion and cation exchange-based

prefiltration was performed using the Sartobind Q and Sartobind S, respectively. Prefiltration of mAb B was not performed in line with the virus filter. Figure 3.2 below shows the workflow for prefiltration and virus filtration.



**Figure 3.2:** Decoupled Prefiltration and Virus Filtration Workflow (Prefiltration was not Inline)

In the above workflow, the mAb was filtered with a 0.2-micron PES filter before adsorptive prefiltration using the requisite prefilter. Buffer formulations were selected such that the flowthrough fraction was the mAb product and was subsequently filtered with the BioEX virus filter. Before mAb prefiltration, the prefilter was equilibrated with sample buffer (20 mM sodium acetate at either pH 5 with 200 mM NaCl, pH 7.5 without salt, and pH 8.6 with 200 mM NaCl) at 2 ml/minute for 30 minutes. 90 ml of the mAb was prepared as feed and constituted in the same buffer as the equilibration buffer. Prefiltration was followed by a buffer chase of 20 ml buffer (same buffer as the mAb) at 2 ml/minute. 40 ml of elution buffer (20 mM sodium acetate at pH 5 or 8.6 with 1 M NaCl for IEX-S and IEX-Q; 20 mM sodium acetate buffer, pH 7.5 no salt for HIC) was used to elute the foulant species at 2 ml/minute from the prefilter. The FPLC showed adsorptive and desorptive events in real-time. The fractions were then analyzed.

The prefiltration membrane was installed on an FPLC (GE Pharmacia, Boston, MA). HIC prefiltration was performed at pH 5 with salt, pH 7.5 with salt, and pH 8.6 with salt. Buffer A had the same composition as the mAb buffer with 200 mM NaCl. A lower ionic strength buffer

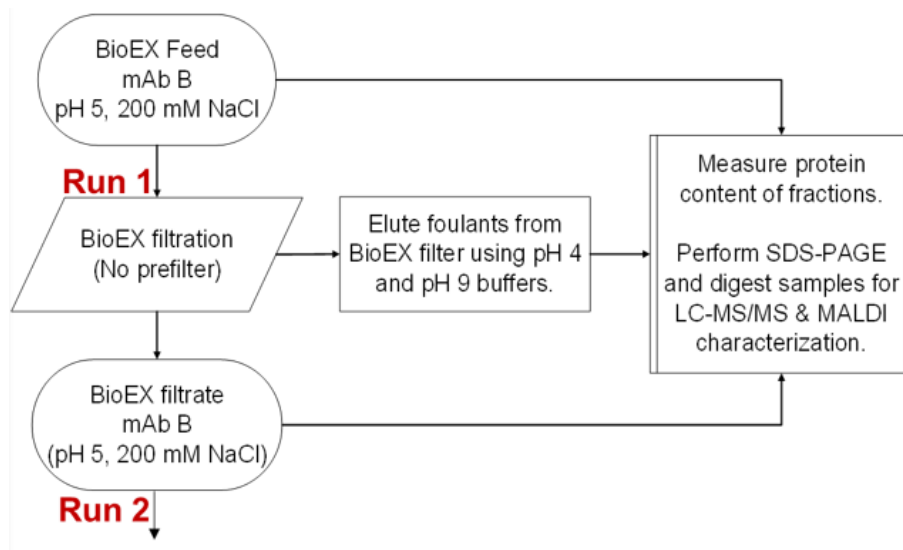
of the same pH as the mAb with 0 mM NaCl was used as buffer B (elution buffer) during HIC prefiltration. Sartobind S and Sartobind Q prefiltration required 200 mM NaCl in buffer A at pH 5 and pH 8.6 but 0 mM NaCl in buffer A at pH 7.5. Buffer B had high ionic strength (1 M NaCl) during IEX (Sartobind S and Sartobind Q) chromatography.

A 0.2- $\mu\text{m}$  polyethersulfone (PES) bottle top filter was used to remove large aggregates before prefiltration and virus filtration (normalizing mAb feed aggregate levels). Prefiltration was performed in flowthrough mode across all prefilters, and the mAb was collected as flowthrough fractions. A buffer wash step was performed after flowthrough, and an elution step was also performed. All fractions were collected for characterization. The flowthrough fraction was immediately available for virus filtration.

Visual leak integrity tests were performed on the BioEX virus filters at 14.5 psi for 20 seconds before flushing air out from the system. Reservoir pressure was controlled by an Ashcroft pressure gauge (Part number: EW-68334-15; 0-100 psi, resolution 0.1, accuracy  $\pm 0.5$  full-scale). Deionized water filtered with a 0.2- $\mu\text{m}$  bottle top filter was added to the Planova™ Pressure Reservoir (Asahi Kasei, Japan). The BioEX filter was then flushed with 40 L/m<sup>2</sup> of DI water and 40 L/m<sup>2</sup> of equilibration buffer. We performed virus filtration in constant-pressure, dead-end filtration mode. The flowthrough fractions during prefiltration were used as the BioEX feed. The cumulative mass of the BioEX filtrate was acquired in real-time using a BalanceLink software connected to a Mettler Toledo scale (Columbus, OH).

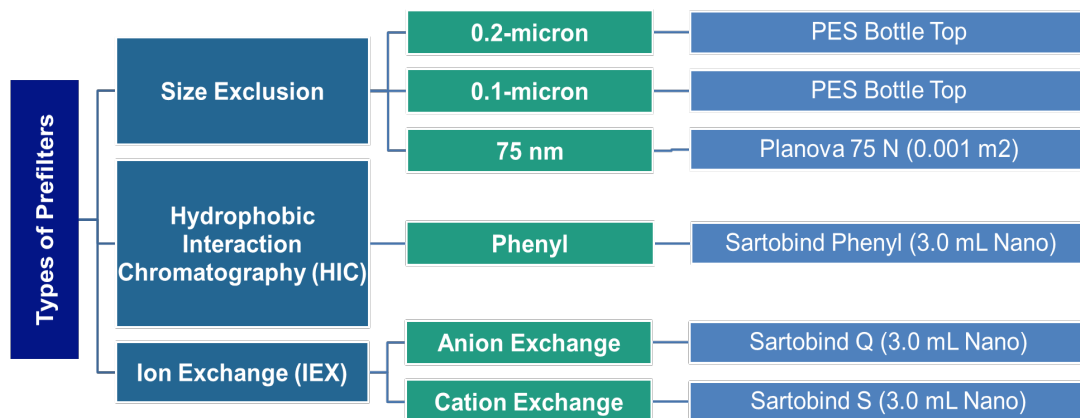
A no prefiltration baseline involved removing large aggregates using a 0.2- $\mu\text{m}$  bottle top filter before BioEX virus filtration. Virus filtration without prefiltration was performed using mAb B feed at the above-stated buffer conditions without HIC or IEX prefiltration.

Figure 3.3 below shows the workflow for virus filtration without prefiltration. The permeate from BioEX filter 1 was introduced as feed to BioEX filter 2.



**Figure 3.3:** Workflow for BioEX Filtration in Series for mAb B without Prefiltration

Virus filtration with the BioEX virus filter was also performed downstream of size exclusion-based prefilters (Planova 75N, 0.1- $\mu\text{m}$ , and 0.2- $\mu\text{m}$  PES bottle top filters). The BioEX virus filter was subsequently flushed with 40 L/m<sup>2</sup> of buffer chase and pH 4 elution buffers. All fractions were collected and subsequently characterized. Figure 3.4 below shows the various specifications of prefilters used for the study.



- **Protein:** mAb B (pI = 7.1 – 8.0, MW = 148 kDa)
- **Condition:** 20 mM sodium acetate buffer in the following conditions
  - Stable: pH 7.5 without salt (BioEX, HIC, IEX-S, IEX-Q, size-based prefilters)
  - Less stable: pH 5 with 200 mM NaCl (BioEX, HIC, IEX-S, IEX-Q, size-based prefilters)
  - Less stable: pH 8.6 with 200 mM NaCl (BioEX, HIC, IEX-S, IEX-Q, 0.2-micron prefilter)
- **Base prefilter:** Sterilizing-grade 0.2-micron PES filter  
(considered as no prefilter)
- **Virus filter:** Planova BioEX (Asahi Kasei)
- **Prefilters:** Sartobind phenyl membrane adsorber (HIC 'prefilter')  
Sartobind S membrane adsorber (IEX-S 'prefilter')  
Sartobind Q membrane adsorber (IEX-Q 'prefilter')  
Size exclusion-based prefilters (0.2-micron, 0.1-micron and Planova 75N [75 nm])

**Figure 3.4:** Specification of Prefilters and Buffer Conditions used for mAb B Study

The Planova 75N is used in the plasma fractionation industry. Here we investigated its effectiveness as a size-exclusion prefilter which would remove larger species that could foul the virus filter. It has a nominal pore size of 75 nm. Planova 75N prefiltration was not performed on an FPLC. The Planova 75N was connected to a Planova pressure vessel containing the mAb at 5 g/L. The operating pressure of 14 psi was supplied from a pressurized nitrogen bottle. The permeate was collected on a weighing balance and recorded for flux calculations. The other size-

exclusion prefilters were bottle top filters (0.1-micron and 0.2-micron). These are sterilizing grade filters that are typically used to filter all buffer streams prior to introduction to the manufacturing process. Bottle top filters are manually handled with a low vacuum used to pull the permeate from the feed along the walls of the receiving bottle to prevent aggregation.

Sartobind membrane adsorbers were adopted as adsorptive prefilters. These include the Sartobind phenyl (HIC prefilter) and the ion exchange prefilters (Sartobind S and Sartobind Q). The ion exchange prefilters were implemented in flowthrough mode by adding 200 mM NaCl to the buffer when the absolute value  $|\text{pH} - \text{pI}| > 0.5$  to maintain high mAb transmission ( $>0.95$ ). Multimodal prefilters were not used for this study.

### **3.2.3 Hydrophobic Interaction Chromatography Based Prefiltration**

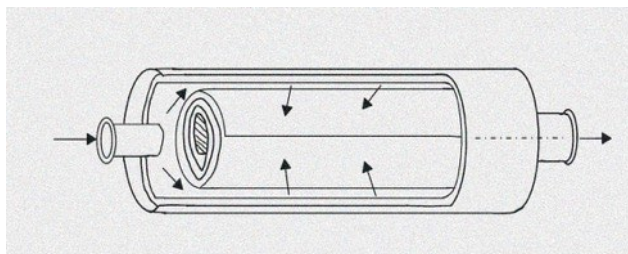
Hydrophobic interaction chromatography (HIC) prefiltration was used to purify monoclonal antibodies by leveraging the difference in hydrophobicity between native conformation mAbs and denatured mAbs or aggregates. A Sartobind phenyl membrane adsorber (HIC 'prefilter') was selected. The membrane matrix is made of stabilized, reinforced cellulose and is functionalized with phenyl ligands. This prefilter has a bed volume of 3 ml and a nominal pore size greater than  $3\mu\text{m}$ . The average pore size is  $3 - 5\mu\text{m}$ . HIC prefilters are single mechanism prefilters. The HIC prefilter is mounted on an FPLC in a flowthrough configuration to observe the molecular interactions in real-time using the in-built spectrophotometer.

The prefilter was equilibrated at 2 ml/minute with the requisite buffer condition at pH 5, 7.5 or 8.6 for 30 minutes before prefiltration of mAb B feed (90 ml at 5.4 g/L). Prefiltration was always performed at 2 ml/minute including the equilibration and wash fractions. Buffer chase



(20 ml) was used to wash off loosely bound mAb from the prefilter over ten minutes followed by 40 ml of elution buffer (same buffer as equilibration buffer without salt) at pH 5, 7.5 or 8.6.

Prefilter flowthrough fractions were collected for virus filtration. The HIC elution fraction (eluate) was also collected for further analysis. Figure 3.5 below shows the schematic of a sartobind phenyl prefilter.



**Figure 3.5:** Cross-sectional Area of a Sartobind Phenyl (HIC) Membrane Adsorber

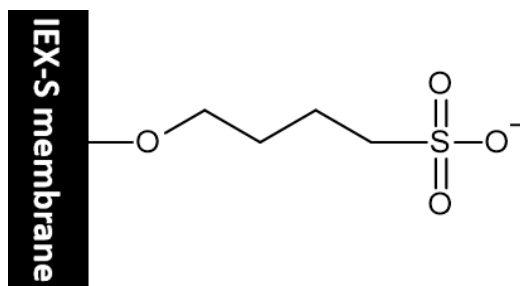
The prefilter membrane is tightly bound inside the housing. The fluid enters the prefilter capsule and flows around the membrane housing under the feed pressure, which forces the fluid to pass through the membrane into the interior flow path (inner core) of the prefilter. This flowthrough fraction is the prefiltered product of the membrane.

### 3.2.4 Cation Exchange Chromatography-Based Prefiltration

The prefilter was equilibrated at 2 ml/minute with the requisite buffer condition at pH 5, 7.5, or 8.6 for 30 minutes before prefiltration of mAb B feed (90 ml at 5.4 g/L). Prefiltration was performed at 2 ml/minute, including the equilibration and wash fractions. Buffer chase (20 ml) was used to wash off loosely bound mAb from the prefilter over ten minutes, followed by 40 ml of elution buffer over 20 minutes (same buffer as equilibration buffer with 1 M NaCl) at pH 5, 7.5, or 8.6.

Strong cation exchange membranes or resins are materials with the attribute of displaying permanent negatively charged ligands on the surface, which can then be used to partition cationic species from a sample. Negatively charged exchangers bind positively charged ions (cations). Cation exchange materials are classified as strong or weak, depending on whether cation exchange properties change with buffer pH [21].

Partitioning of mAbs occurs by selective adsorption based on the mAb surface charges at prevailing pH and salt concentration. The cation exchange chromatography (CEX) membrane adsorber (IEX-S 'prefilter') we selected is the Sartobind S membrane adsorber (IEX-S), which has sulfonic acid ligands ( $\text{SO}_3^-$ ) and a permanent negatively charged surface. The membrane matrix is made of stabilized, reinforced cellulose and is functionalized with sulfonic acid, as shown in Figure 3.6 below.



**Figure 3.6:** Sartobind-S Matrix-Ligand Structure

IEX-S membrane adsorbers have an affinity for positively charged biomolecules due to the ligand chemistry. The prefilter used for this work had a membrane volume of 3 ml and a nominal pore size greater than  $3\mu\text{m}$ . The average pore size is 3 -  $5\mu\text{m}$ . This prefilter was mounted in an FPLC to perform prefiltration in the flowthrough mode. When the process feed stream is introduced into the cation exchange prefilter, foulants with cationic characteristics bind to the oppositely charged functional groups on the IEX-S ligand through Coulombic attraction.

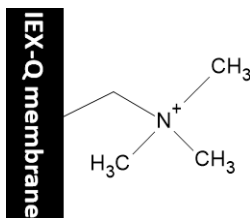
Following Coulomb's law, the attractive forces between cationic species in the feed stream and oppositely charged functional groups on the cation exchange ligand is due to electrostatic forces.

### 3.2.5 Anion Exchange Chromatography-Based Prefiltration

The prefilter was equilibrated at 2 ml/minute with the requisite buffer condition at pH 5, 7.5, or 8.6 for 30 minutes before prefiltration of mAb B feed (90 ml at 5.4 g/L). Prefiltration was performed at 2 ml/minute, including the equilibration and wash fractions. Buffer chase (20 ml) was used to wash off loosely bound mAb from the prefilter over ten minutes, followed by 40 ml of elution buffer over 20 minutes (same buffer as equilibration buffer with 1 M NaCl) at pH 5, 7.5 or 8.6.

Strong anion exchange prefilters are membranes with the attribute of displaying permanent positively charged ligands on the surface, which can then be used to partition anionic species (with a negative charge) from a mobile phase. Positively charged exchangers bind negatively charged ions (anions) by adsorption.

A typical anion exchange chromatography (AEX) membrane is the Sartobind Q membrane adsorber (IEX- Q), which has quaternary ammonium ligands and a positively charged surface. The membrane matrix comprises stabilized, reinforced cellulose whose surfaces are functionalized with quaternary ammonium by hydrogel grafting. The Sartobind-Q matrix-ligand structure is shown in Figure 3.7 below.



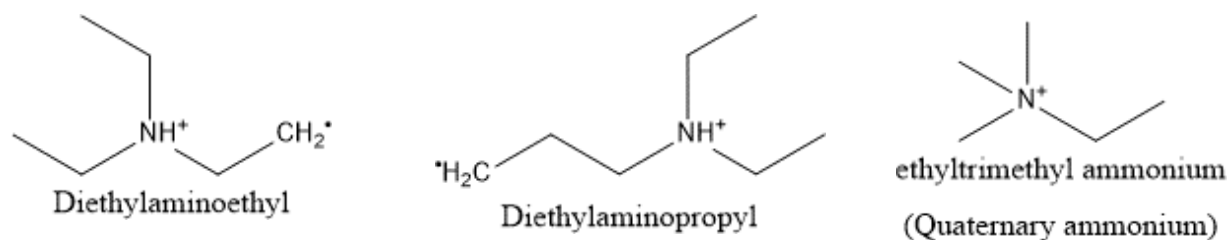
**Figure 3.7:** Sartobind-Q Matrix-Ligand Structure

Sartobind-Q prefilter used in this work had a membrane volume of 3 ml and a nominal pore size greater than 3 $\mu$ m. The average pore size is 3 - 5 $\mu$ m. Table 3.1 below shows the chemistry of some anion exchange ligands.

**Table 3.1:** Structure and Potency of some Anion Exchange Ligands

Anion exchangers	Potency	Functional group
Quaternary ammonium (Q)	strong	-CH <sub>2</sub> -N <sup>+</sup> -(CH <sub>3</sub> ) <sub>3</sub>
Diethylaminoethyl (DEAE)	weak	-CH <sub>2</sub> -CH <sub>2</sub> -N <sup>+</sup> -(CH <sub>2</sub> -CH <sub>3</sub> ) <sub>2</sub>
Diethylaminopropyl (ANX)	weak	-CH <sub>2</sub> -CHOH-CH <sub>2</sub> -N <sup>+</sup> -(CH <sub>2</sub> -CH <sub>3</sub> ) <sub>2</sub>

The strength of anion exchanger ligands represents the charge state and anion exchangeability of the functional groups within the ligand at different solution pH values. The strength and weakness of anion exchangers do not refer to these exchangers' binding affinity but rather the propensity to exchange anions at different pH conditions. The chemical structure of some weak and strong anion exchange ligands is shown in Figure 3.8 below.



**Figure 3.8:** Typical Ligands used to Functionalize Anion Exchange Membranes

Diethylaminoethyl and diethylaminopropyl ligands have hydrogen atoms in their backbone and are prone to deprotonation. Quaternary ammonium has no hydrogen atom in the

backbone and is not susceptible to deprotonation. Strong anion exchangers show little to no variation in ion exchange capacity with a pH change, unlike weak anion exchangers.

### **3.2.6 Capillary Electrophoresis (CE) Characterization**

A pharmaceutical analysis system (PA800 plus) by SCIEX (Redwood City, CA) was used to characterize the various filtration fractions using various modes. The capillary electrophoresis instrument (PA 800 plus) is a preferred choice for pharmaceutical characterization of mAb filtration fractions to identify MW variants, charge variants, glycovariants, and impurities. The mAb fractions to be characterized must be desalted and normalized to uniform concentrations before sample preparation using the SCIEX protocols. Up to 72 samples can be loaded at once. Characterization takes place sequentially based on the programmed software instructions.

The instrument parameters included a 50  $\mu\text{m}$  capillary ID and a 30 cm capillary length. The distance from the capillary inlet to the transparent detection window was 20cm. Bare fused silica capillaries were used for CE-SDS or IgG purity/heterogeneity assay. The advantages of CE include nanoliter injection volumes and exceptional peak resolution using over 1000000 theoretical plates.

Sample preparation for CE-SDS of mAb B involves desalting the filtration fractions with a 10 kDa MWCO centrifugal filter and reconstituting with DI water to 2 g/L. 10 $\mu\text{l}$  of desalted mAb B filtration fractions was added to 90  $\mu\text{l}$  of proprietary SCIEX gel buffer and loaded onto the instrument. SCIEX CE-SDS equipment operation protocol was followed for data acquisition and interpretation. During CE-SDS or IgG purity analysis, 15kV was applied across the capillary to separate the biomolecules by size only. The induced electric field caused sample components

to migrate differentially from the inlet to the capillary outlet. A photodiode array detector was used to measure absorbance yielding an electropherogram in real-time.

The PA800 plus was also used to perform capillary zone electrophoresis (charge variant analysis) of the mAb fractions. In the charge variant analysis mode, the bare fused silica capillary was used. All fractions were desalted and reconstituted in DI water. The samples were loaded in 200  $\mu$ l vials at 2 g/L into the instrument. SCIEX CZE running protocol was followed to obtain the electropherogram. The sample components migrate across the capillary by electroosmotic flow from the inlet to the outlet. Based on the relative migration rates, distinct peaks are obtained for the various IgG charge variants in the sample. The UV detector was installed during CZE characterization, and a voltage of 30kV was applied across the capillary.

The UV detector was also used during capillary isoelectric focusing (cIEF) characterization of mAb fractions. Whereas CZE shows the various charge variants, cIEF shows the peak distributions of isoforms and their respective isoelectric points. The pI of a biomolecule is the pH value at which the molecule's net charge is zero. Capillary isoelectric focusing (cIEF) is used to determine the pI distribution of components in a sample. During cIEF, the capillary was filled with proprietary SCIEX ampholytes, which comprise molecules with acidic and basic moieties that become zwitterionic at their pI. After the sample was injected into the capillary, a continuous pH gradient was created in the non-flowing ampholyte. Biomolecules migrate bi-directionally to the point in the capillary where their net charge is zero (pI) before the ampholytes are discharged with the detector determining the retention time of each component using UV at 280 nm.

The goodness of fit for the pI markers were determined before using those to determine sample component pIs. The pI markers used were pI = 4.1, 5.5, 7, 9.5, and 10. Proprietary synthetic peptides from SCIEX's cIEF kit were used as the pI markers.

After sample preparation, the PA 800 plus was used to perform a fast-glycan analysis of the mAb fractions to cleave the glycans. mAb fractions were concentrated or diluted to 1.1 g/L using centrifugal filters before deglycosylation. 2  $\mu$ l of recombinant glycosidase (PNGase F from Promega, Madison, WI) was used to deglycosylate 18  $\mu$ l of the mAb fractions after the addition of 1  $\mu$ l of 1 M DTT to cleave disulfide bonds. A 10 kDa molecular weight cutoff filter (VWR Life Science, Radnor, PA) was used to separate the released glycans from the deglycosylated mAbs.

Solid-phase extraction using proprietary SCIEX kit materials was used to purify the released glycans using immobilized ligands on magnetic beads. Sequential rinses using polar and non-polar solvents (water and acetonitrile, respectively) ensured that only pure glycans were captured by the magnetic beads while impurities were decanted off.

A laser-induced fluorescence detector was installed on the PA 800 plus during fast-glycan analysis. At the same time, the purified glycans were tagged with a fluorophore (APTS) during sample preparation. The PA 800 was calibrated with internal standards, and the software possesses a comprehensive glycan database to characterize glycans. SCIEX supplied all of the reagents as part of the cIEF, CZE, fast-glycan, and CE-SDS kits, respectively.

### **3.2.7 Dynamic Light Scattering (Particle Size Analysis)**

Particle size analysis by dynamic light scattering (DLS) was used to determine the particle size distribution of mAb filtration fractions. DLS measures the hydrodynamic radius and,

by extension, the hydrated diameter of biomolecules in a colloidal solution. DLS can also be used to obtain the diffusion interaction parameter of analytes in a solution. DLS was performed using a DelsaNano HC particle size analyzer by Beckman Coulter (Brea, CA). DLS measurements are susceptible to noise signals from ambient dust interference; therefore, the cuvettes were rinsed with ultrapure water. The mAb prefiltration and virus filtration fractions were filtered with a 0.2-micron syringe polyethersulfone filter before DLS measurement.

The instrument was calibrated using 100 nm size standards before starting DLS measurements. A disposable polystyrene cuvette with one cm pathlength (BrandTech, Essex, CT) was used for sample collection for measurement. The instrument software was set at 200 acquisitions, and triplicate runs were performed per filtration fraction. Average hydrodynamic diameter and other diffusion parameters were acquired and recorded for each filtration fraction.

DLS is typically used to quantify the relative intensity of monomers in solution compared to small oligomers and large aggregates. The 0.2- $\mu\text{m}$  filter was used to ensure the removal of large aggregates. DLS can determine whether the molecules in solution have a positive diffusion interaction parameter  $K_D$  (repulsive intermolecular behavior) or a negative  $K_D$  where intermolecular attraction forces dominate [22].

### **3.2.8 Size Exclusion Analysis**

Size exclusion analysis was performed by gel filtration chromatography using a TSKgel G3000SWXL column (7.8 mm ID x 30 cm, and particle size of 5  $\mu\text{m}$ ) made by Tosoh Bioscience (Grove City, OH). The column was installed on a high-performance liquid chromatography instrument (Agilent 1260 Infinity Quaternary LC) manufactured by Agilent Technologies (Santa Clara, CA). The mobile phase was 20 mM sodium phosphate buffer, pH 7.0 with 300 mM



ammonium sulfate. The column was equilibrated with the mobile phase for one hour before sample introduction. The mAb fractions were filtered with a 0.2-micron syringe filter and loaded into 1 ml sample vials. The HPLC was programmed and partitioned the analytes over a twenty-minute run.

### **3.2.9 MALDI Mass Spectrometry**

Matrix-Assisted Laser Desorption/Ionization Time-of-flight (MALDI-TOF) mass spectrometry was used to characterize size and charge variants in the mAb filtration fractions. This MALDI MS instrument was manufactured by Bruker (Billerica, MA). Virus filtration and prefiltration fractions of mAb B were desalted and reconstituted in DI water before MALDI MS. The advantage of using MALDI is rapid and direct ionization of mAbs in solution. mAb samples were either analyzed in the native state or after reducing the disulfide bonds with dithiothreitol (DTT).

For DTT-reduced mAb fractions, 20  $\mu$ L of 10 mM DTT was added to 100  $\mu$ L of mAb fraction at 2 g/L. Samples were heated to 95°C for ten minutes and incubated at room temperature for one hour. A centrifugal filter (10 kDa) was used to desalt the mixture and remove DTT before reconstituting in DI water for MALDI MS.

Sample preparation for mAb B involved desalting in DI water using a centrifugal filter and having a 1-2 g/L final concentration. MALDI technique involves pipetting 1-2  $\mu$ L of each mAb fraction on a MALDI target plate. 1  $\mu$ L of dihydroxybenzoic acid is pipetted on top of the sample to form a crystalline matrix for each fraction. The target plate is then inserted into a mass spectrometer for laser desorption ionization and time of flight spectrometric studies. With MALDI, we can observe the biomolecular components' intact masses and the charge of the

component. The MALDI technique does not decompose the samples and is deemed a soft ionization technique for obtaining intact sample molecules ions.

MALDI-MS was also used to characterize the glycoform distribution in the various filtration fractions. After deglycosylation and purification using the SCIEX procedure described in section 3.26, dihydroxybenzoic acid (DHB matrix) was used to co-crystallize the glycan samples (analyte) from mAb filtration fractions on the MALDI target plate. MALDI spectra were obtained for reduced and non-reduced mAb molecules as well as isolated glycans.

### **3.3 Virus Filtration and Prefiltration Results**

#### **3.3.1 BioEX Filtration of mAb B without Prefiltration**

The Planova BioEX virus filter was used to filter 5 g/L mAb B without prefiltration at pH 5, pH 7.5, and pH 8.6, respectively, with the earlier described formulation conditions. mAb B feed was filtered with a 0.2- $\mu\text{m}$  sterile filter, and this was standardized as a no-prefiltration case. The feed volume of mAb B to the BioEX filter was 90 ml (290 L/m<sup>2</sup>). The mAb was then filtered with a BioEX virus filter at a constant pressure of 45 psi. Figure 3.9 below shows the flux decay associated with mAb B filtration through the BioEX virus filter. The figures on the left plot throughput on the X-axis while the figures on the right plot time as the X-axis. The flux starts at a maximum value with ultrapure water filtration. The pre-use buffer flush follows the water flush. The flux data are stitched together for visual clarity. The flux across the BioEX filter remains high during buffer flush but rapidly decays at the onset of mAb filtration and recovers to varying degrees with buffer chase after mAb filtration. Protein recovery and mass balance for no prefiltration BioEX filtration at pH 5 with salt, pH 7.5 without salt, and pH 8.6 are shown in Table 3.2 below.

**Table 3.2:** Mass Balance/Protein Content for BioEX Filtration of mAb B without Prefiltration in 20 mM Sodium Acetate Buffer, pH 5 with Salt, pH 7.5 without Salt, and pH 8.6 with Salt.

BioEX, mAb B, pH 5, 200mM NaCl (no prefiltration)	Abs @ 280nm	Abs @ 280nm	Abs @ 280nm	Abs	Dilution factor	Conc. (mg/mL)	Volume (mL)
	1	2	3	Average			
mAb B fresh stock	0.916	0.906	0.909	0.9103	10	5.647	90
BioEX feed after 0.2um	0.894	0.897	0.895	0.8953	10	5.554	58
BioEX filtrate	0.802	0.806	0.806	0.8047	10	4.992	58
BioEX buffer chase	0.817	0.818	0.818	0.8177	2	1.014	15
pH 4 BioEX eluate (no salt)	0.021	0.02	0.02	0.0203	2	0.025	12
pH 9 BioEX eluate	0.007	0.007	0.007	0.0070	2	0.009	10

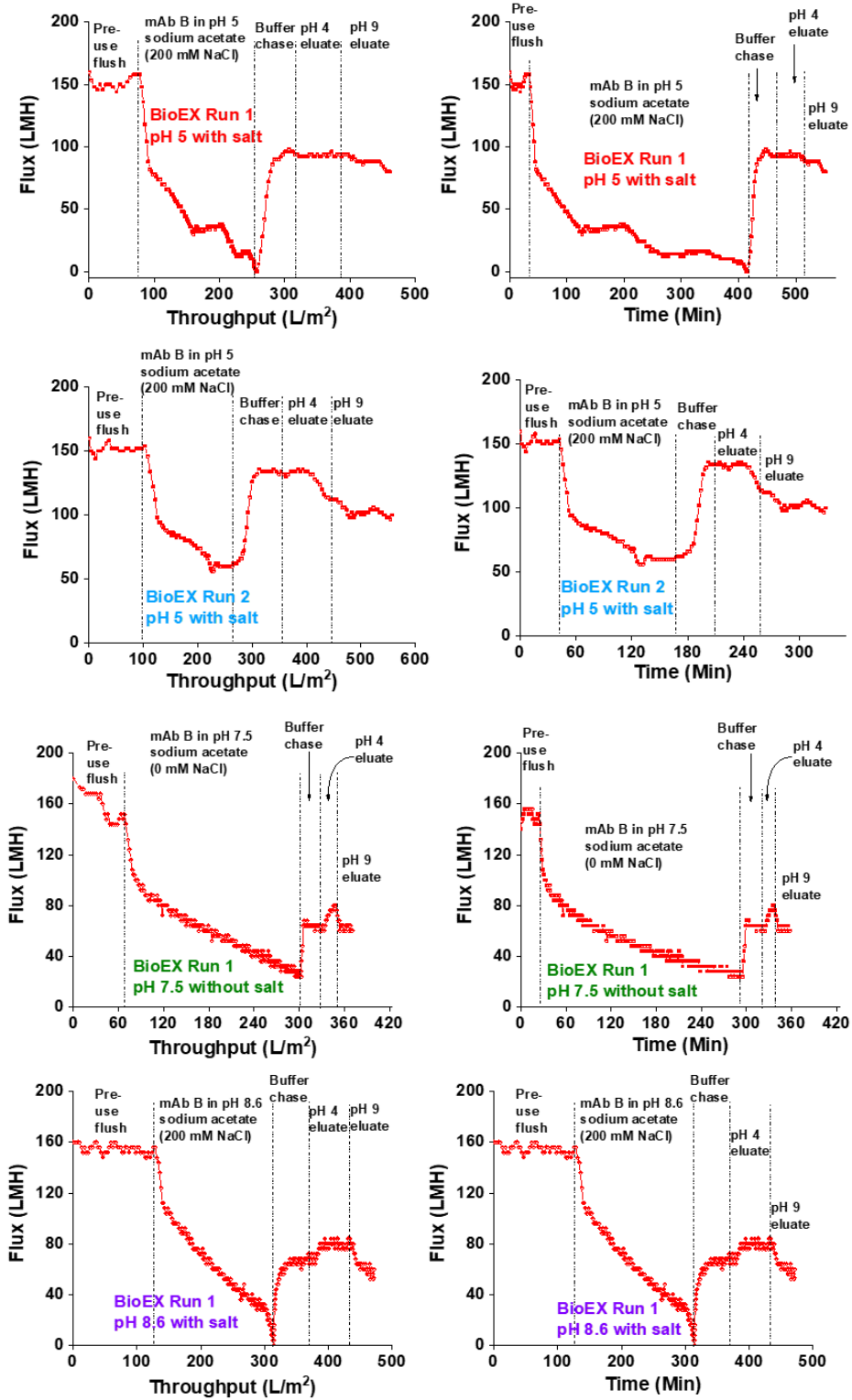
mAb Recovery % **94.743**

BioEX, mAb B, pH 7.5, no salt (no prefiltration)	Abs @ 280nm	Abs @ 280nm	Abs @ 280nm	Abs	Dilution factor	Conc. (mg/mL)	Volume (mL)
	1	2	3	Average			
mAb B fresh stock	0.85	0.848	0.849	0.8490	10	5.27	90
BioEX feed after 0.2um	0.809	0.807	0.808	0.8080	10	5.01	42
BioEX filtrate	0.76	0.762	0.761	0.7610	10	4.72	42
BioEX buffer chase	0.121	0.12	0.121	0.1207	5	0.37	10
pH 4 BioEX eluate (no salt)	0.012	0.012	0.013	0.0123	5	0.04	10
pH 9 BioEX eluate	0.004	0.004	0.005	0.0043	5	0.01	10
pH 4 BioEX eluate with salt	0.008	0.007	0.007	0.0073	1	0.005	11

mAb Recovery % **96.226**

BioEX, mAb B, pH 8.6, 200mM NaCl (no prefiltration)	Abs @ 280nm	Abs @ 280nm	Abs @ 280nm	Abs	Dilution factor	Conc. (mg/mL)	Volume (mL)
	1	2	3	Average			
mAb B fresh stock	0.956	0.95	0.952	0.9527	10	5.910	90
BioEX feed after 0.2um	0.931	0.928	0.93	0.9297	10	5.767	58
BioEX filtrate	0.871	0.87	0.872	0.8710	10	5.403	58
BioEX buffer chase	0.155	0.153	0.154	0.1540	5	0.478	20
pH 4 BioEX eluate (no salt)	0.02	0.019	0.019	0.0193	2	0.024	18
pH 9 BioEX eluate	0.007	0.007	0.008	0.0073	2	0.009	15

mAb Recovery % **96.731**



**Figure 3.9:** BioEX Filtration of 5 g/L mAb B in 20 mM Sodium Acetate, pH 5 with Salt, pH 7.5 without Salt, and pH 8.6 with Salt.

Flux decay is more apparent at pH 5 and 8.6 than at pH 7.5. The flux decay is less decremental at pH 7.5 without salt than at pH 5 with salt. In all three pH conditions, the BioEX filter loses over 80 percent of the initial flux while delivering a throughput of less than 290 L/m<sup>2</sup> that was sterile filtered at the beginning of virus filtration. The mAb is net positively charged at pH 5 and net negatively charged at pH 8.6. Run 2 BioEX filtration involved the permeate from pH 5 run 1 BioEX filtration introduced into a second BioEX filter. Run 2 shows reduced fouling because a portion of the principally fouling species was captured in virus filter run 1. Table 3.3 below summarizes BioEX runs 1 and 2.

**Table 3.3:** mAb B Filtration Parameters for BioEX Runs 1 and 2 without Prefiltration.

EXPERIMENT	Flow parameters across BioEX filter in sequential order							Objectives
	DI water	Pre-use flush pH 5 Sodium acetate (200mM NaCl)	mAb B in pH 5 Sodium acetate (200mM NaCl)	Buffer chase pH 5 Sodium acetate (200mM NaCl)	Elution buffer pH 4 (no salt)	Elution buffer pH 4 with 200mM NaCl	Elution buffer pH 9 (no salt)	
<b>Install new BioEX filter (Run 1)</b> (Complete fouling occurs but recovers with buffer chase to ~ 50% initial flux)	0 g/L 10 mL ~ 130 LMH	0 g/L 10 mL ~ 150 LMH	5.0 g/L 57.6 mL ~ 80 LMH - 0 LMH	1.1 g/L 20 mL ~ 70 LMH	N/A	37 mg/L 20 mL ~ 75 LMH	13 mg/L 20 mL ~ 70 LMH	To perform filtration of mAb B with no prefiltration.
<b>Install new BioEX filter (Run 2)</b> (Feed => filtrate from run 1 BioEX) Partial fouling of filter occurs (~ 80% flux recovery with buffer chase)	0 g/L 10 mL ~ 130 LMH	0 g/L 10 mL ~ 150 LMH	4.76 g/L 55 mL ~ 70 LMH	0.94 g/L 20 mL ~ 120 LMH	N/A	140 mg/L 20 mL ~ 110 LMH	70 mg/L 20 mL ~ 105 LMH	To perform filtration of mAb B filtrate collected from run 1.
<b>Second rinse of BioEX Run 1 filter</b> (~ 60% initial flux recovery with elution buffers)	0 g/L 10 mL ~ 90 LMH	0 g/L 10 mL ~ 90 LMH	N/A	N/A	19 mg/L 20 mL ~ 95 LMH	N/A	12 mg/L 20 mL ~ 75 LMH	To evaluate flux recovery of fouled BioEX run 1 filter using pH swings and ionic strength differences.
<b>Second rinse of BioEX Run 2 filter</b> (~ 90% initial flux recovery with elution buffers)	0 g/L 10 mL ~ 135 LMH	0 g/L 10 mL ~ 135 LMH	N/A	N/A	0 mg/L 20 mL ~ 135 LMH	N/A	4 mg/L 20 mL ~ 110 LMH	To evaluate flux recovery of previously fouled BioEX run 2 filter using pH swings and ionic strength differences.

The application of buffer flush post-mAb filtration results in the flux recovery on the fouled BioEX filter in all conditions. This points to the reversibility of the virus filter fouling as blocked pores become unblocked due to the resolubilization and release by desorption of aggregated biomolecules into filterable molecules. This observation was also reported by Bieberbach et al. [20]. Concentration polarization of mAbs within the virus filter induces localized regions of high mAb concentration on the virus filtration membrane leading to the formation of soluble aggregates that foul the membrane [23]. Soluble aggregates are held by weak non-covalent bonds that can be disrupted into the monomeric form upon mAb dilution by the buffer chase [20].

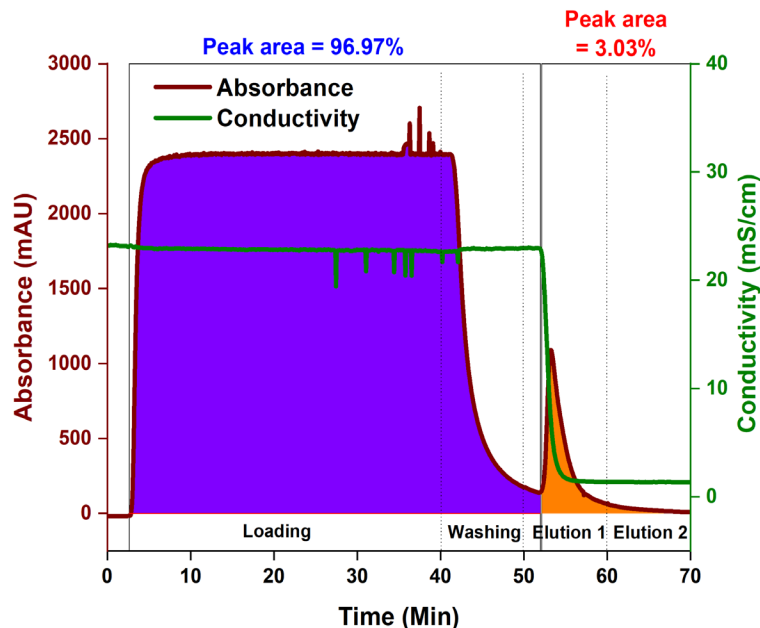
### **3.3.2 Size Exclusion-Based Prefiltration of mAb B**

The 0.2- $\mu\text{m}$ , 0.1- $\mu\text{m}$ , and Planova 75-N were used as prefilters but did not improve BioEX flux (over 70 percent flux decay) seen in the virus filtration flux data. The bottle-top 0.2- $\mu\text{m}$  and 0.1- $\mu\text{m}$  size exclusion-based sterile filters were used as prefilters. Since they are size exclusion filters, no attempt was made to elute species that may be ‘bound’ to the membrane surface. The Planova 75N is typically used as a retrovirus filter and was adopted as a ‘prefilter’ for this work. The Planova 75N was operated from a pressure vessel. Since the Planova 75N is a size exclusion filter, no attempt was made to elute ‘adsorbed’ species from the membrane. BioEX flux after size-exclusion prefilters will be shown in subsequent sections.

### **3.3.3 HIC Prefiltration of mAb B**

HIC prefiltration of pH 5 mAb B in 20 mM sodium acetate with 200 mM NaCl resulted in the chromatogram shown in Figure 3.10 below. Results for the two other pH values are in

Appendix A. A 3 ml Sartobind phenyl membrane adsorber was installed on the FPLC and used as a HIC prefilter.

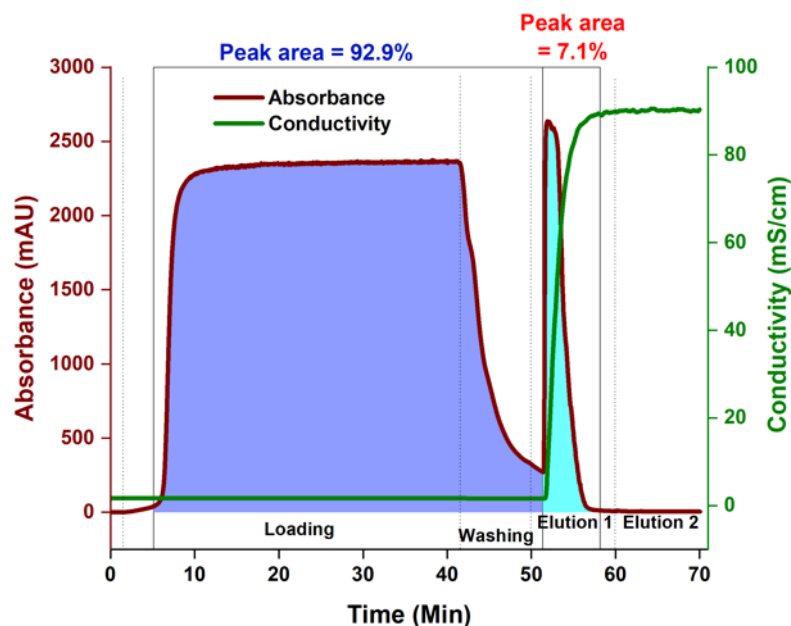


**Figure 3.10:** Chromatogram for HIC Prefiltration of mAb B at pH 5 with 200mM NaCl

Figure 3.10 shows a broad peak representing the mAb flowthrough fraction and a small elution peak indicating the foulants that were removed by the HIC prefilter. UV absorbance measurement at a wavelength of 280 nm was used to perform a mass balance of the fractions, and over 95% mAb recovery was obtained. These fractions were collected and characterized to obtain molecular-level details about the mAb species in each fraction. The flowthrough fraction was filtered through a BioEX virus filter.

### 3.3.4 IEX-S Prefiltration of mAb B

IEX-S prefiltration of pH 5 mAb B in 20 mM sodium acetate with 200 mM NaCl resulted in the chromatogram shown in Figure 3.11 below. Prefiltration chromatograms for the pH 7.5 without salt condition and pH 8.6 with salt are shown in Appendix A.



**Figure 3.11:** Chromatogram for IEX-S Prefiltration of mAb B at pH 5 with 200 mM NaCl

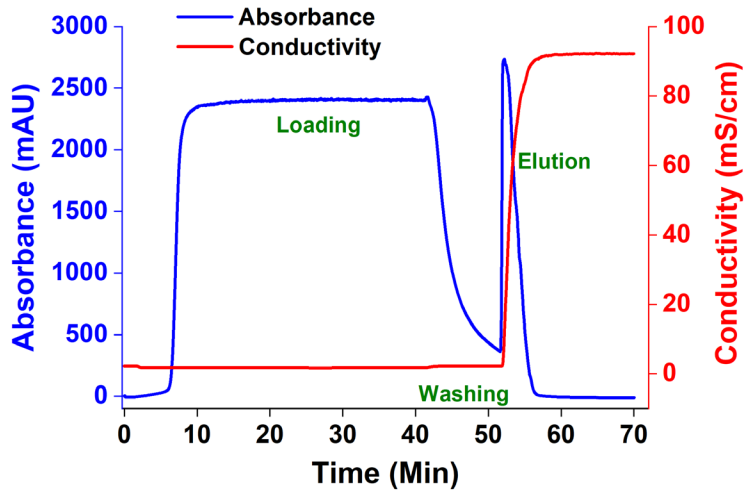
Figure 3.11 shows a broad peak representing the mAb flowthrough fraction and a clearly defined elution peak representing potential foulants that were removed by the cation exchange (IEX-S) prefilter. The presence of 200 mM NaCl prevents all the positively charged mAbs at pH 5 from binding to the negatively charged IEX-S prefilter. Mass balance and protein recovery were performed using UV absorbance measurements at 280 nm, and over 95 percent recovery was obtained.

### 3.3.5 IEX-Q Prefiltration of mAb B

The IEX-Q chromatogram of mAb B at pH 5 with salt did not show an elution peak, as seen in Appendix A. The chromatogram for IEX-Q prefiltration at pH 8.6 with salt showed a small elution peak (also in Appendix A). IEX-Q prefiltration of mAb B in pH 7.5, 20 mM



sodium acetate buffer without salt resulted in the chromatogram shown in Figure 3.12 below.



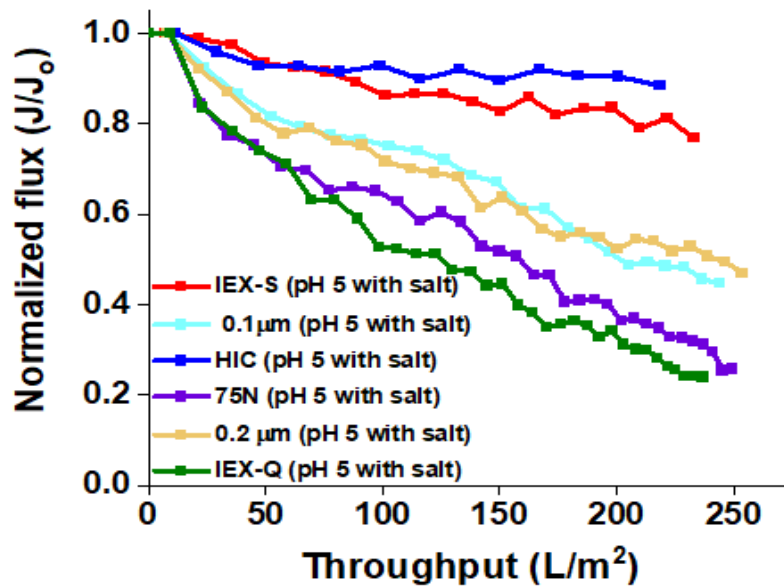
**Figure 3.12:** Chromatogram for IEX-Q Prefiltration of mAb B at pH 7.5 without Salt

IEX-Q prefiltration of mAb B using a Sartobind Q membrane adsorber effectively removes fouling species that can cause flux decay in the BioEX virus filter at pH 7.5 without salt. The absence of salt at pH 7.5 enabled proper capture of foulant species by the positively charged IEX-Q ligand.

### 3.3.6 Composite BioEX flux data for mAb B in different buffer conditions with IEX-Q, IEX-S, HIC, and Size-Based Prefilters

Adsorptive prefiltration of 5 g/L mAb B in the corresponding buffers was performed with the HIC, IEX-S, and IEX-Q membrane adsorbers in the flowthrough mode at three pH conditions (5.0, 7.5, and 8.6) described in section 3.2 earlier. BioEX virus filtration was then performed with the prefilter flowthrough fractions. 90 ml of feed mAb was loaded to the prefilter, and 80 ml of prefilter flowthrough was loaded to the BioEX filter after prefiltration. Figure 3.13 below shows the normalized flux values for the BioEX virus filter after prefiltration at pH 5 with the

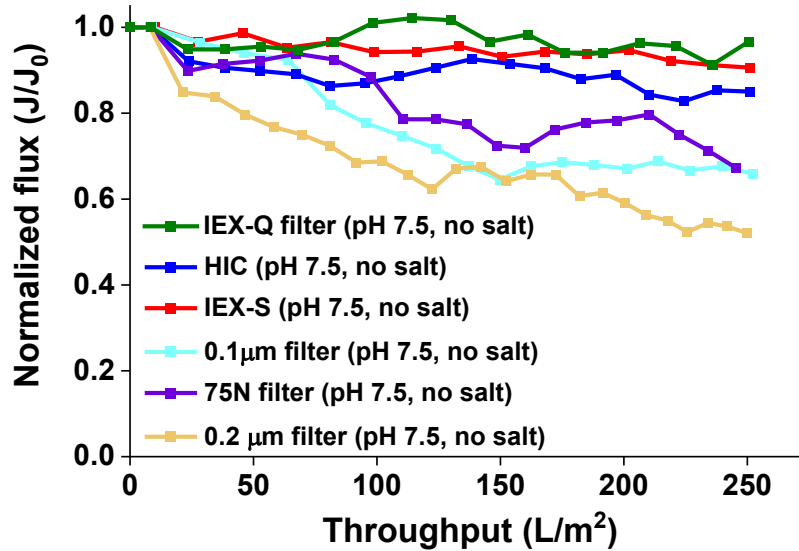
various modes of prefilters.



**Figure 3.13:** mAb B Flux through a BioEX Filter after Prefiltration (pH 5 with 200mM NaCl)

Figure 3.13 shows that size exclusion-based prefilters do not improve BioEX filter flux and are ineffective in foulant capture. The 0.2- $\mu\text{m}$ , 0.1- $\mu\text{m}$ , and 75N prefilters resulted in over 50 percent BioEX flux decay over 250 L/m<sup>2</sup> of feed mAb B (5 g/L in 20 mM sodium acetate buffer, at corresponding buffer condition). Conversely, the HIC membrane adsorber (prefilter) showed the best improvement of mAb B flux through the BioEX filter at pH 5 with less than 10 percent flux decay over 250 L/m<sup>2</sup> of feed. Referring to the earlier chromatograms in Figures 3.10 and 3.11, the HIC with a smaller elution peak area performed better than the IEX-S prefilter with double the HIC's elution peak area. The HIC membrane adsorber shows improved foulant removal (mAb charge variants and denatured mAbs) than other adsorptive and size-based prefilters in 20 mM sodium acetate, pH 5 with salt.

Figure 3.13 shows that the IEX-S prefilter performs well at pH 5 for mAb prefiltration with less than 20 percent flux decay over a mAb throughput of  $\sim 250 \text{ L/m}^2$ . The adsorptive anion exchange prefilter (IEX-Q) did not prevent flux decay at pH 5. mAb B is overwhelmingly positively charged at pH 5 and may not bind the positively-charged IEX-Q ligands. The net charge ( $\pm z$ ) of mAbs changes with buffer pH due to acid-base protonation/deprotonation events on surface-exposed chemical moieties of the mAb [24-26]. Figure 3.14 below shows the normalized flux values for the BioEX virus filter after prefiltration at pH 7.5 with the various modes of prefilters.

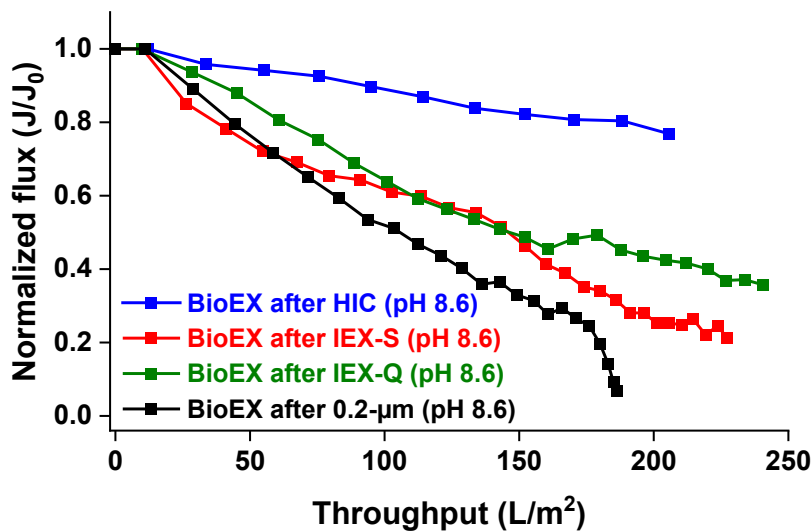


**Figure 3.14:** mAb B Flux through BioEX Filter after Prefiltration (pH 7.5 no Salt, Except for HIC where 200 mM NaCl is Required for Hydrophobic Interaction Chromatography)

Figure 3.14 shows that size exclusion-based prefilters do not perform well at pH 7.5. the ion exchange (IEX-Q and IEX-S) and the hydrophobic interaction chromatography (HIC) prefilters improve mAb flux through the BioEX filter at pH 7.5. HIC adsorptive prefilters cannot function effectively without high conductivity buffers. HIC, IEX-S, and IEX-Q membrane

adsorbers all had steady mAb flux with about ten percent flux decay over 250 L/m<sup>2</sup> of mAb. All three adsorptive prefilters effectively captured principal foulants of the virus filter at pH 7.5.

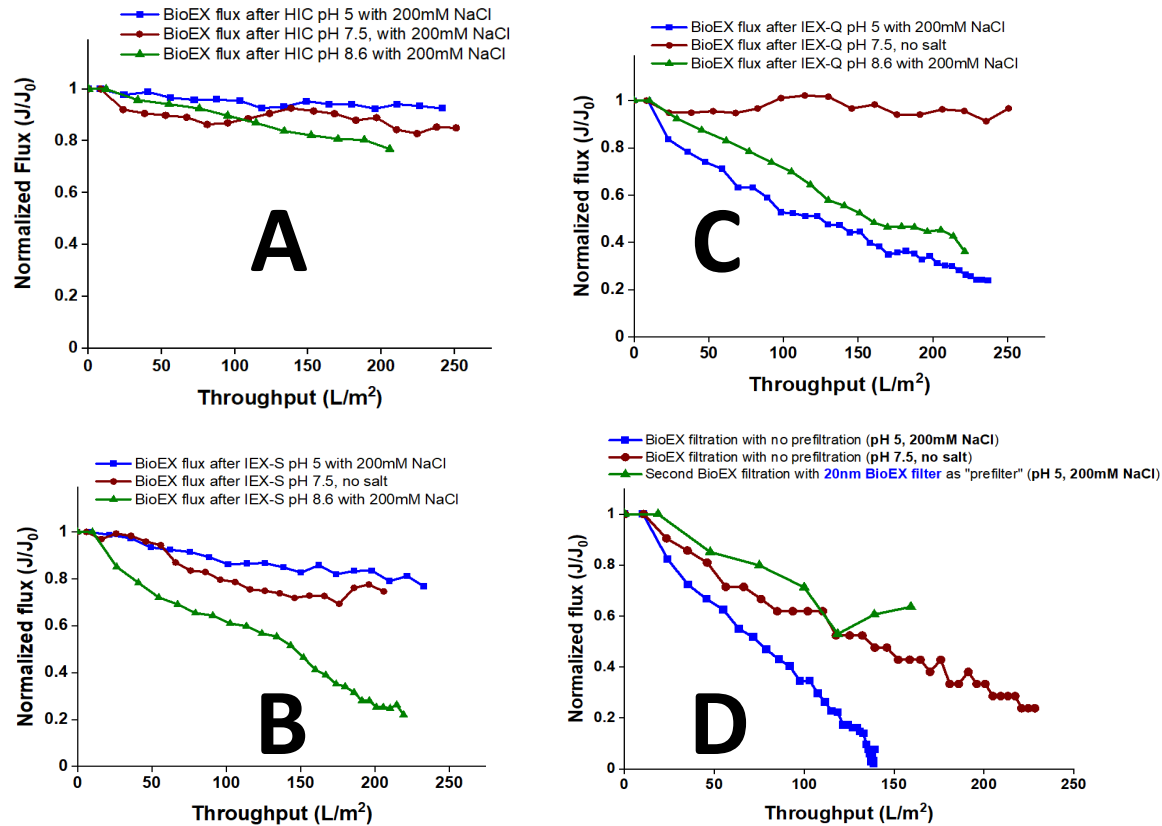
Figure 3.15 below shows the normalized flux values for the BioEX virus filter after prefiltration of mAb B in pH 8.6 sodium acetate with salt using adsorptive prefilters and 0.2-  $\mu$ m sterile filter.



**Figure 3.15:** mAb B Flux through the BioEX Filter after Prefiltration with Different Prefilters (pH 8.6 Buffer with 200 mM NaCl)

All adsorptive prefilters typically capture mAb aggregates. The HIC prefilter preferentially adsorbs denatured monomeric variants, oligomers with increased hydrophobicity, and post-translationally modified mAb variants.

Figure 3.16 below shows mAb B flux through the BioEX filter sorted according to prefilter type at different buffer conditions.



**Figure 3.16:** Composite Figure for mAb B Flux at pH 5 with Salt, pH 7.5 without Salt, and pH 8.6 with Salt through the BioEX Filter According to Prefilter Mechanisms (A) HIC. (B) IEX-S. (C) IEX-Q. (D) No Prefiltration.

Figure 3.16 shows that the presence of salt facilitates HIC prefilter performance. HIC prefiltration results in BioEX flux above 80 percent at pH 5 with salt, pH 7.5 with salt, and pH 8.6 with salt. IEX-S and IEX-Q prefilters do not perform well at pH 8.6, probably because salt does not favor electrostatic adsorption of biomolecules, and mAb B is unstable in pH 8.6 buffer (above pI of mAb B). IEX-Q prefilters do not perform well during prefiltration of mAb B at pH 5 and 8.6 in the presence of salt. Table 3.4 below summarizes the biophysical characteristics of ion exchange ligands and mAb variants at pH 5, 7.5, and 8.6, respectively.

**Table 3.4:** Net Charge of mAb Variants at pH 5, 7.5, and 8.6 and Suggested Membrane Adsorbers Based on Virus Filtration and Prefiltration Studies

	Net charge in pH 5, 20 mM sodium acetate with salt	Net charge in pH 7.5, 20 mM sodium acetate without salt	Net charge in pH 8.6, 20 mM sodium acetate with salt
<b>Sartobind S ligand (SO<sub>3</sub><sup>-</sup>)</b>	Negative	Negative	Negative
<b>Sartobind Q ligand (NH<sub>4</sub><sup>+</sup>)</b>	Positive	Positive	Positive
<b>Acidic variant (pI ~ 7.1)</b>	Positively charged (+)	Negatively charged	Negatively charged (- -)
<b>Main variant (pI ~ 7.5)</b>	Positively charged (+ +)	Almost zero	Negatively charged (- -)
<b>Basic variant (pI ~ 8.0)</b>	Positively charged (+ + +)	Positively charged	Negatively charged (-)
	Preferred ligand in pH 5, 20 mM sodium acetate with salt	Preferred ligand in pH 7.5, 20 mM sodium acetate without salt	Preferred ligand in pH 8.6, 20 mM sodium acetate with salt
<b>Acidic variant <i>mainly binds to</i></b>	HIC, Sartobind S	HIC, Sartobind Q	HIC, Sartobind Q
<b>Main variant <i>mainly binds to</i></b>	HIC, Sartobind S	HIC, Sartobind S and Q equally	HIC, Sartobind Q
<b>Basic variant <i>mainly binds to</i></b>	HIC, Sartobind S	HIC, Sartobind S	HIC, Sartobind Q
<b>Effective prefilter for mAb B at pH 5, 7.5 and 8.6 respectively</b>	HIC > Sartobind S only (Sartobind Q is very poor)	Sartobind Q > HIC > Sartobind S (All perform well in decreasing order)	HIC only (Sartobind S and Q didn't improve flux)

Table 3.4 shows that Sartobind Q performs well at pH 7.5 without salt. Use of Sartobind Q at pH 7.5 results in the best BioEX flux behavior than other prefilter types. Acidic mAb variants may be a principal precursor of multimerization, denaturation, and BioEX fouling.

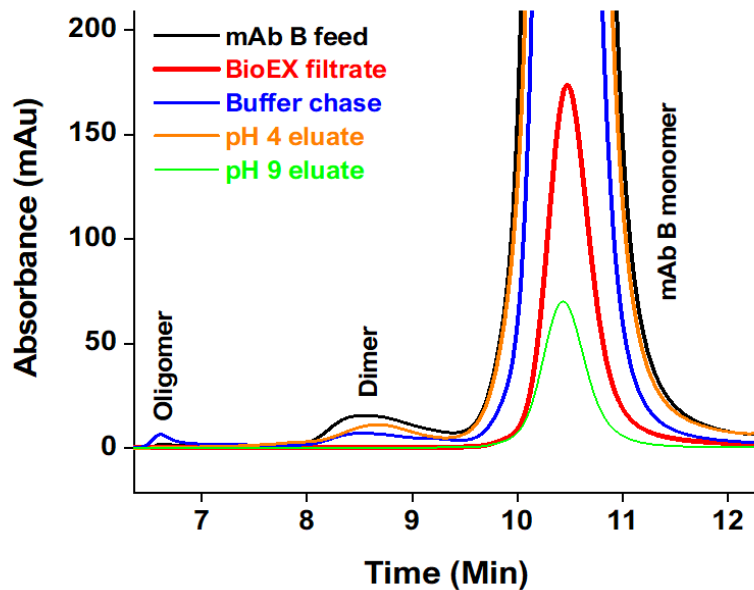
### 3.4 Dynamic Light Scattering (DLS) of mAb B Fractions in pH 5 Sodium Acetate with Salt

Particle size analysis of mAb B fractions was performed using dynamic light scattering. The results are shown in Figure F1 (appendix F) and represent the hydrodynamic diameter

distribution for mAb B HIC prefiltration, IEX-S prefiltration, and BioEX filtration fractions at pH 5 with salt, where IEX-Q was shown not to be effective.

### 3.5 Size Exclusion Chromatography Analysis of mAb B BioEX Filtration Fractions

A size exclusion chromatography (SEC) was used to perform a size-based analysis of BioEX filtration fractions of mAb B in pH 5 acetate buffer (200 mM NaCl) without prefiltration. pH 4 and pH 9 sodium acetate buffers were used to elute foulants from the fouled BioEX filter. All these fractions were characterized using SEC. The mobile phase (20 mM sodium phosphate buffer, pH 7.0 with 300 mM ammonium sulfate) was carefully selected to obtain proper peak resolution of the monomeric and multimeric forms, as shown in Figure 3.17 below.



**Figure 3.17:** SEC Spectra of mAb B BioEX Filtration Fractions

Figure 3.17 shows the presence of multimers in the buffer chase fraction, which can be due to reversible aggregates being washed out of the membrane to restore the virus filter flux. Dimers were present in significant amounts in the buffer chase, pH 4 eluate fraction, and mAb

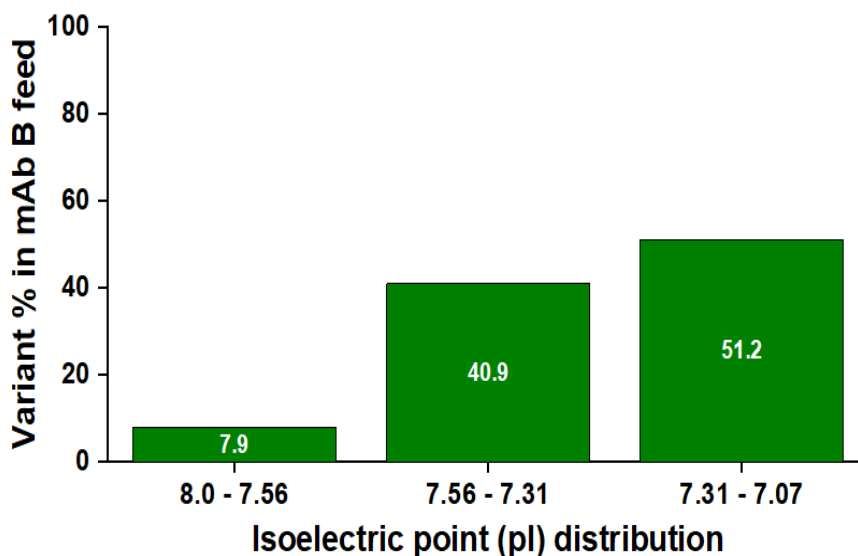
feed fraction without prefiltration. The BioEX filtrate has no dimer content due to the 20 nm cutoff of the virus filter. mAb monomers have a hydrodynamic diameter of around 11-12 nm. SEC characterization was also performed for HIC prefiltration and IEX-S prefiltration fractions, as shown in Appendix E. Overall, very little multimer content was observed in the fractions, reinforcing the reversibility of aggregated species. Supplementary SEC data is shown in Appendix E.

### **3.6 Capillary Electrophoresis Characterization of mAb B Fractions**

#### **3.6.1 Capillary Isoelectric Focusing (cIEF) Of mAb B Samples**

Biophysical property analysis of mAb B feed involves the determination and quantification of mAb B variants along the pI spectrum. The pH 7.5 condition was selected because mAb B is within its pI at pH 7.5 and, most notably, there is no salt present at pH 7.5. The PA 800 plus instrument does not tolerate 50 mM NaCl or more. Figure 3.18 shows the isoelectric point distribution ratio of acidic, main, and basic variants of mAb B in the feed sample as determined using capillary isoelectric focusing (cIEF) on the pharmaceutical analysis system.





**Figure 3.18:** Quantification of Peak Areas for cIEF Electropherogram of mAb B Feed at pH 7.5 without Salt

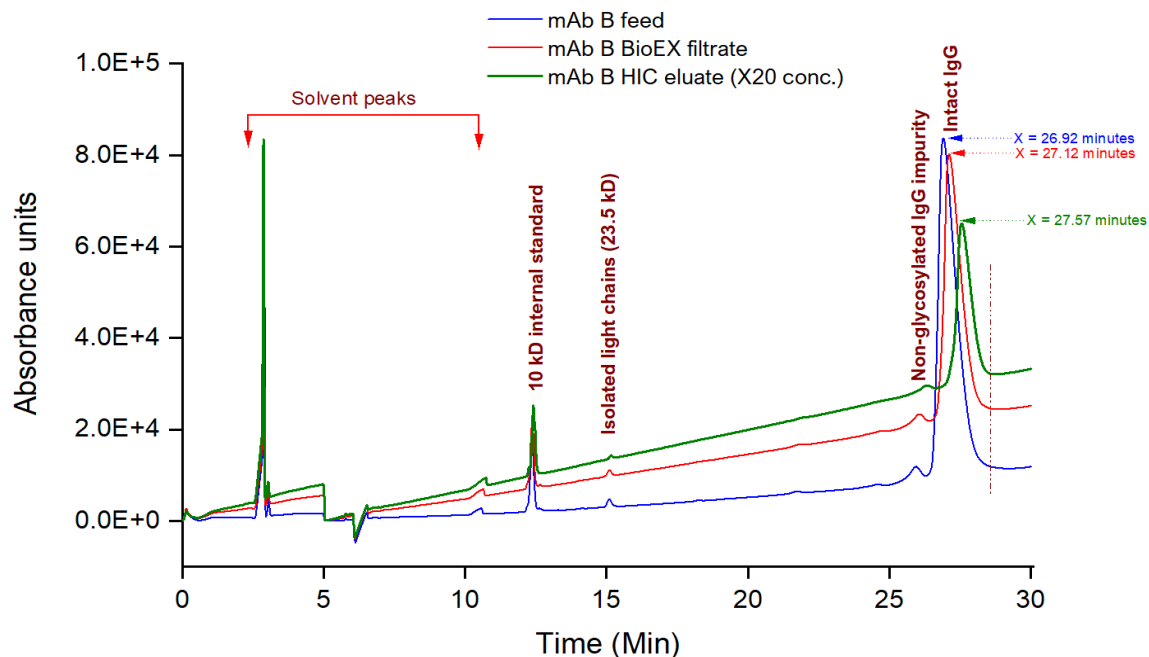
Microheterogeneity of mAbs due to post-translational modifications often results in changes in biophysical and biochemical properties such as isoelectric point [27-29], which is observed in the cIEF spectra of mAb B. Given the pI distribution in Figure 3.18, the central peaks are typically referred to as main or principal variant peaks with pI ranging from 7.3 - 7.6 [29]. mAb B variants with pI values below 7.3 are called acidic variants. Conversely, mAb B variants with pI above 7.6 are basic variants.

According to the cIEF spectra peak integrations and quantification, mAb B feed has 51.2 percent acidic variants, 40.9 percent main variants, and 7.9 percent basic variants.

### **3.6.2 Capillary Electrophoresis CE-SDS Analysis of mAb B Fractions Constituted in DI water after Desalting using Centrifugal Filters**

CE-SDS obtains the monomeric quality profile of a mAb sample in terms of product purity and size heterogeneity. CE-SDS was used to characterize the molecular components

present in mAb B fractions and the size variation of component peaks, as shown in Figure 3.19 below.



**Figure 3.19:** CE-SDS for mAb B Purity Analysis from Capillary Electrophoresis (PA800 Plus)

BioEX feed, permeate, and HIC eluate samples were selected and characterized as shown on the electropherograms in Figure 3.19. Small peaks of fragmented light chains were observed at 23.5 kDa. Small but unglycosylated mAb monomers preceded the large peaks for the mAb monomeric molecules [30]. The HIC eluate peak showed slightly higher peak retention times than the BioEX feed and permeate, further validating that monomeric mAb variants have microheterogeneity in size, charge, and hydrophobicity [31, 32]. The HIC prefilter preferentially captures hydrophobicity-induced mAb variants.

### 3.6.3 Capillary Zone Electrophoresis (Charge Variant Analysis) of mAb B Fractions

Bind-and-elute chromatography with gradient elution from a cation exchange column was used to partition charge variants of mAb B. mAb B was initially loaded on a Sartobind S

membrane adsorber in pH 5 sodium acetate without salt (buffer A), and an elution buffer B (pH 8.6 with salt). Gradient elution from pH 5 to 8.6 was too steep for a suitable peak resolution of the charge variants, and a working pH closer to buffer B's pH was selected. The Capto S (5 ml) impact column, a higher binding capacity cation exchange column, was selected for further work. Buffer A was optimized at pH 6.5, 20 mM sodium acetate without salt, while buffer B was 20 mM sodium acetate buffer, pH 8.6 with 200 mM NaCl. Gradient elution was optimized for better peak resolution and collection of elution fractions with charge variant partitioning.

Loading of 900 ml of 0.5 g/L mAb B in 20 mM sodium acetate buffer, pH 6.5 without salt, was performed on the FPLC at 1 ml/min. Fractions were eluted by gradient elution (from 0 percent buffer B to 100 percent buffer B in 100 minutes). The bind-and-elute chromatograms are shown in Appendix C. The elution fractions were prepared for charge variant analysis using the pharmaceutical analysis system. The electropherograms for each fraction were integrated according to acidic peak groups, main and basic peak groups, then quantified as shown in Table 3.5 below.

**Table 3.5:** Capillary Zone Electrophoresis Peak Analysis for Capto S Fractions of mAb B

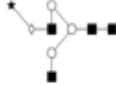
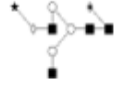
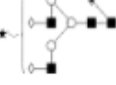

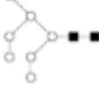
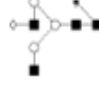


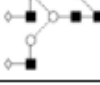
Capto S fractions	Basic charge variants	Dominant mAb isoform	Acidic charge variants
mAb B feed	13.9	41.6	44.5
Eluate fraction 2	15.1	55.1	29.8
Eluate fraction 3	15.7	55.1	33.2
Eluate fraction 4	13.9	42.3	43.8
Eluate fraction 5	10.1	37.5	52.4
Eluate fraction 6	10.7	36.6	52.7
Pooled eluate fractions	13.2	44.8	42

The acidic charge variants were 44.5 percent of the mAb feed and 29.8 percent of eluate fraction 2. The percentage of acidic variants increased from elution fractions 2 to elution fraction 6 and indicating that some acidic variants have a strong affinity to the cation exchange column. Buffer pH values below 7.0 would keep the mAbs positively charged and easily captured by cation exchange columns in bind-and-elute mode [32]. Sartobind S performed well as a prefilter for mAb B in pH 5 sodium acetate with salt. Low ionic strength buffers are also favored to prevent the competitive binding of buffer ions to the negatively charged cation exchange ligands. The percentages of main (dominant) mAb variants decreased from eluate fraction 2 to eluate fraction 6, which is the inverse trend of the acidic variants. Pooled eluate fractions had variant percentages, which closely tracked mAb variant percentages in the feed.

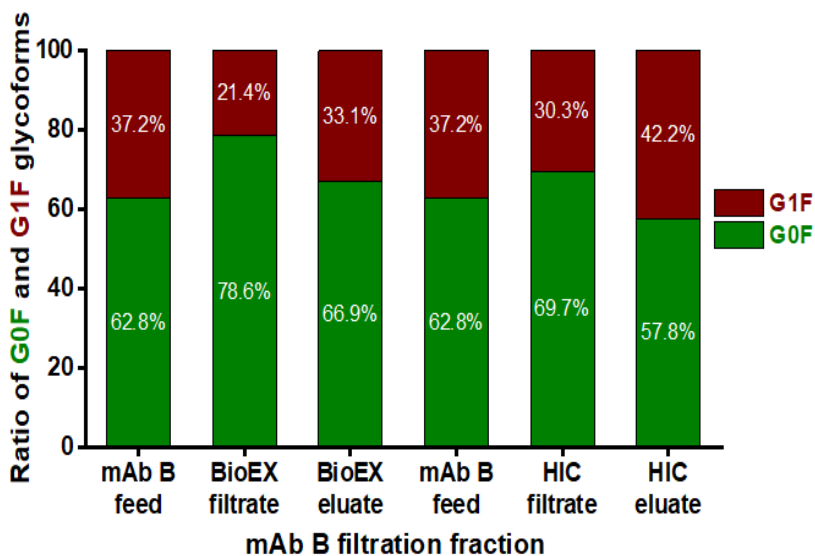
#### **3.6.4 Glycan Analysis of mAb B Fractions**

Filtration fractions were deglycosylated to characterize the glycan profile and distribution of glycoforms per filtration pool. BioEX filtration fractions of mAb B (pH 7.5 acetate buffer without salt) and without prefiltration were prepared for deglycosylation. The fractions were treated with sodium dodecyl sulfate, dithiothreitol (to reduce the disulfide bonds), and Triton X-100 before glycan cleavage by N-glycosidase F (PNGase F). A 10 kDa centrifugal filter was used to remove mAb fragments, while solid-phase extraction was used to purify the glycans removed from each mAb fraction for analysis using either MALDI-MS or capillary electrophoresis. Table 3.6 below shows the glycan structures.

**Table 3.6:** Characteristics of Glycans Identified in mAb B Fractions

<u>Annotations</u>	Glycan ID	Chemical Structure	Monoisotopic mass (g/mol)
Contains Sialic acid residue	A2(6)G1S1		1769.6
Contains Sialic acid residue	FA2(6)G1S1		1915.69
Contains Sialic acid residue	FA2G2S1		2077.75
<b>(G0F) Most abundant glycoform (least MW)</b>	FA2		1462.54
High mannose	M7 [D2]		1558.54
<b>G1F (Highest % increase from feed to eluate)</b>	FA2(6)G1		1624.6
	FA2(3)G1		1624.6
	A2BG2		1843.67
G2F	FA2G2		1786.65

The various glycans have differences in molecular mass, and depending on mAb glycoform, these introduce slight differences in molecular mass (size variants). Each mAb typically has only one glycan appended to each heavy chain on asparagine-297 (N-297). Glycan occupancy can thus be a determinant of mAb properties primarily in the case where a mAb may have no glycan appended or mono-glycosylated instead of two glycans per mAb. Figure 3.20 shows the glycan profile of mAb B fractions restricted to the two dominant glycoforms comprising over 90 percent of the glycans present.



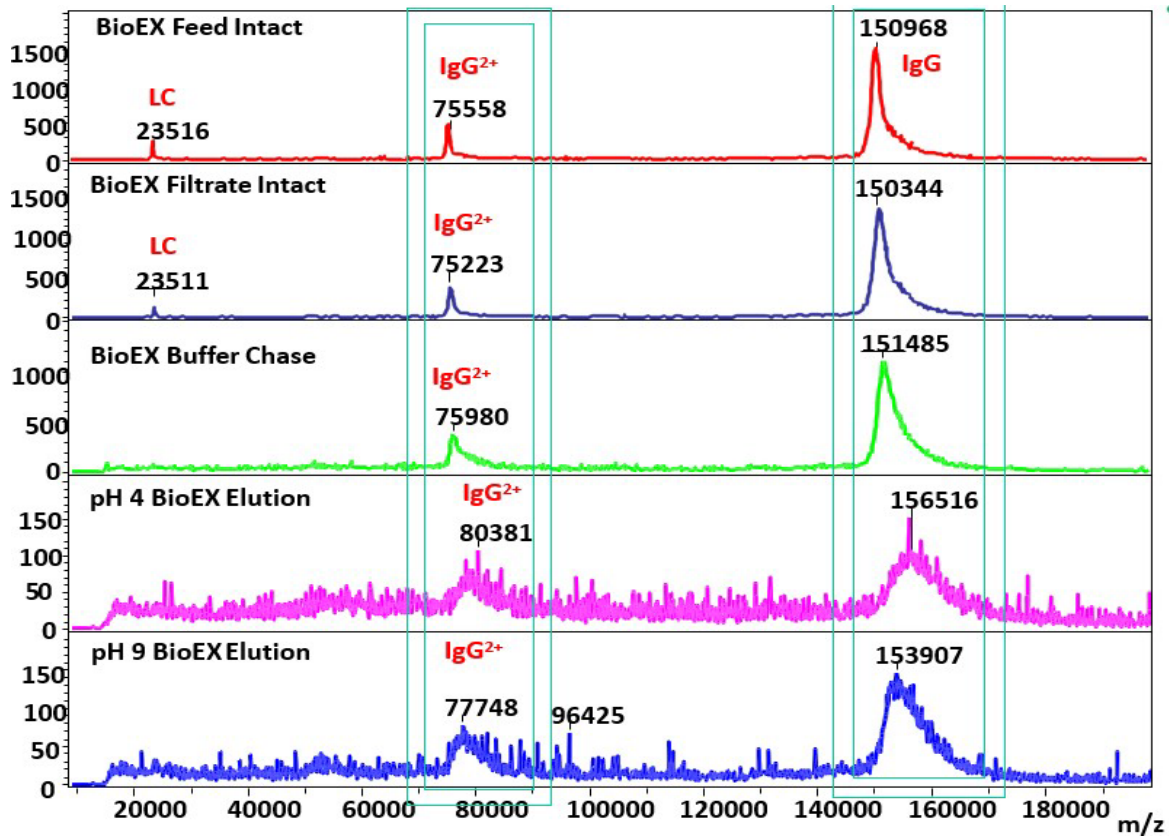
**Figure 3.20:** Glycan Analysis for Quantification of G0F and G1F Glycoforms per Filtration Fraction of mAb B (pH 7.5, 20 mM Sodium Acetate Buffer, without Salt)

The dominant glycoform (G0F) with a molecular weight of 1463 Da was highly represented in the BioEX filtrate, while the G1F glycoform with a molecular weight of 1625 Da was highly represented in the HIC eluate. The HIC eluate components are known to comprise the principal foulants of the virus filter, and it can be deduced that the G1F ratio is directly proportional to the fouling propensity of a mAb pool. G1F increases by 12 percent from the BioEX filtrate to the BioEX eluate and increases 12 percent from the HIC prefilter permeate to the HIC eluate. Conversely, G0F abundance is deduced to correlate with good behavior and filterability of a mAb pool across a virus filter. Future studies are required to evaluate the aggregation propensity of mAb monomers according to the glycovariant profile of each pool.

### 3.7 MALDI MS Analysis of mAb B Fractions

MALDI MS was performed on the various filtration fractions to evaluate the size heterogeneity of the mAb monomers in the filtration fractions, as shown in Figure 3.21 below.

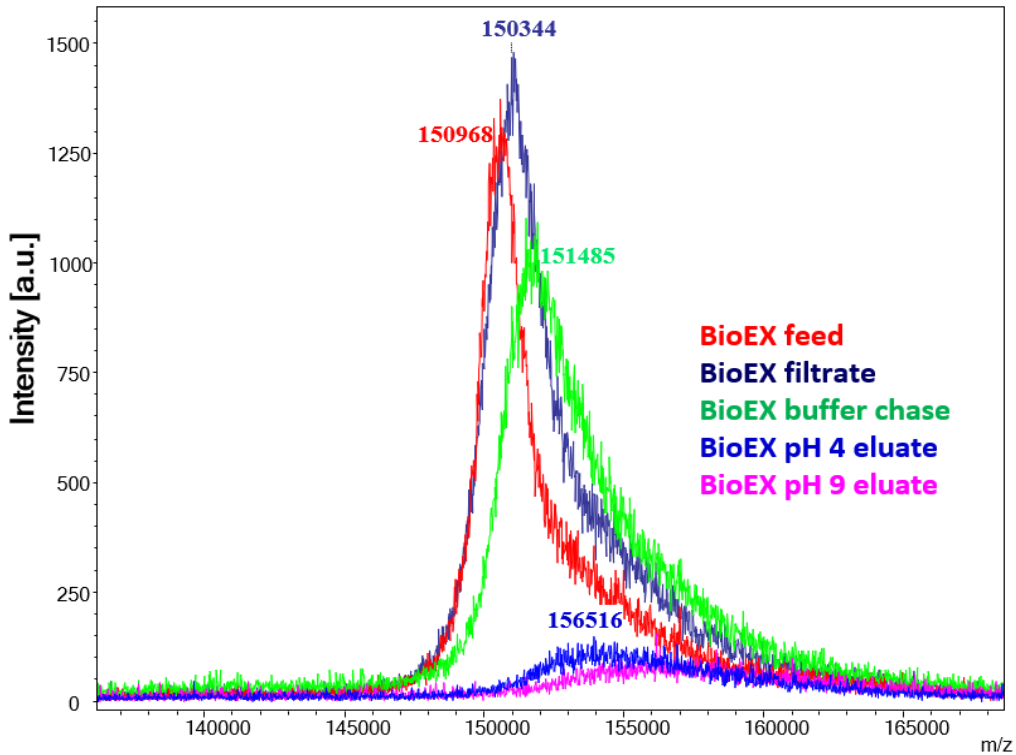
The mAb fractions were intact monomers because they were not reduced using (DTT). The eluate fractions were concentrated (x40) using a 10,000 Da MWCO centrifugal filter.



**Figure 3.21:** MALDI MS Spectra of mAb B BioEX Fractions without Prefiltration

The molecular weight of intact mAb B monomer in elution fractions pH 4 and 9 is significantly higher than the monomeric mAb B molecular weight in the BioEX feed and filtrate fractions. The monomeric peak for mAb B feed (150,968 Da) is centered ~600 Da higher than the BioEX filtrate. The buffer chase monomeric peak (151,485 Da) is centered ~1200 Da higher than the BioEX filtrate. The peak for pH 4 eluate is 5000 Da higher than the central peak position for the buffer chase. The pH 9 eluate peak is centered at ~153,907 Da, significantly higher than the feed and filtrate peaks, though with much lower intensity.

Double ionized forms of the mAb were observed within the 77,000 Da – 80,000 Da range. The principal fouling variants were enriched in the buffer chase and eluate fractions. They have higher molecular weights than the main isoform of mAb B in the feed. Figure 3.22 below shows a zoomed-in overlay plot for the monomeric variant peak per BioEX fraction.



**Figure 3.22:** Zoomed-in MALDI Spectra for Monomeric mAb B Peaks in BioEX Fractions

Figure 3.22 shows the relative peak intensities of fractions and peak width overlap at the higher molecular weight region (150,000 – 165,000 Da). This overlap around 165,000 Da shows that the higher molecular weight fractions are marginally enriched in the pH 4 and pH 9 buffer elution fractions and not artifacts of the buffer condition. MALDI mass spectrometry was performed for cation exchange (IEX-S) prefiltration fractions after desalting with a spin column, as shown in Figure 3.23 below. The zoomed-in inset occurs in the 150,000 Da region.



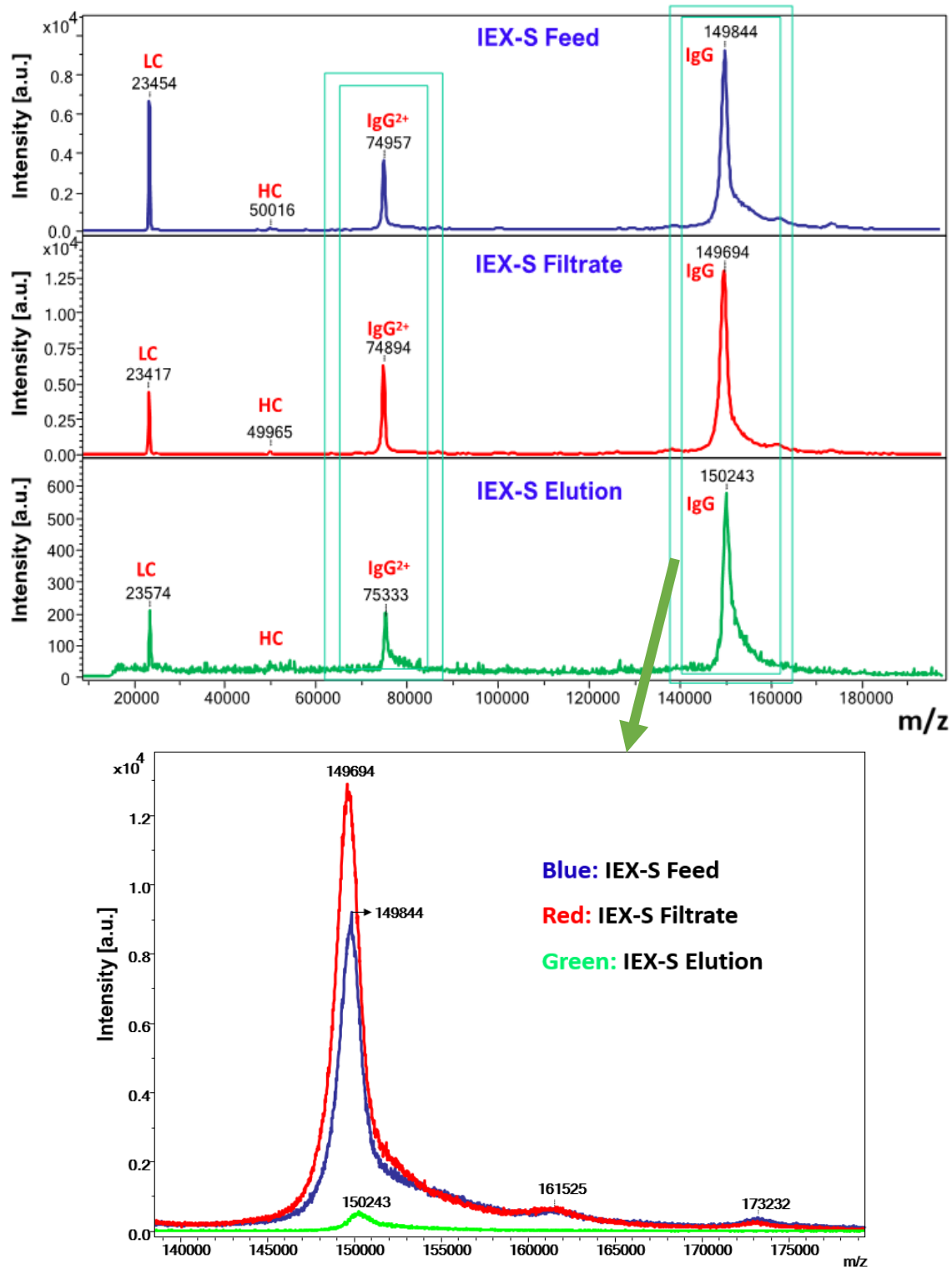


Figure 3.23: MALDI-MS Spectra for mAb B IEX-S Prefiltration Fractions (Inset at 150 kDa)

Consistent with the observations for the BioEX filtration fractions, the higher molecular weight monomeric variants are enriched in the IEX-S eluate fraction. The eluate peak is centered at 150.3 kDa, while the IEX-S permeate is centered at 149.7 kDa. The peak at 161.5 kDa is postulated to be a heavily glycosylated mAb B variant and is not visible in the eluate fraction because of the low eluate concentration. The peak at 173.2 kDa is postulated to be mAb B monomers (150 kDa) bound to isolated fragments of light chain (23.5 kDa).

MALDI MS analysis was performed for the HIC prefiltration fractions (feed, filtrate, and eluate) and mAb B feed (titrated to pH 4, 5, and 9) to understand whether pH variation introduces artifacts into MALDI spectra. The spectra are shown in Figure 3.24 below.

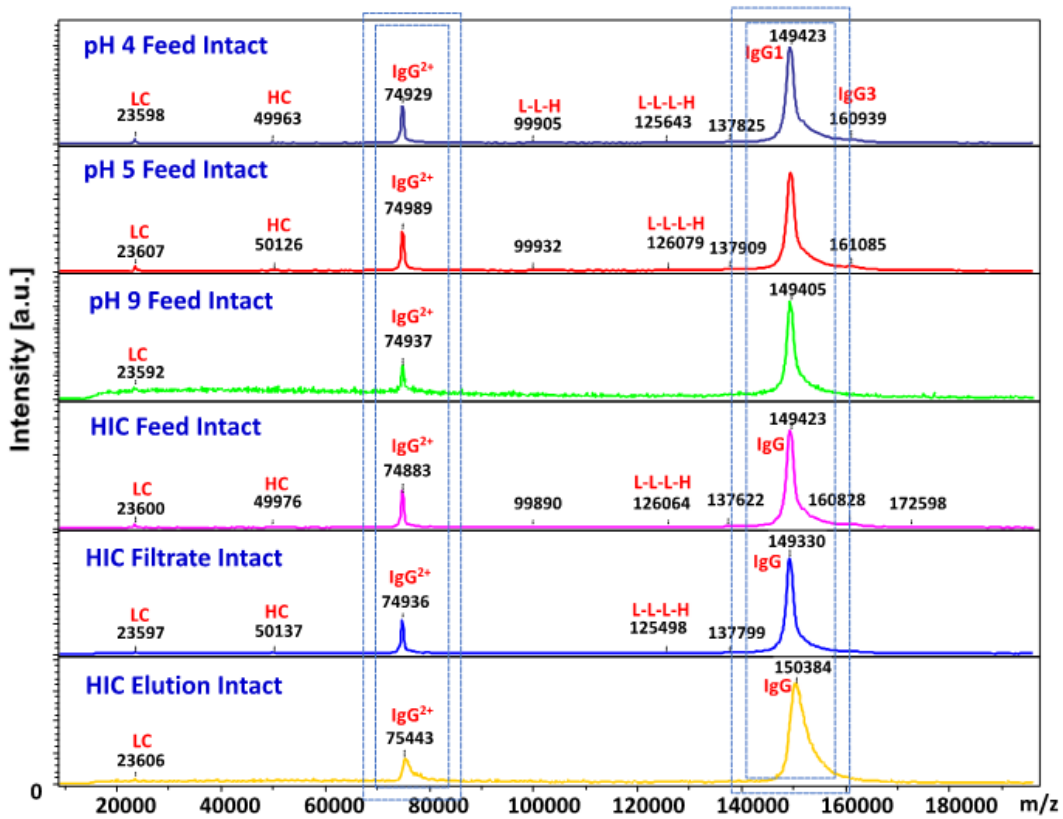
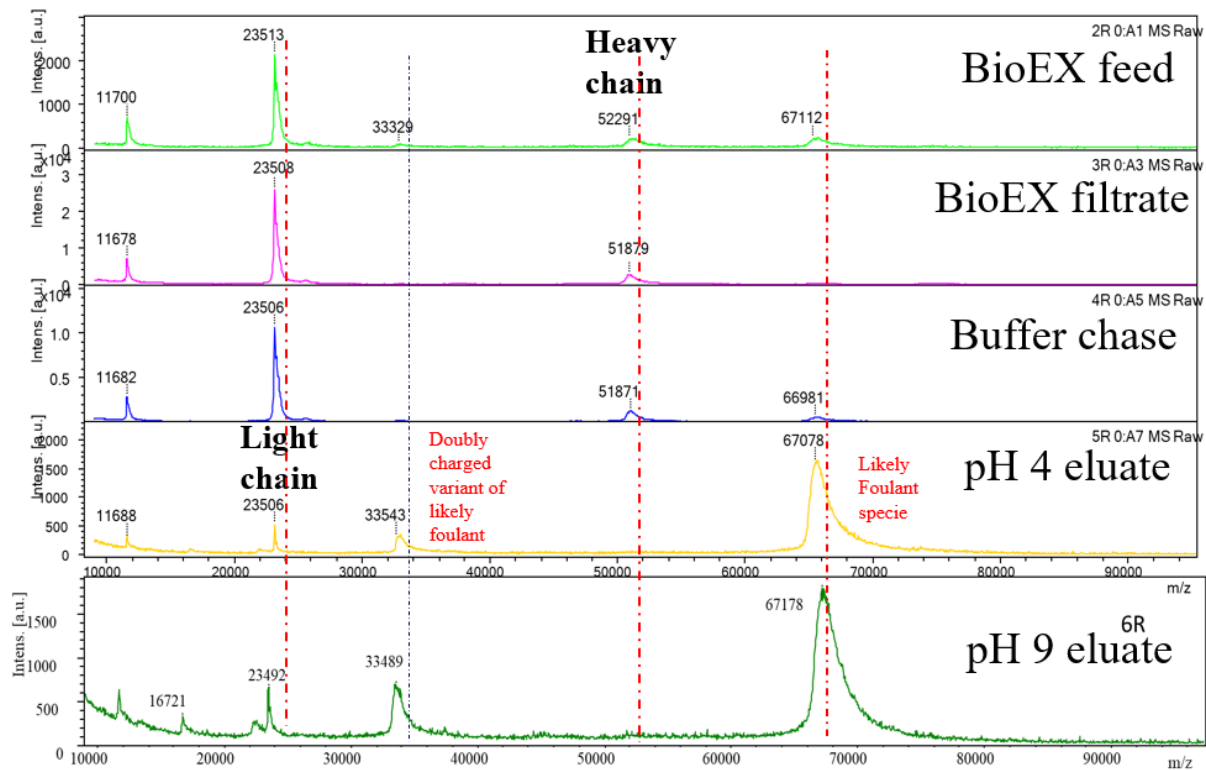


Figure 3.24: MALDI MS of HIC Prefiltration Fractions and mAb B Feed at Different pH

Figure 3.24 shows that between pH 4 and pH 9, mAb B monomer peaks are centered at 149,400 Da +/- 100 Da, and therefore, titration of mAb B feed to different pH values does not introduce size artifacts into the MALDI spectrum. This condition was evaluated since pH 4, and pH 9 eluates were at different pH conditions compared to the feed and permeate (filtrate) fractions. The HIC feed and filtrate fractions had a similar MW of 149400 Da +/- 100 Da, unlike the HIC eluate, which was enriched with a higher MW variant at 150,384 Da. The HIC eluate was at a much lower concentration than the feed and had to be concentrated (x40) using a centrifugal PES filter (10 kDa MWCO).

We also performed MALDI MS for mAb fractions after dithiothreitol reduction of the disulfide linkages joining the heavy and light chains of mAb B, as seen in Figure 3.25 below.

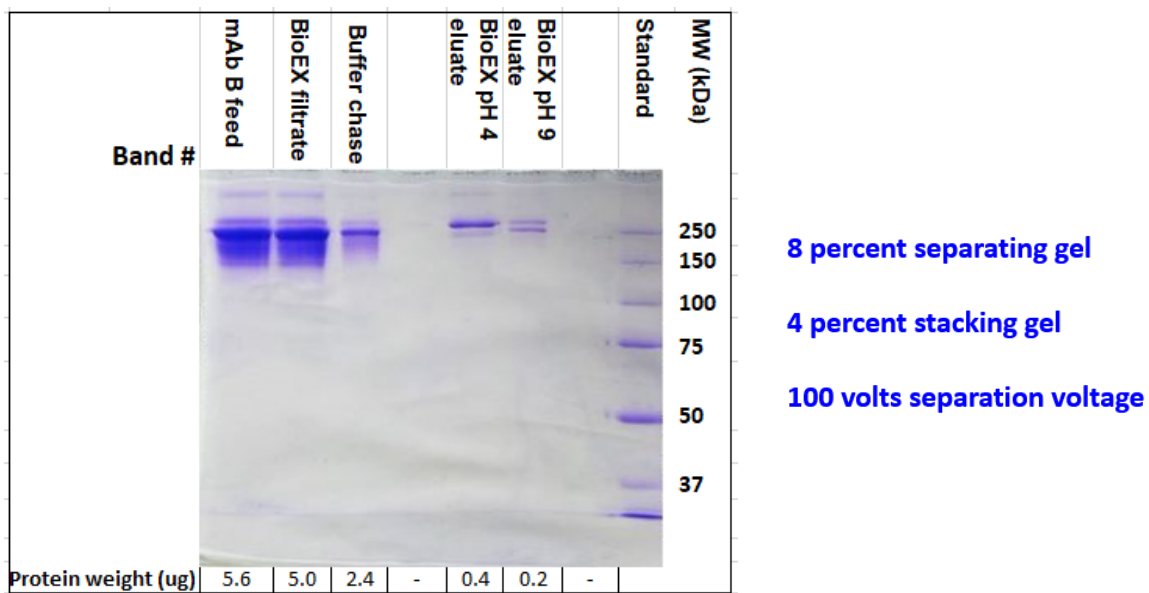


**Figure 3.25:** MALDI MS Spectra of DTT-reduced mAb B BioEX Filtration Fractions

Figure 3.25 shows the enrichment of a 67000 Da mAb fragment in the elution fractions at pH 4 and pH 9. This 67,000 Da peak is marginally present in the buffer chase fraction and not noticeable in the BioEX feed and filtrate fractions. It is hypothesized that this fragment is from a monomeric mAb variant after DTT reduction. Denatured variants have higher hydrophobicity and induce multimerization with subsequent fouling of virus filters.

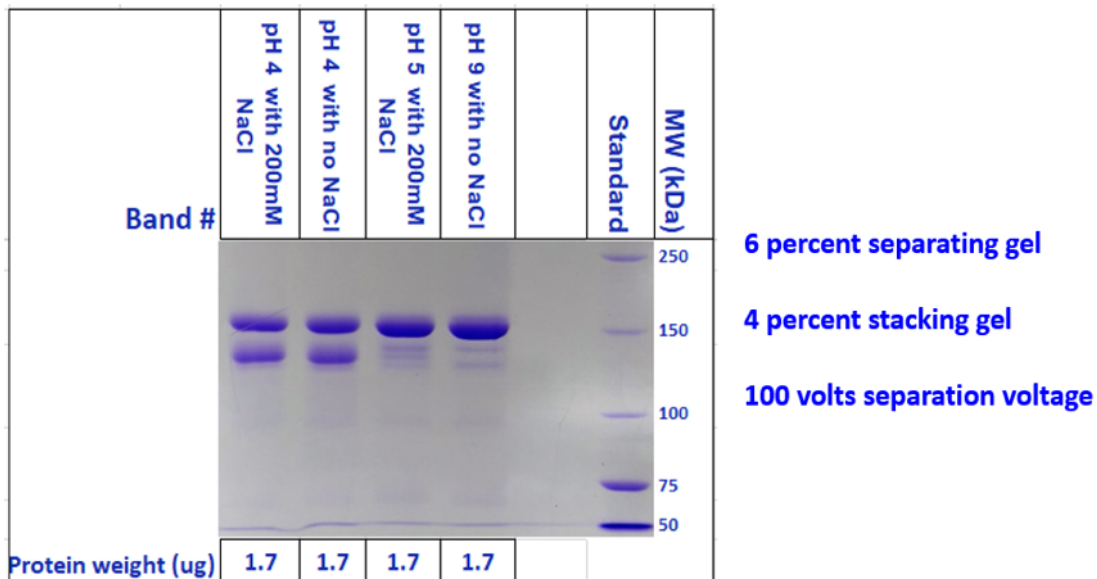
### 3.8 Sodium dodecyl sulfate (SDS) polyacrylamide gel electrophoresis (PAGE) analysis

Gel electrophoresis was used to analyze the monomeric size variation of mAb B filtration fractions. SDS PAGE is an electrochemical technique that ensures all the biomolecules present have the same mass/charge ratio and migrate in the same direction at different rates. The negatively charged sulfate groups on SDS impart a net negative charge to all analytes in the gel such that mAb migration from cathode to anode down the gel is based on molecular weight only. Figure 3.26 below shows the electrophoretogram for BioEX filtration fractions without prefiltration.



**Figure 3.26:** SDS PAGE of mAb B BioEX Filtration Fractions without Prefiltration

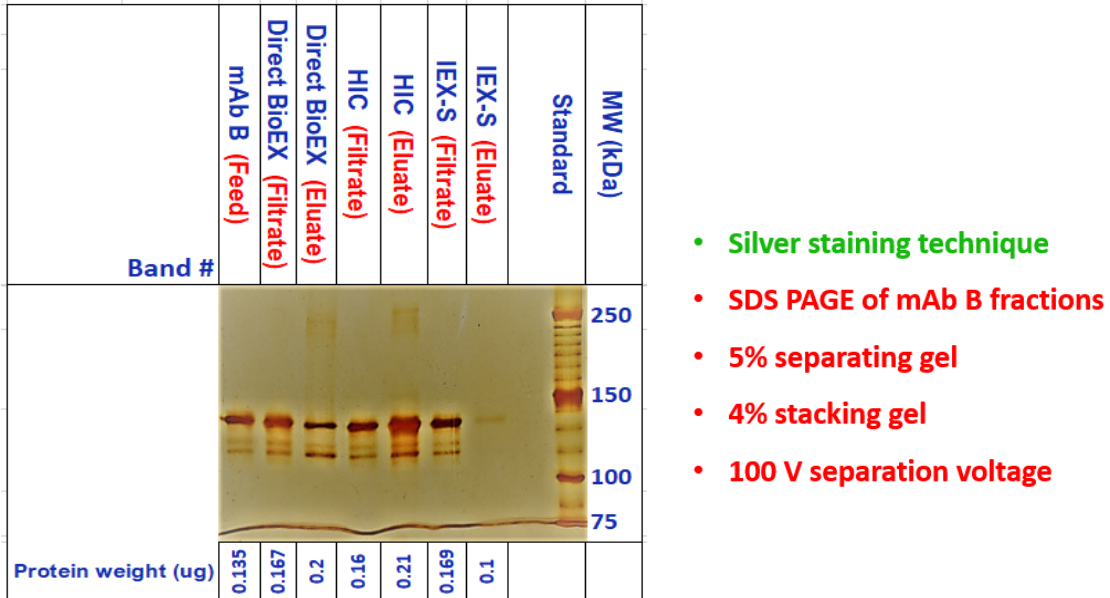
We performed SDS PAGE with non-reducing gel buffers, 8 percent polyacrylamide gel for the separating gel, and 4% for the stacking gel with a voltage of 100V. The non-reducing gel ensures that the mAb monomers do not break down into heavy (50 kDa) and light (25 kDa) chains. Consistent with the MALDI MS results, the elution fractions have a higher percentage of higher molecular weight mAb variants. The higher MW variants weighed between 151.5 kDa and 156 kDa. The main variant weighed between 149 and 150 kDa. Eight percent separating gel was discovered to be insufficiently porous for mAb B, and the gel porosity was increased by reducing the polyacrylamide percentage from 8 percent to 6 percent. In Figure 3.27 below, mAb B feed was incubated in different buffer pH and salt conditions before SDS PAGE to observe any attribute changes.



**Figure 3.27:** SDS PAGE of mAb B Feed Titrated to Different pH Values

Figure 3.27 shows that the presence or absence of salt at pH 4 did not significantly alter the mAb monomer bands. Between pH 5 and pH 9, there was no significant difference between the bands. SDS PAGE is not a sufficiently high-resolution technique for studying microheterogeneity in therapeutic proteins. Figure 3.28 below shows the SDS PAGE spectra for

BioEX, HIC, and IEX-S prefiltration fractions using the silver staining protocol for SDS PAGE gels.

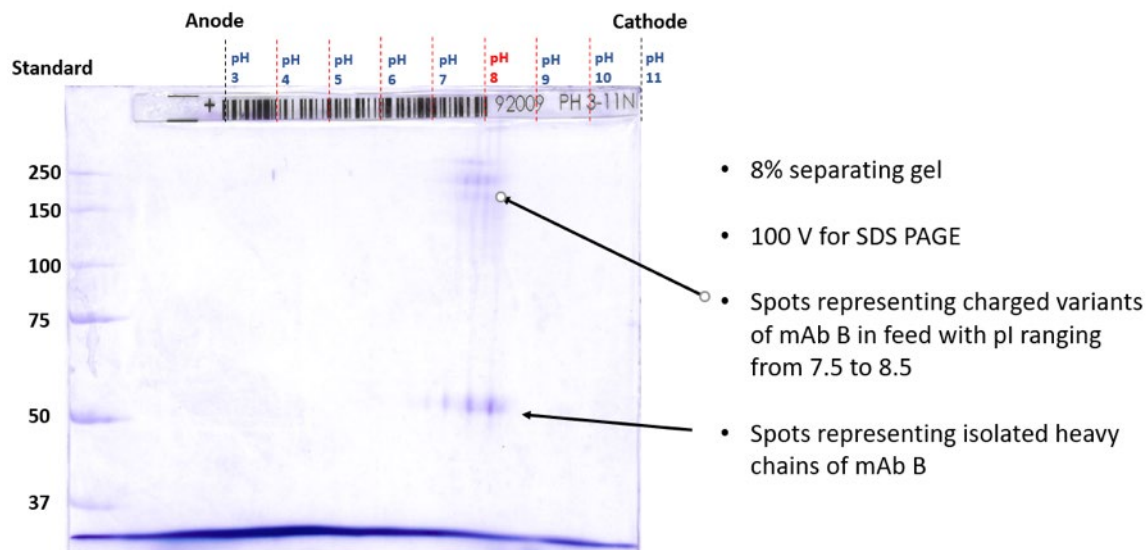


**Figure 3.28:** SDS PAGE of mAb B BioEX (No Prefiltration), HIC, and IEX-S Filtration Fractions

The silver staining gel technique obtained high-resolution electrophoretograms at low analyte loading. HIC eluate clearly showed an enrichment of the higher molecular weight monomeric band than the HIC filtrate. The IEX-S eluate showed a similar trend but was at a low concentration. The separating gel (5 percent polyacrylamide) was deduced to be more porous than desired; hence the mAb bands are slightly below 150 kDa.

2D PAGE partitions biomolecules according to charge and size. The immobilized pH gradient (IPG) strip partitions mAb variants according to pI. Figure 3.29 below shows a 2-dimensional PAGE analysis of the mAb B feed. One dimension shows the molecular mass, while the other dimension shows the isoelectric point. 2D PAGE is not as accurate as CE-SDS;

however, 2D PAGE allows validating results obtained using other techniques.



**Figure 3.29:** 2D PAGE of mAb B Feed in a Non-reducing Buffer Condition

Figure 3.29 shows the monomeric variants of mAb B at spots spread out between pI 7.5 and pI 8.5 (+/- 0.5 pH units). The process was not sufficiently developed; hence, the presence of mAb streaking and relatively high level of fragmentation into heavy chains and light chains. The charge variants (acidic, main, and basic) are visible at the intact mAb size marker (150 kDa) and the size marker of the heavy chain (50 kDa).

### 3.9 Conclusion

Prefiltration is an effective means of improving the filterability of mAbs through a virus filter when the right prefilter type is selected to remove the fouling species. The importance of cheaper membrane-based prefilters cannot be overemphasized due to virus filter costs and the single-use nature of virus filters. With new biologic modalities coming onstream and the pressure of biosimilar competition, a clearly defined model for prefilter selection is crucial. The

biopharmaceutical industry has previously relied on empirical means to determine adequate prefilters for the novel mAbs that come to the market every year.

Size exclusion prefilters did not improve the flux of mAb B, thereby validating the generally accepted research position that virus filter fouling is attributed to small oligomers less than 50 nm in size but larger than 20 nm. The smallest size-based prefiltration membrane we evaluated was 75 nm nominal pore-sized.

HIC membrane adsorbers are a ready option for downstream processing. HIC removes fouling species in moderate to high ionic strength buffers. Denatured mAb monomers are more hydrophobic than the native mAb monomers and are therefore captured by HIC prefilters. HIC membranes function well within several pH units of physiological pH (pH 7) in the presence of salt, as shown in the pH 5, pH 7.5, and pH 8.6 prefiltration data.

HIC prefilters are not significantly affected by the net charge variability of mAbs in buffers of different pH. However, as seen in section 4 of this work, HIC prefilter performance can be affected by some excipients such as arginine that ensure mAb stability in buffer formulations. Excipients that reduce viscosity or modulate hydrophobic interaction may affect the effectiveness of HIC prefilters.

Cation exchange prefilters work well when moderate ionic strength buffers are used, and the mAb's net charge is opposite the intrinsic charge of the prefiltration membrane. IEX-S performs well at pH 5 with salt because the salt prevents the binding of all mAb species to the membrane but permits the oppositely charged variants (potential foulants) to be captured.

Anion exchange membrane adsorbers are the best option for mAb B at pH 7.5 without salt. At pH 7.5, mAb B is within its pI region (7.1 - 8.0), where the net charge is zero or close to



zero, and monomeric charge variants that foul the virus filter are captured on the IEX-Q prefilter. The acidic charge variants of mAb B, especially the sialic acid glycoforms, are hypothesized to be captured by the positively-charged IEX-Q membrane adsorber.

## References

1. Wickramasinghe, S.R., et al., Virus Removal and Virus Purification, in Current Trends and Future Developments on (Bio-) Membranes. 2019. p. 69-96.
2. Godawat, R., et al., Periodic counter-current chromatography -- design and operational considerations for integrated and continuous purification of proteins. *Biotechnol J*, 2012. 7(12): p. 1496-508.
3. Konstantinov, K.B. and C.L. Cooney, White Paper on Continuous Bioprocessing May 20–21 2014 Continuous Manufacturing Symposium. *Journal of Pharmaceutical Sciences*, 2015. 104(3): p. 813-820.
4. Rayfield, W.J., et al., Prediction of viral filtration performance of monoclonal antibodies based on biophysical properties of feed. *Biotechnology Progress*, 2015. 31(3): p. 765-774.
5. Adan-Kubo, J., et al., Microscopic visualization of virus removal by dedicated filters used in biopharmaceutical processing: Impact of membrane structure and localization of captured virus particles. *Biotechnol Prog*, 2019. 35(6): p. e2875.
6. Kavara, A., et al., Recent advances in continuous downstream processing of antibodies and related products, in *Approaches to the Purification, Analysis and Characterization of Antibody-Based Therapeutics*. 2020. p. 81-103.
7. Namila, N., *The Effects of Solution Condition on Virus Filtration Performance*. 2020, University of Arkansas: Ann Arbor. p. 191.
8. Chiang, M.J., et al., Validation and optimization of viral clearance in a downstream continuous chromatography setting. *Biotechnol Bioeng*, 2019. 116(9): p. 2292-2302.
9. Shirataki, H., et al., Analysis of filtration behavior using integrated column chromatography followed by virus filtration. *Biotechnol Bioeng*, 2021. 118(9): p. 3569-3580.
10. Johnson, S.A., et al., Virus filtration: A review of current and future practices in bioprocessing. *Biotechnol Bioeng*, 2021.
11. Roche, J. and C.A. Royer, Lessons from pressure denaturation of proteins. *J R Soc Interface*, 2018. 15(147).

12. Kosiol, P., Membranes for virus removal by size exclusion, in Department of Chemistry. 2018, University of Duisburg-Essen: Germany.
13. Dengl, S., et al., Aggregation and Chemical Modification of Monoclonal Antibodies under Upstream Processing Conditions. *Pharmaceutical Research*, 2013. 30(5): p. 1380-1399.
14. Paul, A.J., K. Schwab, and F. Hesse, Direct analysis of mAb aggregates in mammalian cell culture supernatant. *BMC Biotechnology*, 2014. 14(1): p. 99.
15. Vazquez-Rey, M. and D.A. Lang, Aggregates in monoclonal antibody manufacturing processes. *Biotechnol Bioeng*, 2011. 108(7): p. 1494-508.
16. Fekete, S., et al., Method development for the separation of monoclonal antibody charge variants in cation exchange chromatography, Part I: salt gradient approach. *J Pharm Biomed Anal*, 2015. 102: p. 33-44.
17. Cai, K., et al., Virus removal robustness of ion exchange chromatography. *Biologicals*, 2019. 58: p. 28-34.
18. Barnard, J.G., et al., Investigations into the fouling mechanism of parvovirus filters during filtration of freeze-thawed mAb drug substance solutions. *J Pharm Sci*, 2014. 103(3): p. 890-9.
19. Charcosset, C., 4 - Virus filtration, in *Membrane Processes in Biotechnology and Pharmaceutics*, C. Charcosset, Editor. 2012, Elsevier: Amsterdam. p. 143-167.
20. Bieberbach, M., et al., Investigation of fouling mechanisms of virus filters during the filtration of protein solutions using a high throughput filtration screening device. *Biotechnol Prog*, 2019. 35(4): p. e2776.
21. Sadek, P.C., *Illustrated Pocket Dictionary of Chromatography*. 2004: Wiley.
22. Yadav, S., S.J. Shire, and D.S. Kalonia, Factors affecting the viscosity in high concentration solutions of different monoclonal antibodies. *J Pharm Sci*, 2010. 99(12): p. 4812-29.
23. Billups, M., et al., Antibody retention by virus filtration membranes: Polarization and sieving effects. *Journal of Membrane Science*, 2021. 620.
24. Robinson, J., D. Roush, and S.M. Cramer, The effect of pH on antibody retention in multimodal cation exchange chromatographic systems. *J Chromatogr A*, 2020. 1617: p. 460838.
25. Rohani, M.M. and A.L. Zydney, Role of electrostatic interactions during protein ultrafiltration. *Adv Colloid Interface Sci*, 2010. 160(1-2): p. 40-8.

26. Vlasak, J. and R. Ionescu, Heterogeneity of monoclonal antibodies revealed by charge-sensitive methods. *Curr Pharm Biotechnol*, 2008. 9(6): p. 468-81.
27. Liu, H., et al., Characterization of recombinant monoclonal antibody charge variants using WCX chromatography, icIEF and LC-MS/MS. *Anal Biochem*, 2019. 564-565: p. 1-12.
28. Xu, Y., et al., Structure, heterogeneity and developability assessment of therapeutic antibodies. *MAbs*, 2019. 11(2): p. 239-264.
29. King, C., et al., Characterization of recombinant monoclonal antibody variants detected by hydrophobic interaction chromatography and imaged capillary isoelectric focusing electrophoresis. *J Chromatogr B Analyt Technol Biomed Life Sci*, 2018. 1085: p. 96-103.
30. Wagner, E., et al., Determination of size variants by CE-SDS for approved therapeutic antibodies: Key implications of subclasses and light chain specificities. *J Pharm Biomed Anal*, 2020. 184: p. 113166.
31. Joshi, S., et al., Monitoring size and oligomeric-state distribution of therapeutic mAbs by NMR and DLS: Trastuzumab as a case study. *Journal of Pharmaceutical and Biomedical Analysis*, 2021. 195.
32. Sadavarte, R., et al., Rapid preparative separation of monoclonal antibody charge variants using laterally-fed membrane chromatography. *J Chromatogr B Analyt Technol Biomed Life Sci*, 2018. 1073: p. 27-33.

## 4.0 Impact of Buffer Conditions on Filterability of Monoclonal Antibodies

### 4.1 Introduction

A different, industrially relevant mAb is the subject of this section. Quality by design philosophy requires a molecular-level understanding of the product quality attributes of mAbs for effective process design, development, and quality assurance [1]. mAbs are multi-domain polypeptides with anisotropic tendencies derived from varied surface patches [2, 3]. The presence of orientation-dependent patches on the exposed regions of a mAb can lead to anomalous mAb-mAb interactions or mAb-filter interactions [4-8].

When a positively charged patch interacts with a negatively charged patch on an adjacent mAb molecule, soluble multimerization can occur due to attractive electrostatic interactions [4]. The anisotropic nature of mAbs implies asymmetric charge variations along the surface of a mAb [8]. mAbs have been shown to have surface patches with asymmetric spectra of hydrophobicity and hydrophilicity, which can have different fouling tendencies [9].

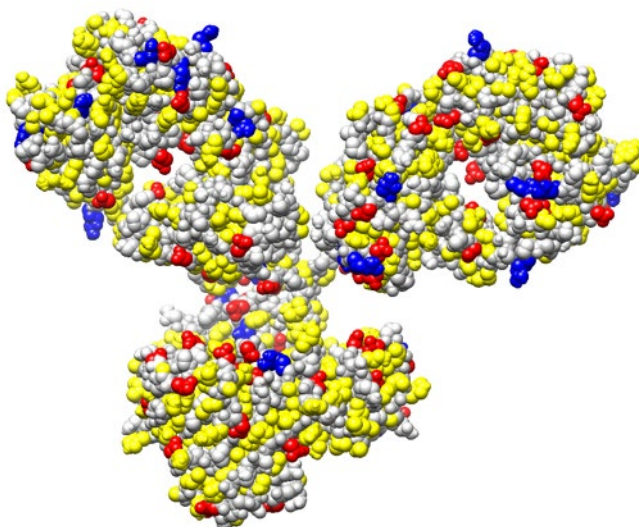
Over 1300 amino acids come together to form a mAb through secondary, tertiary, and quaternary structures. These amino acids have different characteristics, including polar versus non-polar, hydrophobic versus hydrophilic, and positively charged versus negatively charged. As a result, the biophysical characteristics of the surface-exposed residues change when the buffer properties are different [10]. In mAb studies, biophysical characteristics are considered holistically as net characteristics or discrete-wise at the domain or surface-patch level.

As a result of property change in different aqueous environments, mAbs must be carefully screened for buffer conditions with the best stability and least multimerization propensity [11, 12]. Mass spectrometry with multi-attribute monitoring (MAM-MS) is becoming

a technique of choice for characterizing mAb molecular attributes all at once [1, 13-15]. pH and ionic strength turbidimetric titrations have been used to study mAb multimerization propensity in aqueous buffers. High throughput screening has also become a technique of choice for research organizations.

Turbidimetric measurements can determine the role of excipients on mAb stability using a UV spectrophotometer at 340 nm. Generally, spectrophotometers give turbidity generalizations on the macro level without discretizing the product's molecular characteristics. Pharmaceutical analysis systems such as the PA 800 plus have become a technique of choice for product quality and attribute analysis.

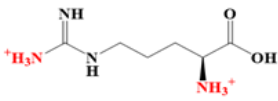
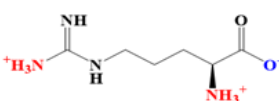
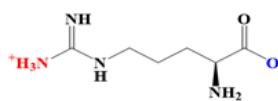
Anomalous behavior of mAbs becomes prevalent at low ionic strengths hence the usefulness of cation exchange prefiltration and anion exchange prefiltration at specific pH values. Figure 4.1 below shows the charge and hydrophobicity anisotropy of a mAb.



**Figure 4.1:** Charge and Hydrophobicity Asymmetry of IgG2a mAb. (RBSB Protein Databank). Positively Charged Residues in Blue, Negatively Charged Residues in Red, and Hydrophobic Residues in Yellow.

Figure 4.1 shows the charge asymmetry of a mAb at a defined pH value which changes when buffer pH changes [16, 17] because the residues or patches protonate at lower pH values than the mAb's pI and deprotonate at higher pH values. The hydrophobic patches, shown in yellow, interact with other hydrophobic patches on adjacent mAbs or adsorptive membranes when the salt concentration is sufficient. Arginine is an amino acid that is frequently used as a buffer excipient. Arginine, as shown in Table 4.1 below, has a distal guanidine group with a pKa of 13.8 [18].

**Table 4.1:** Changing Charge States of Arginine at Different Buffer pH Values.

	pH 2	pH 7	pH 10
Arginine			
Net charge (+/-)	(+2)	(+1)	0

In the table above, the terminal amine ( $\text{NH}_3^+$ ) is protonated at physiological pH but becomes deprotonated beyond pH 12. The carboxyl group is always deprotonated except below pH 2.1, where it becomes  $\text{COOH}$ . The arginine example is a microcosm of what happens to most amino acids that are surface exposed on a mAb in varying buffer conditions. Charge anisotropy attributes should be carefully considered to minimize multimerization and fouling of virus filters.

## 4.2 Materials and Methods

### 4.2.1 Materials

Reagents used were Sodium chloride (molecular biology grade > 98% purity), L-arginine monohydrochloride (cell-culture grade > 98.5% purity), Sodium phosphate monobasic monohydrate (ACS reagent, > 98% purity), Sodium phosphate dibasic (reagent plus, >99%

purity), OmniPur sodium acetate trihydrate (molecular biology grade > 99% purity), Glycine (for electrophoresis, > 99% purity), Acrylamide for synthesis (79-06-1) and glacial acetic acid (100% purity) sourced from MilliporeSigma (Billerica, MA).

L(+)-Histidine (>98% purity), tris(hydroxymethyl)aminomethane (biotechnology grade, 99% purity), Ammonium sulfate (proteomics grade, > 99.5% purity), and Sodium dodecyl sulfate (biotechnology grade, > 99% purity) were sourced from VWR Life Science (Radnor, PA). Nalgene™ rapid-flow™ sterile single-use bottle top filters (0.2 µm and 0.1 µm) were purchased from ThermoFisher Scientific (Waltham, MA). Ultrapure water with a resistivity of 18.2 MΩ was used for buffer formulation. Precision protein plus MW standard and Bromophenol blue indicator, Supelco (115-39-9), were sourced from Bio-Rad laboratories (Hercules, CA). Dithiothreitol (molecular biology grade, >99% purity) was purchased from Gold Biotechnology (St. Louis, MO).

Other selected prefilters were Viresolve prefilter (VPF) provided by MilliporeSigma (Billerica, MA), Sartobind® Phenyl nano 3 mL, Sartobind® Q nano 3 mL, 8 mm bed height, and Sartobind® S nano 3 mL, 8 mm bed height provided by Sartorius (Göttingen, Germany). The selected virus filter was Planova BioEX (membrane surface area 0.0003m<sup>2</sup>) provided by Asahi Kasei Medical (Tokyo, Japan) and the Viresolve Pro (VPro) provided by MilliporeSigma (Billerica, MA).

TangenX Sius PDn Cassette (30 kDa MWCO, mPES, 0.1 m<sup>2</sup>) was sourced from Repligen (Marlborough, MA). SDS MW analysis kit (PN: 390953), Fast glycan labeling and analysis kit (PN: B94499), CZE rapid charge variant analysis kit (PN: C44790), and Advanced cIEF starter kit (PN: A80976) were sourced from SCIEX (Redwood City, CA).

#### 4.2.2 Monoclonal Antibody Sample Preparation and Buffer Conditions

An industrially relevant mAb M was provided by a biopharmaceutical company. It had been processed through three chromatographic polishing steps. In the previous section, we studied mAb B, which was subjected to the industry-standard two polishing steps. The isoelectric point (pI) of mAb M ranged from 5.95 to 6.55. 10.9 g/L mAb M was initially constituted in a buffer containing 20 mM histidine and 150 mM arginine, pH 5.11. 100 ml portions of mAb M were subsequently ultrafiltered and diafiltered into pH 5 buffers of 20 mM sodium acetate, 0 M NaCl, and 200 mM NaCl. The final volume and concentration were 200 ml and 5 g/L respectively. Several 50 ml portions of mAb M were retained in the original arginine plus histidine buffer. 200 ml aliquots of 10.9 g/L mAb M were also buffer exchanged into buffers of 20 mM histidine only, pH 5.11 and pH 6.7. pH 6.7 buffers were titrated with glacial acetic acid and tris base. Final mAb concentrations after UF/DF were 10 g/L and diluted to 5 g/L with corresponding buffers when required.

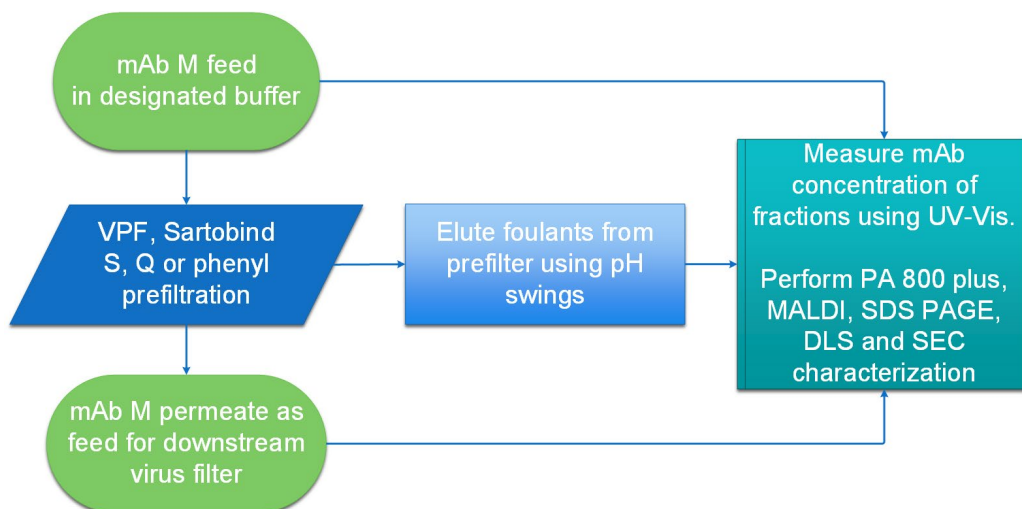
The desired mAb concentrations were 5 g/L and 10 g/L, respectively. mAb stock concentration was measured by UV spectrophotometric analysis at 280 nm using Genesys10 UV Scanning System (Waltham, MA) with VWR quartz spectrophotometer cell (path length 1 cm; West Chester, PA). mAb concentration and turbidity were determined by measuring the absorbance at 280 and 340 nm, respectively.

Buffer exchange was performed by ultrafiltration and diafiltration (UF/DF) of mAb M using five diafiltration volumes on a TangenX Sius™ LSn HyStream 30kDa tangential flow filtration (TFF) Cassette (Marlborough, MA). Buffer pH and conductivity were measured using Orion Star™ A215 pH/conductivity benchtop multiparameter meter from ThermoFisher Scientific (Waltham, MA). mAb fractions were immediately used for prefiltration or virus



filtration following buffer exchange or stored at 4°C for less than one week. Aliquoted mAbs were stored for extended periods at -80°C.

HIC and IEX-S prefiltration of 10 g/L or 5 g/L mAb M was performed using the Sartobind phenyl and Sartobind S membrane adsorbers (3 ml membrane volume), respectively. From mAb B studies in the previous section, it had been established that size-exclusion-based prefilters were ineffective for preventing virus filter flux decay. The research focus was placed on adsorptive and multimodal prefilters in this section. Prefiltration of mAb M using the VPF prefilters and Sartobind membranes was performed in the decoupled prefiltration mode before virus filtration. Figure 4.2 below shows the workflow for prefiltration and virus filtration.



- **Protein:** mAb M (pI = 5.95 – 6.55, MW = 149 kDa)
- **Condition:**
  - 20mM histidine and 150 mM arginine buffer, pH 5.11, without salt (BioEX only)
  - 20 mM histidine buffer, pH 5.11, without salt (VPro, VPF, BioEX)
  - 20 mM histidine buffer, pH 6.7, without salt (VPro, HIC, IEX-S)
  - 20 mM sodium acetate buffer, pH 5.0, without salt (BioEX only)
  - 20 mM sodium acetate buffer, pH 5.0, with 200mM NaCl (BioEX, HIC)
- **Base prefilter:** Sterilizing-grade 0.2-micron PES filter (considered as no prefilter)
- **Virus filter:**
  - Planova BioEX (Asahi Kasei)
  - Viresolve Pro (MilliporeSigma)
- **Prefilters:**
  - Viresolve prefilter (VPF)
  - Sartobind phenyl membrane adsorber (HIC 'prefilter')
  - Sartobind S membrane adsorber (IEX-S 'prefilter')

**Figure 4.2:** Decoupled Prefiltration / Virus Filtration Workflow and Filtration Conditions

In the workflow above, 50 ml of mAb M was filtered with a 0.2-micron PES filter before adsorptive prefiltration using the VPF or Sartobind membranes. Elution buffers were used to desorb the fouling species from the prefiltration membrane. The FPLC showed adsorptive and desorptive events in real-time. The fractions were then analyzed. Only VPF prefiltration was performed without the FPLC. Prefiltration conditions are described below.

The prefilters were installed on an FPLC (GE Pharmacia, Boston, MA). Prefiltration was performed in flowthrough mode across all prefiltration membranes, and the mAb was collected as flowthrough fractions. A buffer wash step was performed after flowthrough, and an elution step was also performed. All fractions were collected for characterization. The flowthrough fraction was immediately used for virus filtration.

The prefilters were equilibrated at 2 ml/minute with the requisite buffer condition (earlier described) for 30 minutes before prefiltration of mAb M feed (50 ml at 10 g/L or 5 g/L). Prefiltration was performed at 2 ml/minute, including the equilibration and wash fractions. Buffer chase of the same composition as the feed mAb buffer (20 ml) was used to wash off loosely bound mAb from the prefilter over ten minutes, followed by 40 ml of elution buffer over 20 minutes (same buffer as equilibration buffer with 1 M NaCl for IEX-S). The Sartobind phenyl required no salt elution in acetate buffer; however, 20 mM histidine plus 150 mM arginine was used as elution buffer for HIC when mAb was in 20 mM histidine buffer only.

Viresolve prefilter (VPF) prefiltration was not performed on an FPLC. The Planova 75N was connected to a Planova pressure vessel containing the mAb at 5 g/L. The operating pressure was 14 psi, supplied by a pressurized nitrogen bottle. The permeate was collected on a weighing balance and recorded for flux calculations. For the bottle-top filters (0.2  $\mu\text{m}$ ), filtration was manually handled with a low vacuum pulling the permeate gently along the walls of the receiving bottle to prevent aggregation.

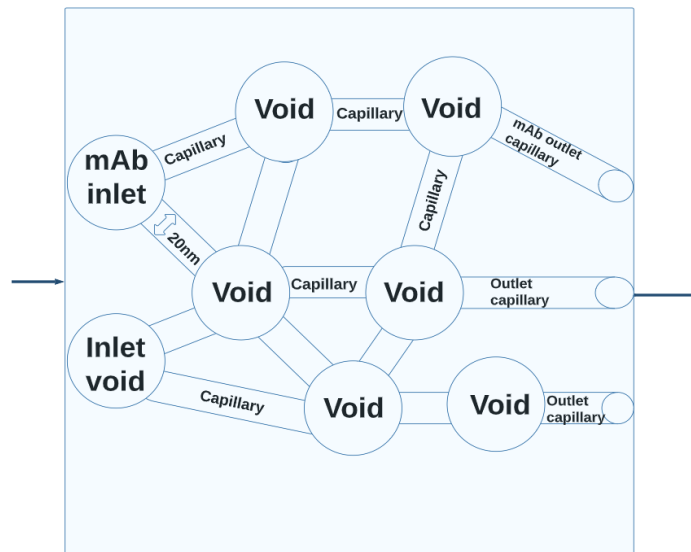
VPro virus filters were operated at 30 psi and equilibrated with 40 L/m<sup>2</sup> of water to remove all the trapped air before buffer and mAb M filtration. Visual leak integrity tests were performed on the BioEX virus filters at 14.5 psi for 20 seconds before flushing air out from the system. Reservoir pressure was controlled by an Ashcroft pressure gauge (Part number: EW-

68334-15; 0-100 psi, resolution 0.1, accuracy  $\pm 0.5$  full-scale). Deionized water filtered with a 0.2  $\mu\text{m}$  bottle top filter was added to the Planova™ Pressure Reservoir (Asahi Kasei, Japan).

The BioEX filter was flushed with 40 L/m<sup>2</sup> of DI water and 40 L/m<sup>2</sup> of formulation buffer. We performed virus filtration in constant-pressure (45 psi), dead-end filtration mode. The flowthrough fractions during prefiltration were used as the BioEX feed. The cumulative mass of the BioEX, VPro, and VPF permeate was acquired in real-time using a BalanceLink software connected to a Mettler Toledo scale (Columbus, OH).

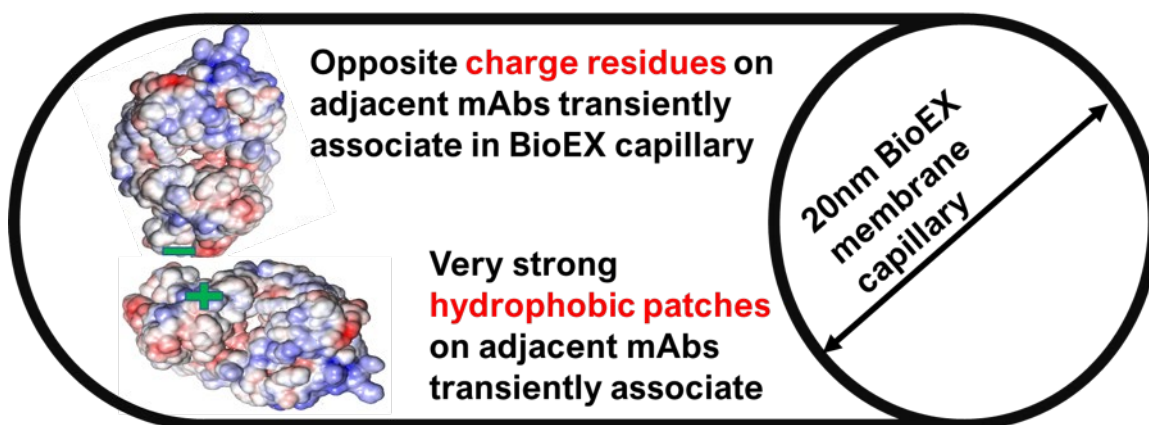
A no prefiltration baseline involved removing any large aggregates using a 0.2- $\mu\text{m}$  bottle top filter before virus filtration. Virus filtration without prefiltration was performed using mAb M feed at the above-stated buffer conditions.

Figure 4.3 below shows the membrane cross-section of the BioEX hollow-fiber virus filter showing the void and capillary structure of each hollow fiber from the inside to the outside.



**Figure 4.3:** Virus Filtration Mechanism of the Planova BioEX [19].

The BioEX works by size exclusion principle utilizing the 20 nm diameter capillary pores. The membrane is made of hydrophilized PVDF hollow fibers. Viruses, mAb dimers, and multimers (> 20 nm) can block the narrow capillary pores. Virus filters are typically designed to have high sieving coefficients for mAbs hence the asymmetric design of the VPro where the open support structure faces the feed stream. In Figure 4.3, the BioEX virus filter shows a void and 20 nm-capillary structure where voids are connected by multiple tortuous capillary paths. Blockage of a few capillaries leaves room for redirection of the mAb product from that void through any other open capillary to the subsequent void or until all capillaries are blocked. Virus filters are designed to maintain high mAb sieving coefficients (>0.95) [20]. Figure 4.4 shows the transport of two adjacent mAb monomers in the 20 nm capillary region of a BioEX filter.



**Figure 4.4:** mAb Monomers Passing Through the 20 nm Capillary of the Planova BioEX

Figure 4.4 theoretically illustrates two mAb monomers with surface charge asymmetry moving through the capillary region of the BioEX membrane. The oppositely charged patches transiently interact due to electrostatics and slow down the flux of protein through the virus filter with the possible outcome of blocking the virus filter pore through soluble multimerization.

### **4.2.3 Capillary Electrophoresis (CE) Characterization**

Capillary electrophoresis was performed using the PA800 plus by SCIEX (Redwood City, CA). Different characterization modes of the pharmaceutical analysis system were employed. Detailed descriptions are presented in section 3.2.6. The PA800 plus has a 50  $\mu\text{m}$  capillary ID and a 30 cm capillary length. The distance from the capillary inlet to the detection window was 20 cm. Bare fused silica capillaries were used for CE-SDS and IgG purity/heterogeneity assay. 15kV was applied across the capillary during CE-SDS and IgG purity analysis to resolve the analytes. A photodiode array detector was used to obtain an electropherogram in real-time.

Capillary zone electrophoresis (charge variant analysis) of the mAb fractions was also performed. Bare fused silica capillary was used in the charge variant analysis mode. Sample components migrate across the capillary by electroosmotic flow from the inlet to the outlet. Based on the relative migration rates, distinct peaks are obtained for the various IgG charge variants in the sample. The UV detector was used during CZE characterization, and a voltage of 30 kV was applied across the capillary. The UV detector was also used during capillary isoelectric focusing (cIEF) characterization of mAb fractions.

### **4.2.4 Dynamic Light Scattering (Particle Size Analysis)**

Dynamic light scattering (DLS) was used to determine the hydrodynamic diameters of mAb molecules in the various filtration fractions. DLS was performed using a DelsaNano HC particle size analyzer by Beckman Coulter (Brea, CA). DLS measurements are susceptible to noise signals from ambient dust interference; therefore, the cuvettes were rinsed with ultrapure water, and the mAb fractions were filtered with a 0.2-micron syringe polyethersulfone filter.

The instrument was calibrated using 100 nm size standards before starting DLS measurements. A disposable polystyrene cuvette with a 1 cm pathlength (BrandTech, Essex, CT) was used for sample collection for measurement. The instrument software was set at 200 acquisitions, and triplicate runs were performed per filtration fraction. Average hydrodynamic diameter and other diffusion parameters were acquired and recorded for each filtration fraction.

DLS was used to evaluate the diffusion interaction parameter  $K_D$ . A positive value denotes repulsive intermolecular forces, and a negative value denotes attractive intermolecular forces [21].

#### **4.2.5 Size Exclusion Analysis**

Size exclusion analysis was performed using a TSKgel G3000SWXL column (7.8 mm ID x 30 cm, and particle size of 5  $\mu$ m) made by Tosoh Bioscience (Grove City, OH). The column was installed on a high-performance liquid chromatography instrument (Agilent 1260 Infinity Quaternary LC) manufactured by Agilent Technologies (Santa Clara, CA). The mobile phase was 20 mM sodium phosphate buffer, pH 7.0 with 300 mM ammonium sulfate. The SEC column was equilibrated with the mobile phase at 0.9 ml/minute for one hour before sample introduction. The mAb fractions in requisite buffers were filtered with a 0.2-micron syringe filter and loaded into 1 ml sample vials. The HPLC was programmed and partitioned the analytes over a twenty-minute run at 0.9 ml/minute. 10  $\mu$ l of samples were injected into the column and analyzed by HPLC.

## **4.2.6 MALDI Mass Spectrometry**

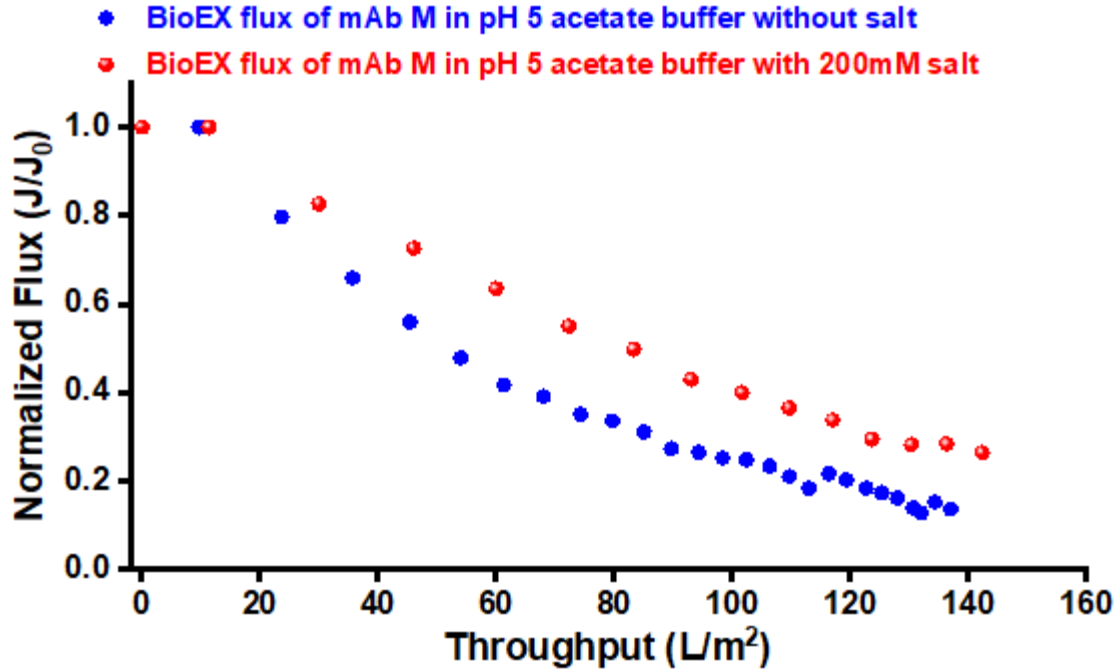
Matrix-Assisted Laser Desorption/Ionization Time-of-flight (MALDI-TOF) mass spectrometry was used to characterize mAb filtration fractions. This MALDI MS instrument was manufactured by Bruker (Billerica, MA). Due to the unstable nature of mAb M, samples were retained in their filtration buffer conditions during mass spectrometry. Desalting was not performed. MALDI-MS involves pipetting 1-2  $\mu\text{L}$  of each mAb fraction on a target plate in filtration buffer condition and co-crystallizing with sinapic acid. The target plate is then inserted into the instrument. MALDI MS outputs the analyte's intact mass and the ionization state of the analyte (singly versus double ionized). MALDI MS does not decompose the samples and is deemed a soft ionization technique for characterization. Sinapic acid was used as the immobilization matrix to co-crystallize the mAb fractions (analyte) on the MALDI target plate.

## **4.3 mAb M Filtration Results**

### **4.3.1 BioEX Virus Filtration of mAb M In Sodium Acetate Buffer without Prefiltration**

The Planova BioEX virus filter was used to filter 5 g/L mAb M in 20 mM sodium acetate buffer with and without salt and no prefiltration at pH 5 with the earlier described formulation conditions. The mAb was filtered with a 0.2-micron bottle top filter. mAb M was then filtered with a BioEX virus filter at a constant pressure of 45 psi. Figure 4.5 below shows the flux decay associated with filtration of mAb M in pH 5 sodium acetate buffer through the BioEX virus filter without adsorptive prefiltration.





**Figure 4.5:** BioEX Filtration of mAb M in pH 5 Sodium Acetate Buffer, with and without Salt.

BioEX filter fouling and flux decay with mAb M is drastic in sodium acetate buffer at pH 5. In the presence and absence of salt, the BioEX filter loses over 80 percent of the initial flux while delivering throughput under 140 L/m<sup>2</sup> of mAb feed. The presence of 200 mM sodium chloride marginally improved the flux decay by 10 percent over the flux decay without salt. mAb M has an isoelectric point range between 5.95 and 6.55. The pH 5 condition is outside the net charge neutrality region of mAb M (pI = 5.95 - 6.55). All mAb M variants would be positively charged at pH 5, which is 1 pH unit below the isoelectric point region. Further characterization was performed to understand the molecular level interactions that lead to rapid fouling and is described further in the results.

Table 4.2 below shows the mass balance of the above BioEX filtration fractions where greater than 96% mAb M recovery was achieved.

**Table 4.2:** Mass Balance of mAb M in pH 5 Sodium Acetate (with and without Salt)

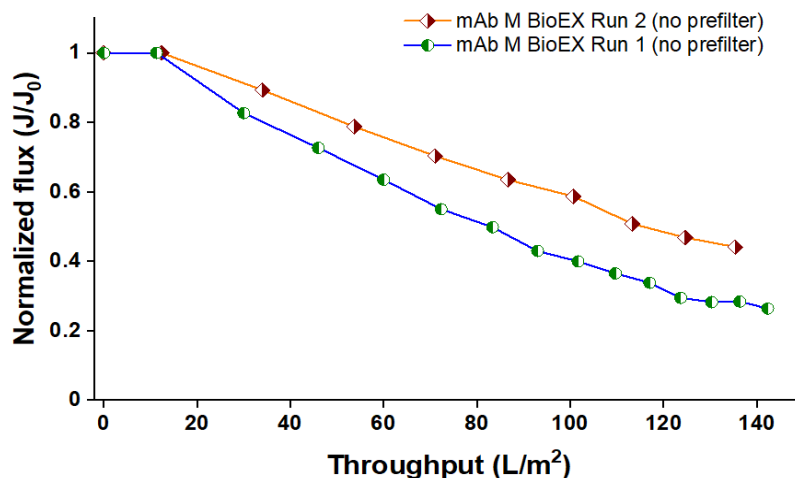
BioEX pH 5 (No prefiltration, no salt)	Abs @ 280nm	Abs @ 280nm	Abs @ 280nm	Absorbance	Dilution factor	Conc. (mg/mL)	Volume (mL)
	<b>1</b>	<b>2</b>	<b>3</b>	<b>Average</b>			
mAb M before 0.2um	0.447	0.450	0.449	0.4487	20	6.064	50.0
mAb M after 0.2um (BioEX feed)	0.437	0.434	0.435	0.4354	20	5.884	42.0
BioEX filtrate (mAb M)	0.410	0.413	0.415	0.4125	20	5.575	42.0
BioEX buffer chase	0.048	0.049	0.050	0.0492	20	0.665	6.0
BioEX mAb recovery	<b>0.96363</b>						

BioEX pH 5 (No prefiltration, with salt)	Abs @ 280nm	Abs @ 280nm	Abs @ 280nm	Absorbance	Dilution factor	Conc. (mg/mL)	Volume (mL)
	<b>1</b>	<b>2</b>	<b>3</b>	<b>Average</b>			
mAb M before 0.2um	0.353	0.352	0.354	0.3530	20	4.770	50.0
mAb M after 0.2um (BioEX feed)	0.345	0.344	0.346	0.3450	20	4.662	43.0
BioEX filtrate (mAb M)	0.314	0.321	0.323	0.3193	20	4.315	44.6
BioEX buffer chase	0.036	0.035	0.033	0.0347	20	0.468	3.0
BioEX mAb recovery	<b>0.96706</b>						

The BioEX filter demonstrated mAb sieving coefficients above 0.96 even though the mAb rapidly fouled the virus filter. In both experimental instances, the application of buffer flush post-mAb filtration resulted in the recovery of flux on the fouled BioEX filter up to 60 percent of initial flux. This phenomenon suggests desorption or reversibility of the fouling species with buffer dilution where soluble multimers resolubilize upon buffer dilution [22].

Further flux experiments were performed with mAb M permeate from the previous BioEX filtration (with salt), where the BioEX run 1 permeate was introduced as feed to a new BioEX filter (designated as run 2 BioEX filter). The flux result is shown in Figure 4.6 below. In both instances, no prefiltration (except 0.2-micron sterile filtration) was performed before virus filtration.



**Figure 4.6:** Run 1 and 2 BioEX Filtration of 5 g/L mAb M in pH 5, 20 mM Sodium Acetate Buffer with 200 mM NaCl, 0.2- $\mu$ m Prefiltration

Run 2 BioEX filtration shows reduced fouling because a significant portion of the principally fouling species was captured in BioEX filter run 1. Buffer dilution of the mAb permeates typically occurs during virus filtration. Consequently, the feed concentration changed from 4.8 g/L for run 1 to 4.4 g/L for run 2, as shown in Table 4.3 below. With a reduced feed concentration in run 2, a better flux performance is typically expected since mAb filterability correlates with feed concentration. Concentration polarization of mAbs is postulated to occur within the capillaries of the BioEX hollow fibers. Concentration polarization is hypothesized to cause apparent high mAb concentration on the membrane's boundary layers, leading to the formation of reversible multimers that foul the membrane [20]. Reversible multimers are joined by non-covalent bonds, which can be disrupted into the monomeric form upon mAb dilution by the buffer chase [22]. The mass balance for mAb concentration of run 1 and run 2 fractions is shown in Table 4.3 below.

**Table 4.3:** Mass Balance for BioEX Run 1 and 2 Fractions of mAb M in pH 5 Sodium Acetate

BioEX pH 5 Run 1 (No prefiltration, with salt)	Abs @ 280nm	Abs @ 280nm	Abs @ 280nm	Absorbance	Dilution factor	Conc. (mg/mL)
	<b>1</b>	<b>2</b>	<b>3</b>	<b>Average</b>		
mAb M before 0.2um	0.353	0.352	0.354	0.3530	20	4.77
mAb M after 0.2um (BioEX feed)	0.345	0.344	0.346	0.3450	20	4.66
BioEX filtrate (mAb M)	0.314	0.321	0.323	0.3193	20	4.32
BioEX buffer chase	0.036	0.035	0.033	0.0347	20	0.47
BioEX mAb recovery	96.71%	<b>With buffer chase</b>				

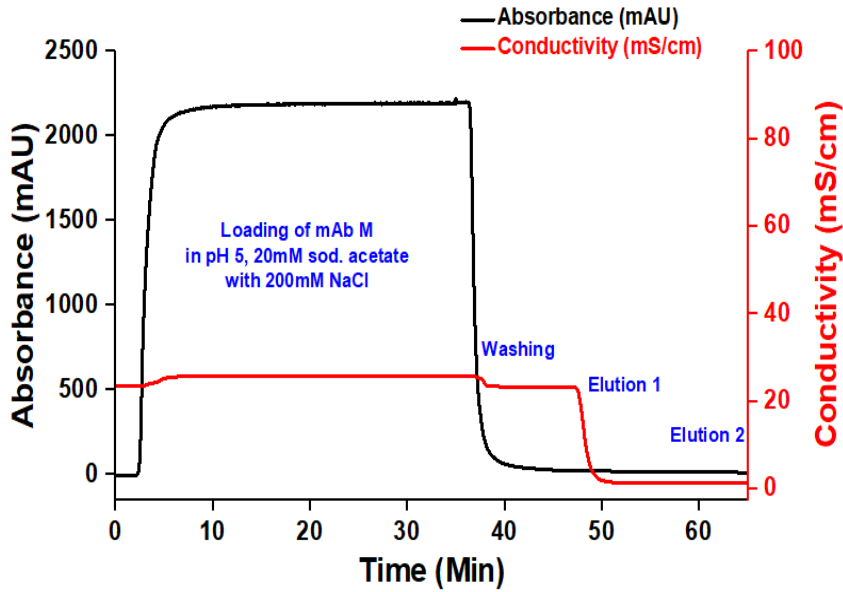
  

BioEX pH 5 Run 2 (No prefiltration, with salt)	Abs @ 280nm	Abs @ 280nm	Abs @ 280nm	Absorbance	Dilution factor	Conc. (mg/mL)
	<b>1</b>	<b>2</b>	<b>3</b>	<b>Average</b>		
mAb M before 0.2um	0.434	0.435	0.432	0.4337	15	4.40
mAb M after 0.2um (BioEX feed)	0.414	0.417	0.408	0.4130	15	4.19
BioEX filtrate (mAb M)	0.382	0.391	0.385	0.3860	15	3.91
BioEX mAb recovery	92.39%	<b>Without buffer chase</b>				

Run 2 feed concentration was slightly lower than run 1 feed concentration because run 1 permeate was reintroduced as run 2 feed. In both instances, high mAb recovery was obtained.

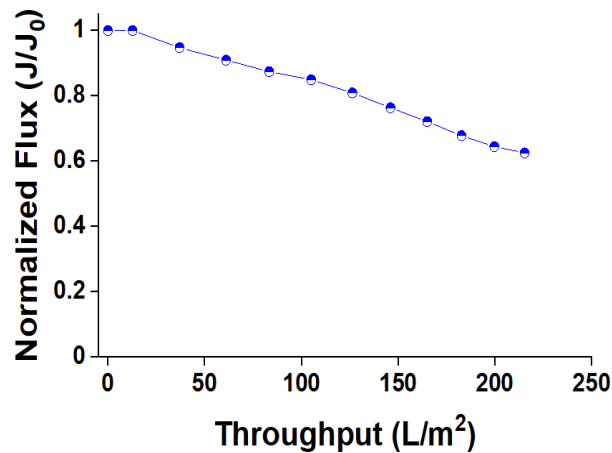
#### 4.3.2 BioEX Filtration of mAb M in Sodium Acetate Buffer with HIC Prefiltration

Hydrophobic interaction chromatography (HIC) prefiltration was used before BioEX filtration of this batch of mAb M in 20 mM sodium acetate buffer, pH 5, and 200 mM NaCl. The resulting chromatogram is shown in Figure 4.7 below.



**Figure 4.7:** Chromatogram for HIC Prefiltration of mAb M at pH 5 with 200 mM NaCl

Figure 4.7 shows a broad peak representing the mAb flowthrough fraction and no distinct elution peak for fouling variants removed by the HIC prefilter. The elution buffer was the same as the loading buffer and could not desorb foulants from the prefilter. The flowthrough fraction was filtered through a BioEX virus filter, as shown in Figure 4.8 below. It resulted in significant flux improvement over the no-prefiltration cases.

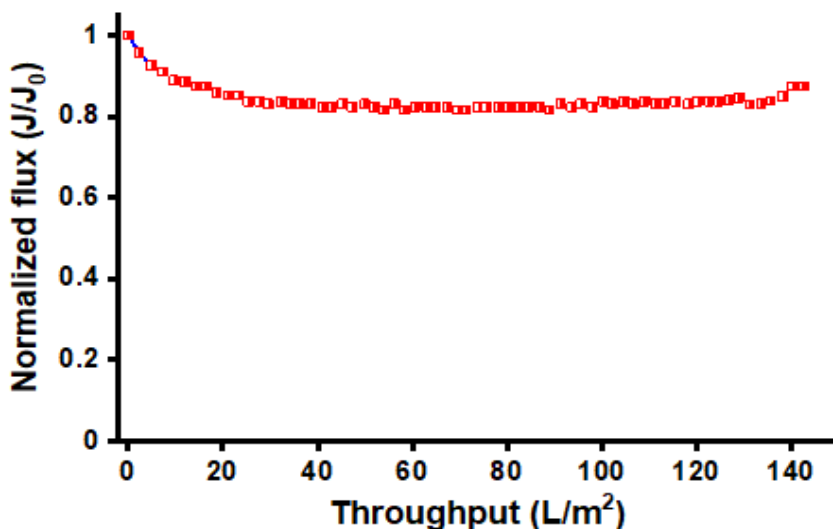


**Figure 4.8:** BioEX Filtration of mAb M in pH 5 Sodium Acetate Buffer after HIC Prefiltration

Figure 4.8 shows that adsorptive prefiltration using a HIC membrane adsorber improved the flux performance of mAb M in pH 5 sodium acetate buffer. Flux decay over a throughput of 220 L/m<sup>2</sup> was about 40 percent. Conversely, over 80 percent flux decay was observed without prefiltration with a throughput of 140 L/m<sup>2</sup>.

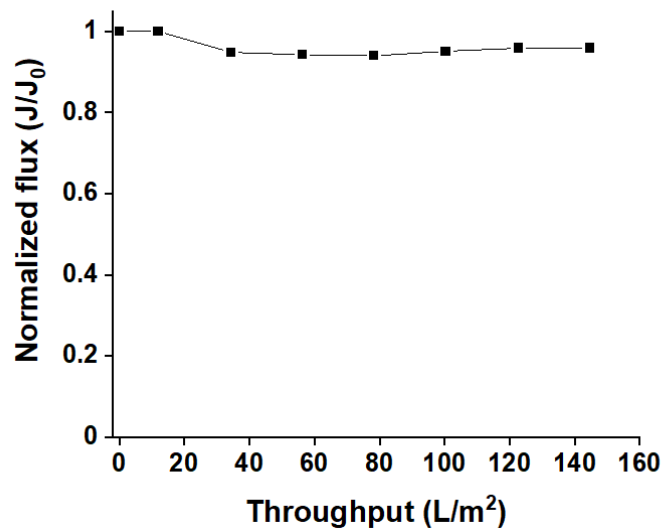
#### 4.3.3 Virus Filtration of mAb M in 20 mM Histidine Plus 150 mM Arginine Buffer Without Prefiltration

This mAb was determined to be unstable during process development and was therefore optimized for storage in 20 mM histidine plus 150 mM arginine at pH 5.11. Virus filtration was performed in this original buffer condition without prefiltration to study the filterability and fouling propensity, as shown in Figure 4.9.



**Figure 4.9:** BioEX Filtration of 5 g/L mAb M in pH 5.11, 20 mM Histidine plus 150 mM Arginine Buffer without Prefiltration

The result shows minor flux decay during mAb M filtration in the original buffer condition with the BioEX virus filter without prefiltration. Arginine is known to reduce hydrophobicity-induced multimerization of monomeric species, resolubilize multimers and facilitate refolding of thermally unfolded proteins [23-26]. Figure 4.10 below shows the BioEX flux data for 10 g/L mAb M in the original histidine plus arginine buffer formulation at pH 5.11.



**Figure 4.10:** BioEX Filtration of 10 g/L mAb M in pH 5.11, 20 mM Histidine Plus 150 mM Arginine Buffer without Prefiltration

Figure 4.10 shows that BioEX filtration of mAb M in the original buffer condition at a mAb concentration of 10 g/L resulted in excellent flux and little fouling. The mass balance of this experiment is shown in Table 4.4 below.

**Table 4.4:** Mass Balance for BioEX Fractions of 10 g/L mAb M in pH 5.11, 20 mM Histidine Plus 150 mM Arginine Buffer

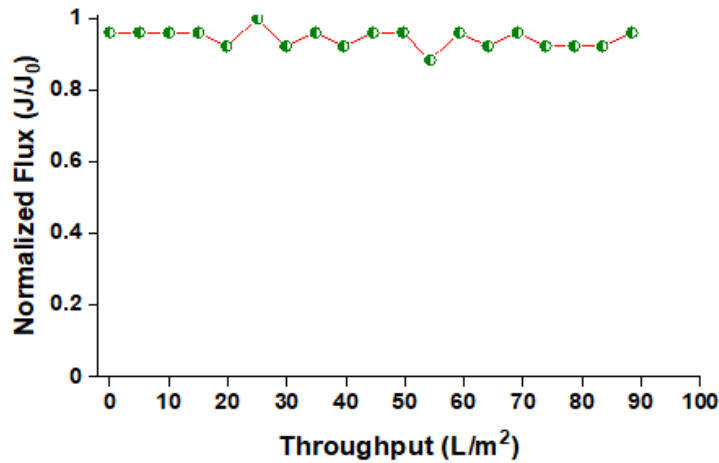
BioEX filtration of mAb M in original buffer (no prefiltration)	Abs @ 280nm	Abs @ 280nm	Abs @ 280nm	Absorbance	Dilution factor	Conc. (mg/mL)
	<b>1</b>	<b>2</b>	<b>3</b>	<i>Average</i>		
mAb M before 0.2um	0.791	0.792	0.792	0.7917	20	<b>10.70</b>
mAb M after 0.2um (BioEX feed)	0.788	0.786	0.786	0.7867	20	<b>10.63</b>
BioEX filtrate (mAb M)	0.78	0.777	0.776	0.7777	20	<b>10.51</b>
<b>BioEX protein recovery</b>	<b>98.86%</b>					

Figure 4.10 shows that little fouling of the virus filter occurred, while Table 4.4 shows that 99 percent of the feed was recovered in the permeate without the need for a buffer chase to resolubilize fouling species.

#### 4.3.4 Virus Filtration of mAb M in 20 mM Histidine (Only) Buffer Without Prefiltration

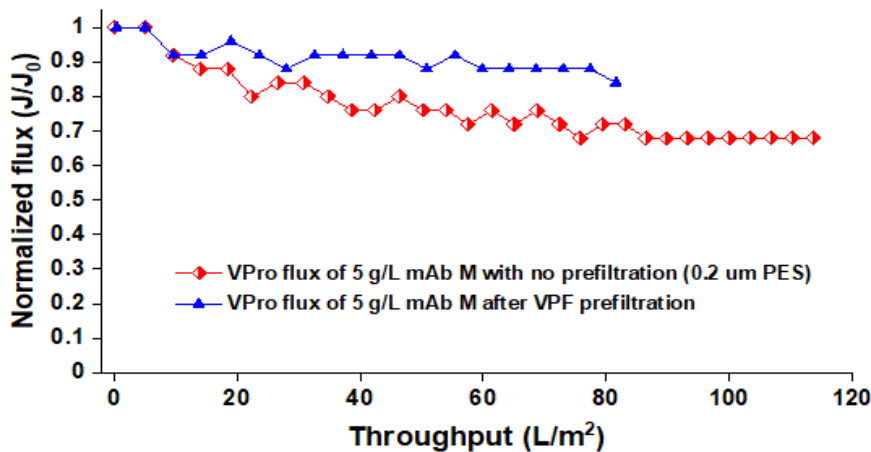
To study the impact of excipients on the filterability of mAb M, we performed buffer exchange and virus filtration after removing arginine from the formulation by buffer exchange using UF/DF. Figure 4.11 below shows the flux of 10 g/L mAb M in 20 mM histidine buffer (only) through the BioEX virus filter at pH 5.11 and without salt.





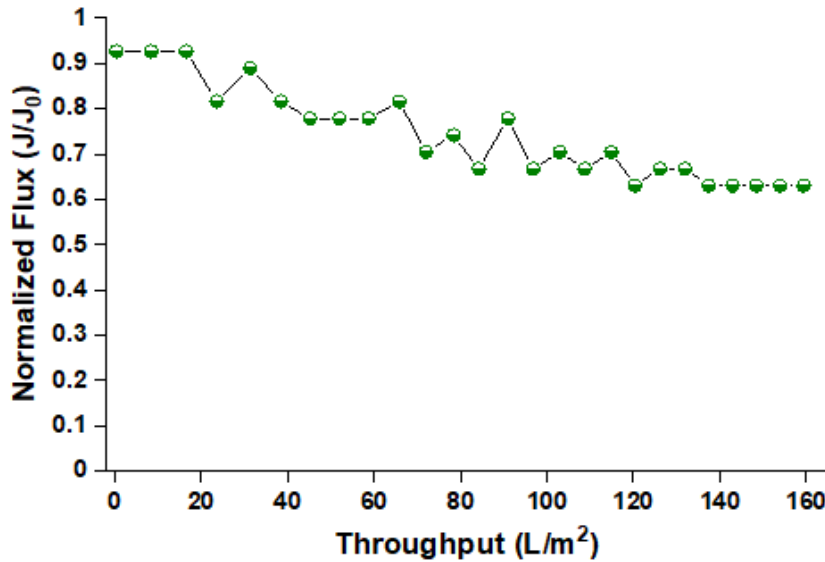
**Figure 4.11:** BioEX Filtration of 10 g/L mAb M in 20 mM Histidine Buffer (without Salt) at pH 5.11 without Prefiltration

After removing arginine from the mAb formulation at pH 5.11, there was still no significant fouling of the BioEX virus filter. Figure 4.12 below shows the flux of 5 g/L mAb M in 20 mM histidine buffer, pH 5.11, through a VPro virus filter with and without Viresolve prefilter (VPF) multimodal prefiltration.



**Figure 4.12:** VPro Filtration of 5 g/l mAb M in pH 5.11, 20 mM Histidine Buffer with and without VPF Prefiltration

Figure 4.12 showed 30 percent flux decay with the VPro virus filter without prefiltration. However, the VPF prefilter resulted in significant improvements in mAb M filterability with less flux decay. It was decided to perform virus filtration of mAb M at pH 6.7, above the pI range for this mAb. Figure 4.13 below shows the VPro flux of 5 g/L mAb M in pH 6.7, 20 mM histidine buffer without prefiltration.

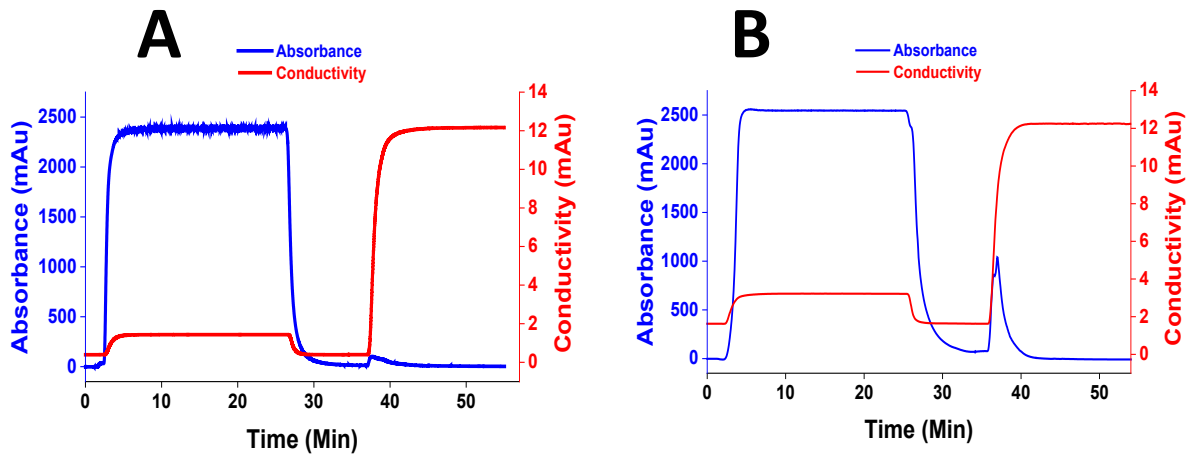


**Figure 4.13:** VPro Filtration of 5 g/L mAb M in 20 mM Histidine Buffer (Only) at pH 6.7 without Prefiltration

At pH 6.7, mAb M showed about 35 percent flux decay on the VPro virus filter without prefiltration. It is hypothesized that reversal of the monomeric net charge of mAb M occurs from a net positive charge at pH 5.11 to a net negative charge at pH 6.7 since the pI of this mAb is between 5.95 and 6.55. Net charge reversal due to pH is theorized to cause monomeric self-association at the membrane boundary layer where concentration polarization occurs.

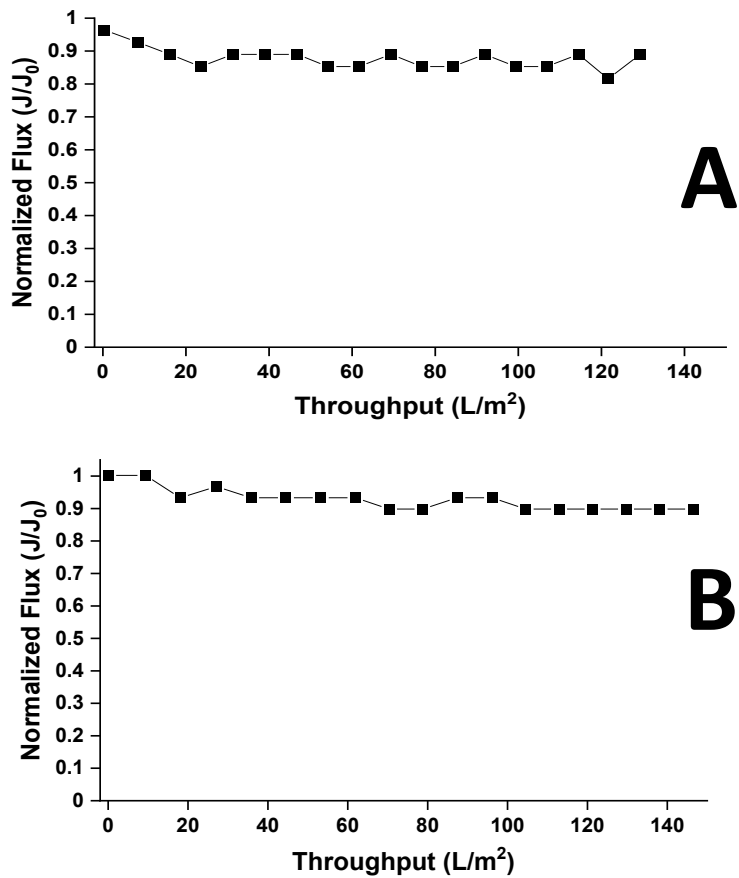
### 4.3.5 Virus Filtration of mAb M in pH 6.7, 20 mM Histidine Buffer with Adsorptive Prefiltration (Sartobind S, Sartobind Phenyl, and Viresolve Prefilter)

Adsorptive prefiltration was performed with the HIC, IEX-S, and VPF prefilters in the flowthrough mode, followed by virus filtration. Figure 4.14 below shows the chromatogram with HIC and IEX-S prefilters for mAb M in 20 mM histidine buffer, pH 6.7.



**Figure 4.14:** (A) HIC Prefiltration of 10 g/l mAb M in pH 6.7, 20 mM Histidine Buffer. (B) IEX-S Prefiltration of 10 g/l mAb M in pH 6.7, 20 mM Histidine Buffer.

From the chromatograms in Figure 4.14, the HIC has a smaller elution peak area compared to the IEX-S prefilter, which is much larger. The HIC prefilter is theorized to optimally target the removal of hydrophobicity-induced foulant species (possibly denatured mAbs) than ion-exchange mechanism adsorptive prefilters. Figure 4.15 below shows the flux behavior of mAb M through the VPro virus filter after HIC and IEX-S prefiltration.



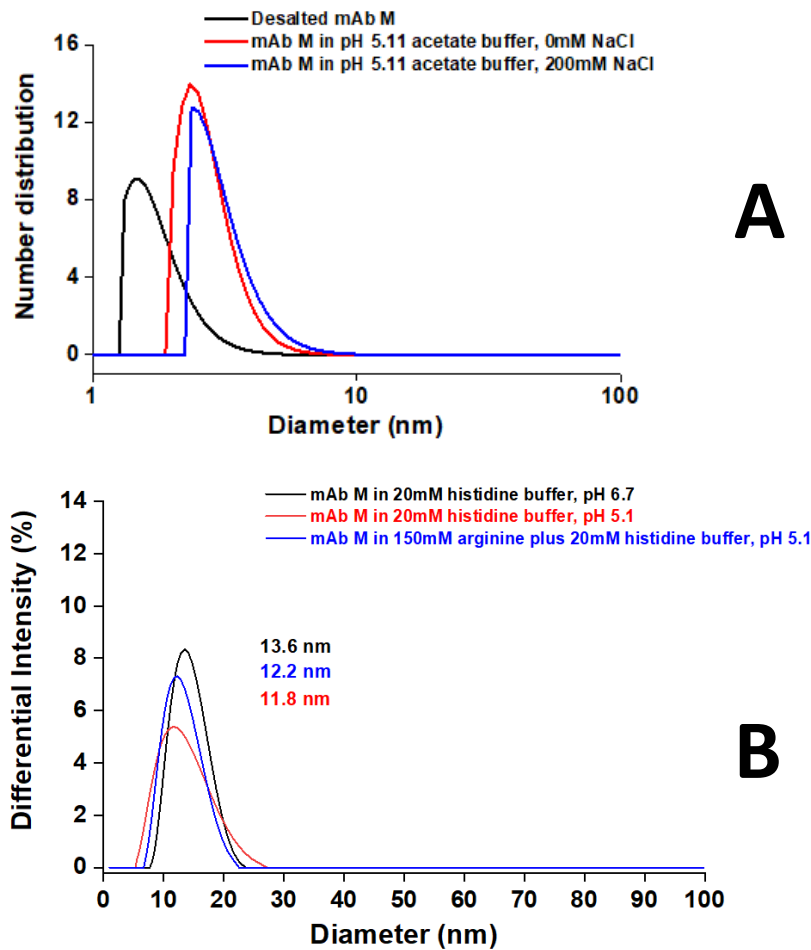
**Figure 4.15:** (A) VPro Filtration of 10 g/l mAb M in pH 6.7, 20 mM Histidine Buffer after HIC Prefiltration. (B) VPro Filtration of 10 g/l mAb M in pH 6.7, 20 mM Histidine Buffer after IEX-S Prefiltration.

Both the HIC and cation exchange prefiltration (IEX-S) significantly improves the flux of mAb M through the VPro virus filter and show less than 10 percent flux decay compared to 30 percent flux decay without prefiltration. All adsorptive prefilters preferentially adsorb denatured variants, multimers with increased hydrophobicity, and post-translationally modified mAb variants with charge asymmetry. The size exclusion-based prefilters do not perform well typically, as shown for the no prefiltration instances where 0.2-  $\mu\text{m}$  sterile filters were used.

## 4.4 mAb M Characterization

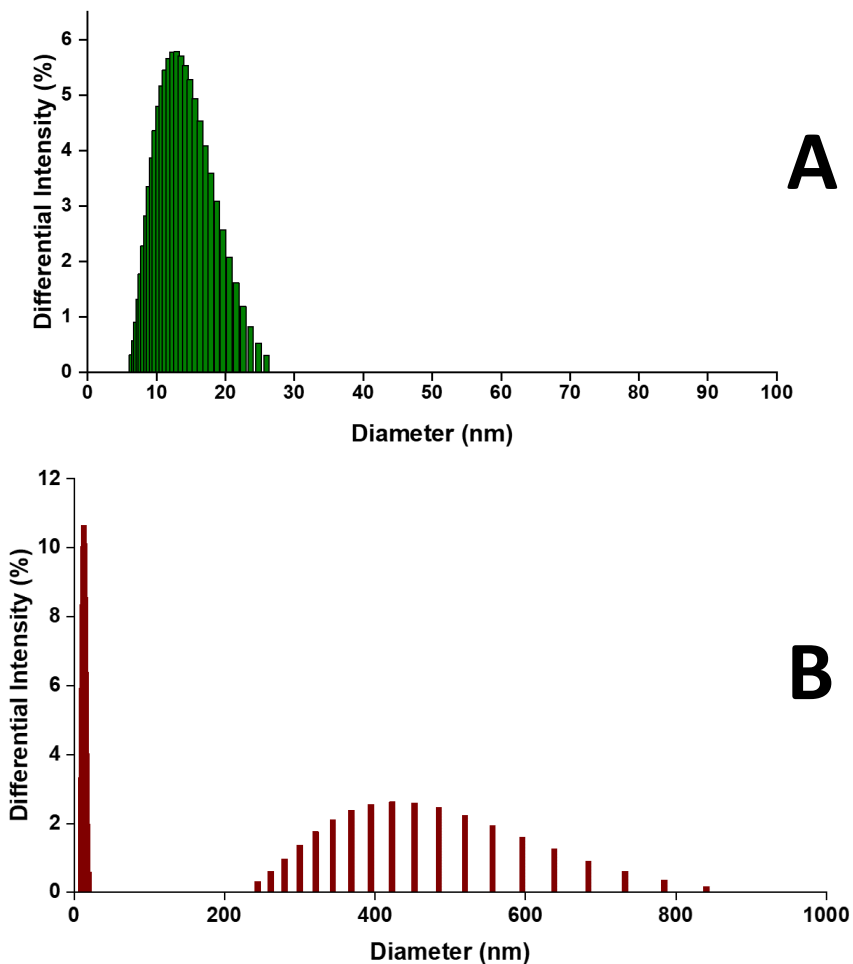
### 4.4.1 Dynamic Light Scattering (DLS) Characterization of mAb M Fractions

Particle size analysis of mAb M fractions was performed using a DelsaNano DLS. Figure 4.16 below shows the size spectra for mAb M filtration fractions in 20 mM sodium acetate buffer, pH 5 (with and without salt), DI water, 20 mM histidine buffer, pH 5.11, pH 6.7, and 20-mM histidine plus 150 mM arginine, pH 5.11.



**Figure 4.16:** (A) DLS of mAb M Fractions in Sodium Acetate Buffer with/without Salt and in DI Water. (B) DLS of mAb M in 20 mM Histidine pH 5.11, pH 6.7, and 20 mM Histidine Plus 150 mM Arginine Buffer Formulations for Stability Studies.

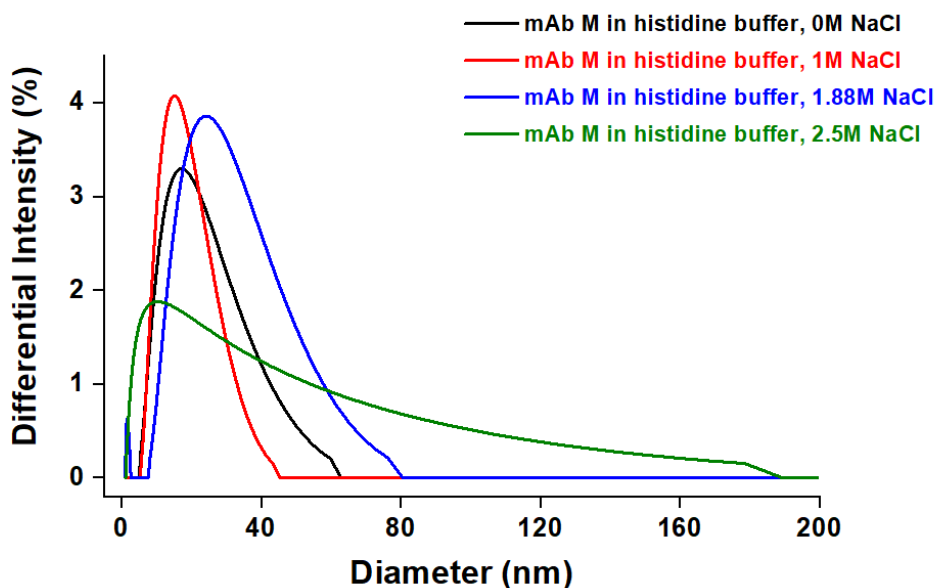
DLS data in Figure 4.16A above reinforces results from CE-SDS, showing that desalting the mAb causes fragmentation. Fragmentation is shown by the black spectrum line with a hydrodynamic diameter of less than 5 nm. Sodium acetate buffer with and without salt also shows a low hydrodynamic diameter for mAb M at less than 9 nm. Figure 4.16B shows that mAb M had the least hydrodynamic diameter in the pH 5.1 histidine buffer, closely followed by the original buffer (pH 5.1 histidine plus arginine). pH 6.7 histidine buffer was the least stable for mAb M. Figure 4.17 below shows the particle size distribution of mAb M in the original buffer (20 mM histidine plus 150 mM arginine).



**Figure 4.17:** (A) Differential Intensity for mAb M in Original Buffer. (B) Differential Intensity for mAb M in pH 5 Sodium Acetate Buffer with Salt after Desalting in DI Water

Figure 4.17A and 4.17B above shows the stability of mAb M in arginine versus when the buffer is desalted and reconstituted in DI water, where it fragments and forms irreversible large aggregates at the same time.

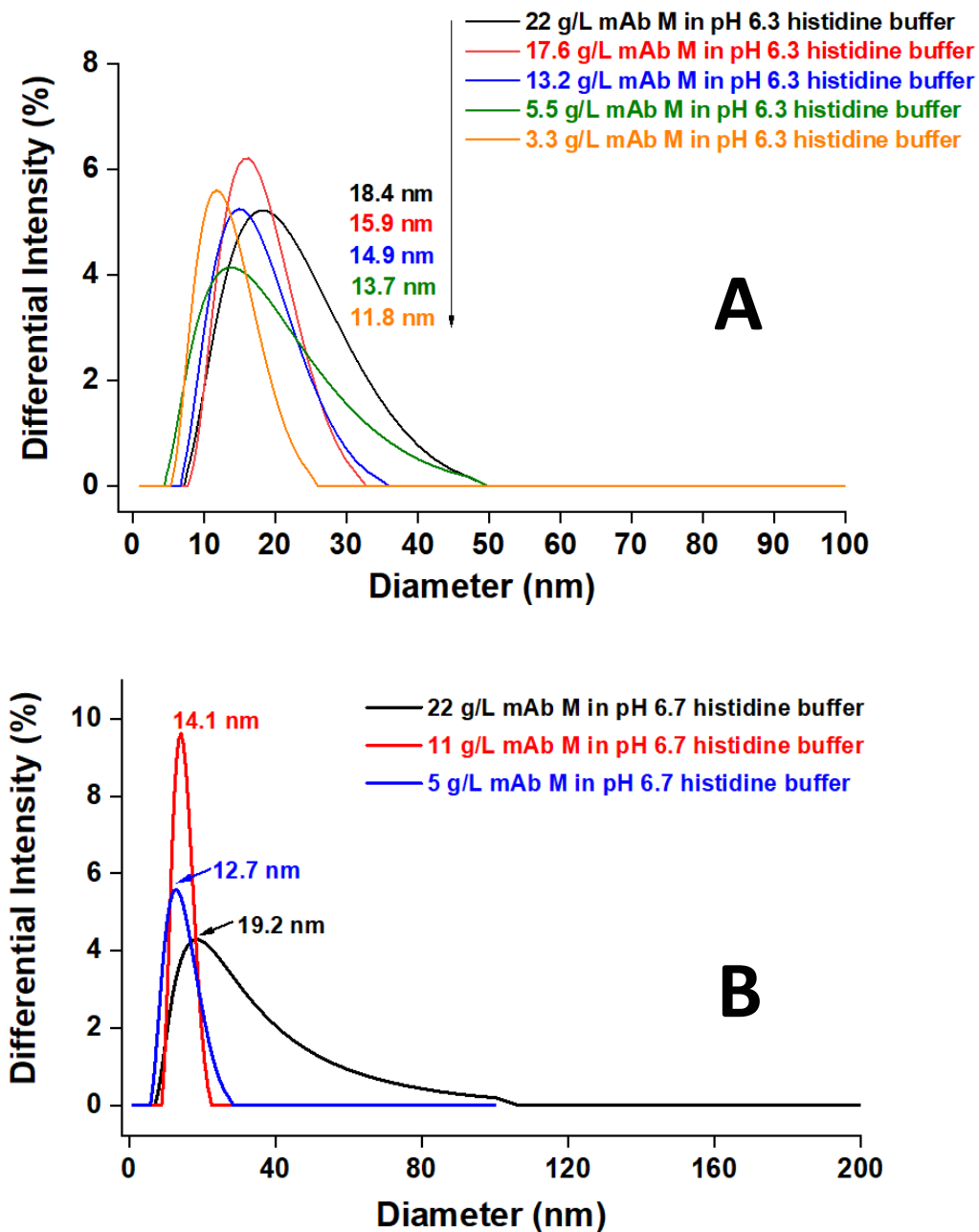
Stability studies for mAb M were designed to obtain further information about the molecular characteristics of mAb M monomers in different salt conditions at its pI. High salt concentrations can denature a mAb. We evaluated the effect of high salt concentrations on mAb M in histidine buffer by titrating to pH 6.3 because pH 6.3 was within the net charge neutrality region of this mAb. Figure 4.18 below shows DLS data for mAb M in 20 mM histidine buffer (pH 6.3 and different ionic strengths).



**Figure 4.18:** Differential Intensity for mAb M in 20 mM Histidine Buffer, pH 6.3 at Different Ionic Strengths

Figure 4.18 shows a direct correlation between salt content and multimerization of mAb M, resulting in increased hydrodynamic diameters. As the salt concentration goes up, the hydrodynamic diameter goes up. Above 1 M NaCl, the mAb monomers multimerize and show

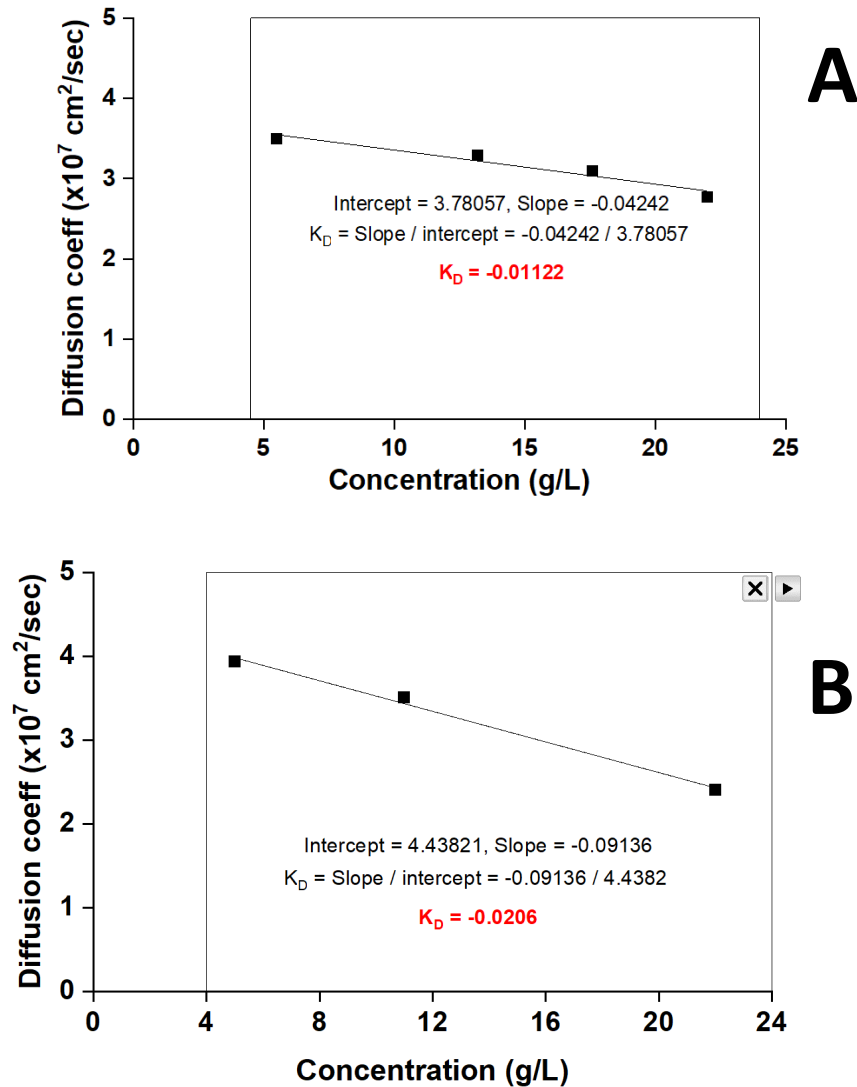
increased turbidity. Figure 4.19 below shows the effect of mAb concentration on the hydrodynamic diameter of mAb m in 20 mM histidine buffer at pH 6.3 and 6.7, respectively.



**Figure 4.19:** (A) DLS Size Analysis of mAb M in 20 mM Histidine Buffer, pH 6.3, at Different Concentrations. (B) DLS Size Analysis of mAb M in 20 mM Histidine Buffer, pH 6.7, at Different Concentrations.



The hydrodynamic diameter of mAb M positively correlates with the mAb concentration at pH 6.3 and 6.7. 22 g/L mAb M had the highest hydrodynamic diameter of 18.4 nm and 19.2 nm at pH 6.3 and 6.7, respectively. 3.3 g/L mAb M in pH 6.3 histidine buffer had the least hydrodynamic diameter of 11.8 nm. The diffusion interaction parameter,  $K_D$ , was obtained for mAb M at the pH conditions of 6.3 and 6.7 in histidine buffer only, as shown in Figure 4.20.

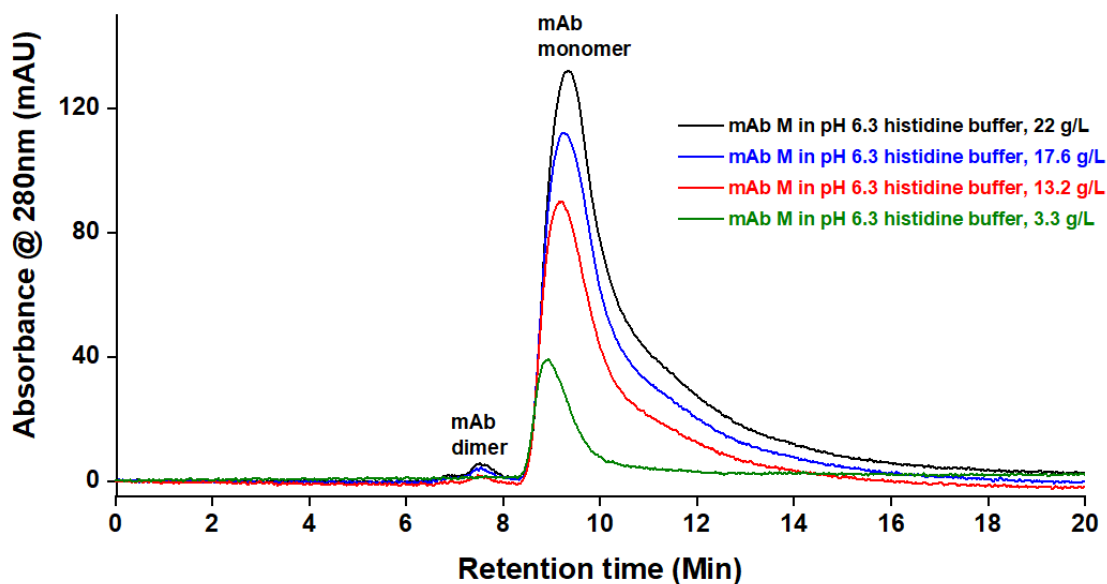


**Figure 4.20:** Plot of Diffusion Coefficient Versus Concentration of mAb M in 20 mM Histidine Buffer at (A) pH 6.3. (B) pH 6.7.

Figure 4.20 above shows that mAb M has a more negative diffusion interaction parameter at pH 6.7 than pH 6.3. A more negative diffusion interaction parameter implies a slightly higher intermolecular attraction force. mAb M, therefore, has a higher multimerization tendency at pH 6.7, which is above its pI range (5.95 - 6.55), than at pH 6.3, which is within its pI range.

#### 4.4.2. Size Exclusion Chromatography Analysis of mAb M Filtration Fractions

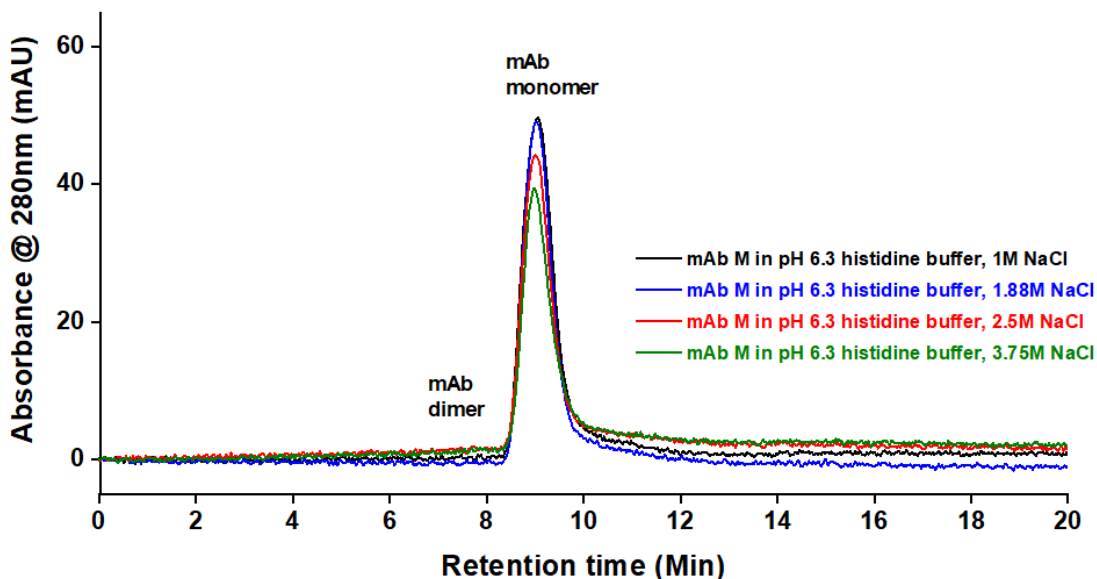
HPLC SEC chromatography was used to perform a size-based analysis of mAb M filtration fractions. The mobile phase was carefully optimized to obtain proper peak resolution of the monomer and multimeric forms. Figure 4.21 below shows the concentration-dependent chromatograms of mAb M constituted in 20 mM histidine buffer, pH 6.3.



**Figure 4.21:** HPLC SEC of mAb M in 20 mM Histidine Buffer, pH 6.3, at Different mAb M Concentrations

Figure 4.21 shows that dimers are present in small percentages at 13.2 g/L, 17.6 g/L, and 22 g/L. The mAb monomeric peak height is directly proportional to the mAb concentration.

However, the addition of NaCl up to 3.75 M did not induce dimerization of 2.5 g/L mAb M in pH 6.3 histidine buffer, as shown in Figure 4.22 below.



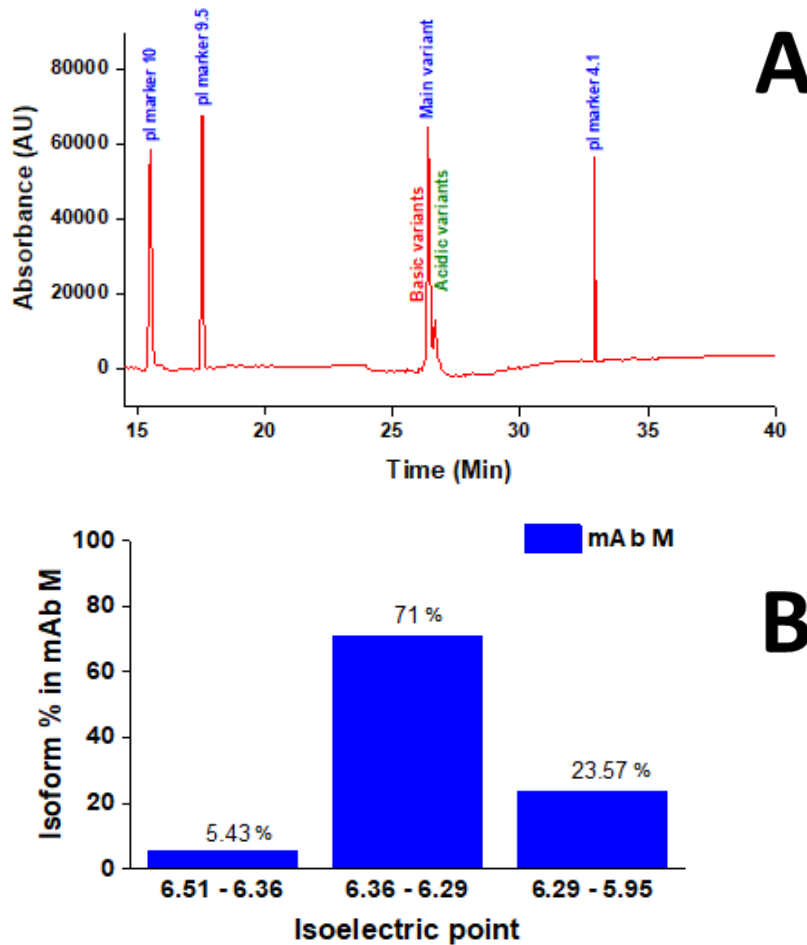
**Figure 4.22:** HPLC SEC of 2.5 g/L mAb M in 20mM Histidine Buffer, pH 6.3, at Different Buffer Salt Concentrations (1 M NaCl, 1.88 M NaCl, 2.5 M NaCl, and 3.75 M NaCl).

mAb M appears to foul virus filters by monomeric self-association of denatured or PTM variants at the surface of virus filtration membranes when in histidine buffer leading to soluble/reversible aggregation. Large irreversible aggregates are not typically found in the filtration fractions at normal buffer conditions, even with changes in salt content.

### 4.4.3 Capillary Electrophoresis Characterization of mAb M Fractions

#### 4.4.3.1 Capillary Isoelectric Focusing (cIEF) of mAb M Sample

Capillary isoelectric focusing data was obtained for mAb M feed to optimize the buffer parameters used in this study. Figure 4.23 below shows the isoelectric point distribution ratio of acidic, main, and basic isoforms of mAb M in the feed sample as determined using the PA 800 plus pharmaceutical analysis system.



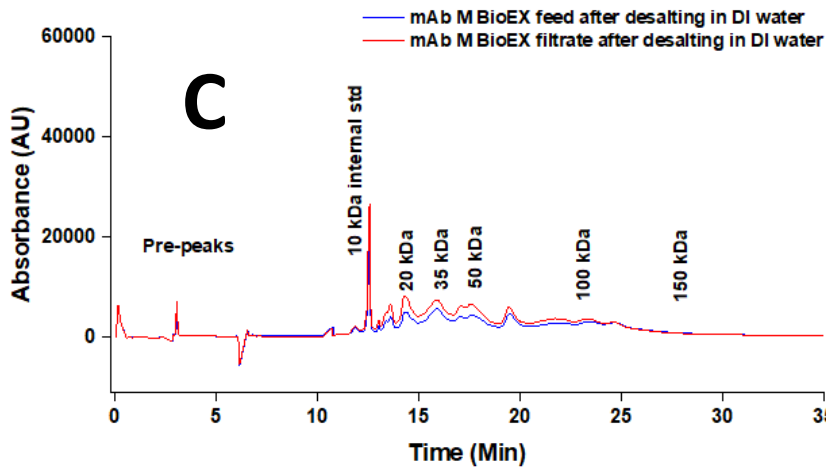
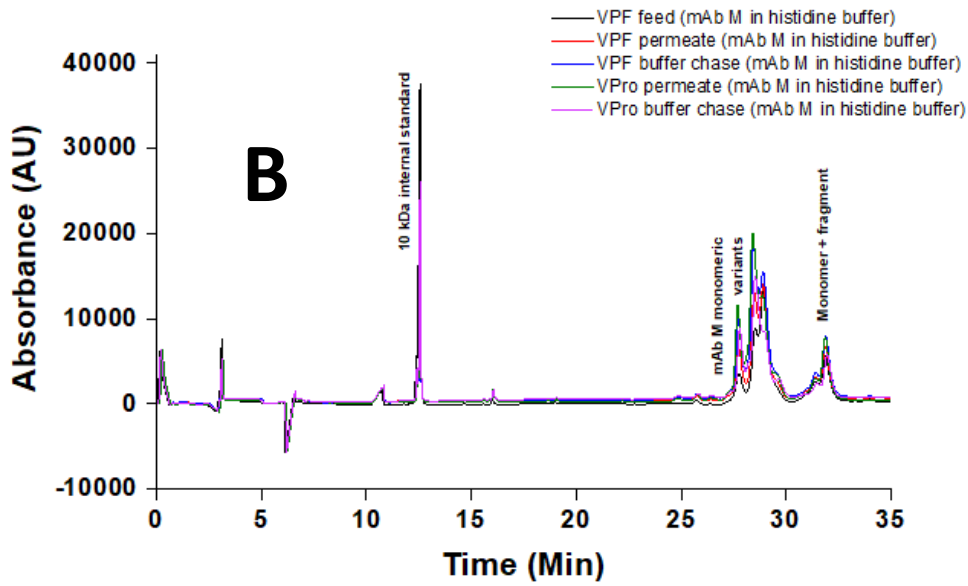
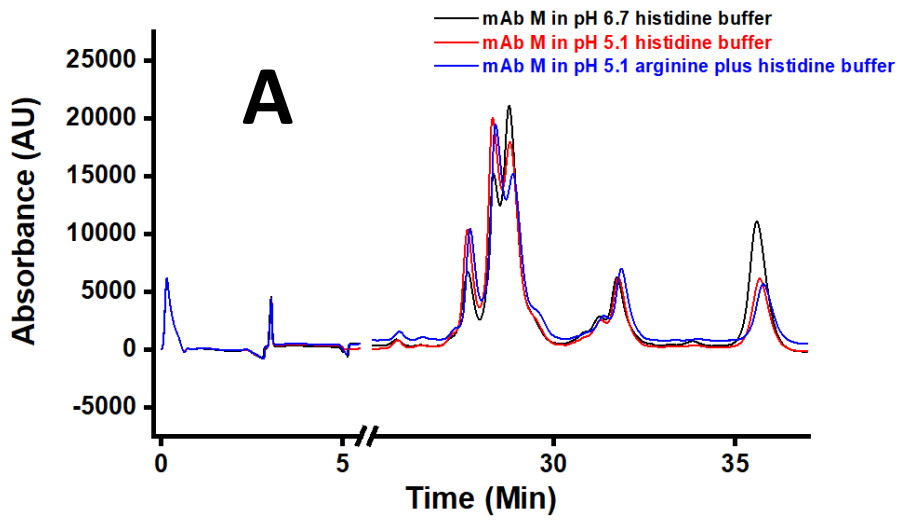
**Figure 4.23:** (A) c-IEF of mAb M in pH 5.11, 20 mM Histidine, 150 mM Arginine Buffer.

(B) Isoform Distribution of mAb M in pH 5.11, 20 mM Histidine, 150 mM Arginine Buffer.

Microheterogeneity of mAbs due to post-translational modifications often results in surface charge asymmetry, hydrophobicity differences, and isoelectric point differences [27-29]. The cIEF spectra of mAb M show three main isoforms, with 5.4 percent of the basic variant, 71 percent of the main variant, and 23.5 percent of the acidic variant. mAb M variants with pI values below 6.29 are acidic variants. Conversely, mAb M variants with pI above 6.36 are basic variants. According to the cIEF spectra peak integrations and quantification, mAb M shows less than half of the acidic variant ratio of the previously studied mAb B.

#### **4.4.3.2 Capillary Electrophoresis CE-SDS Analysis of mAb M Fractions**

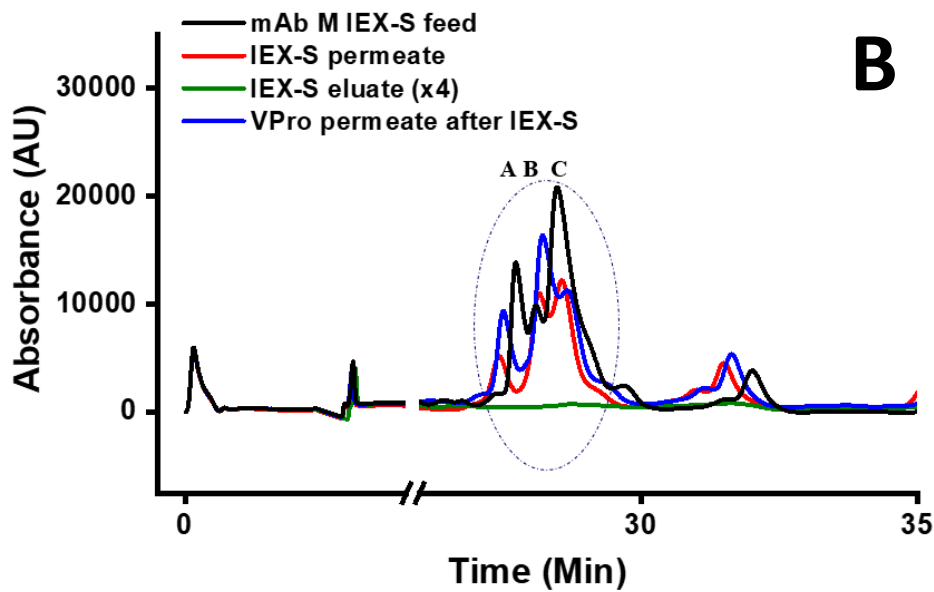
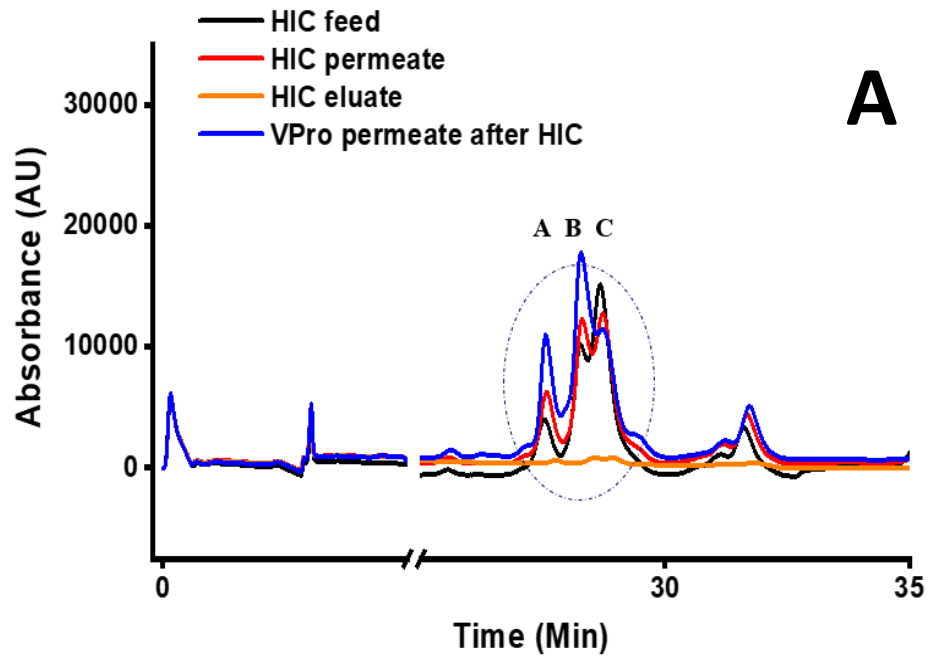
CE-SDS was used to evaluate the purity and size homogeneity of mAb M filtration fractions by capillary electrophoresis on the PA 800 plus. The CE-SDS electropherogram for mAb M in different buffer conditions is shown in Figures 4.24A, 4.24B, and 4.24C below.



**Figure 4.24:** CE-SDS Purity Analysis of mAb M Fractions using PA800 Plus. (A) mAb M in pH 5.11 Histidine plus Arginine Buffer, pH 5.11 and pH 6.7 Histidine Only Buffers, respectively. (B) CE-SDS of mAb M in 20 mM Histidine Buffer, pH 5.11 for VPF and VPro Fractions (C) CE SDS of mAb M BioEX Fractions without Prefiltration (pH 5.11, 200mM NaCl)

Figure 4.24A shows that the mAb peaks do not differ significantly between buffer types with clearly resolved peaks for the monomeric variants and aggregate peaks (monomer plus fragment). pH 6.7 histidine buffer showed the highest percentage area for the higher MW monomeric and higher MW aggregate peaks. Figure 4.24B, where mAb M is in histidine buffer (only), shows the higher molecular weight peaks that consist of one monomer plus an isolated mAb fragment. This higher molecular weight peak was obtained between 171 and 175 kDa. Monomeric mAb variants have been reported to possess microheterogeneity in size, charge, and hydrophobicity [30, 31]. Figure 4.24C shows no monomeric forms of mAb M and suggests mAb instability after desalting, leading to some fragmentation and some irreversible aggregation, as confirmed with DLS.

CE-SDS was performed for the HIC and IEX-S prefiltration fractions to evaluate size variants in the various fractions; feed, permeate, and eluate, as shown in Figure 4.25 below.



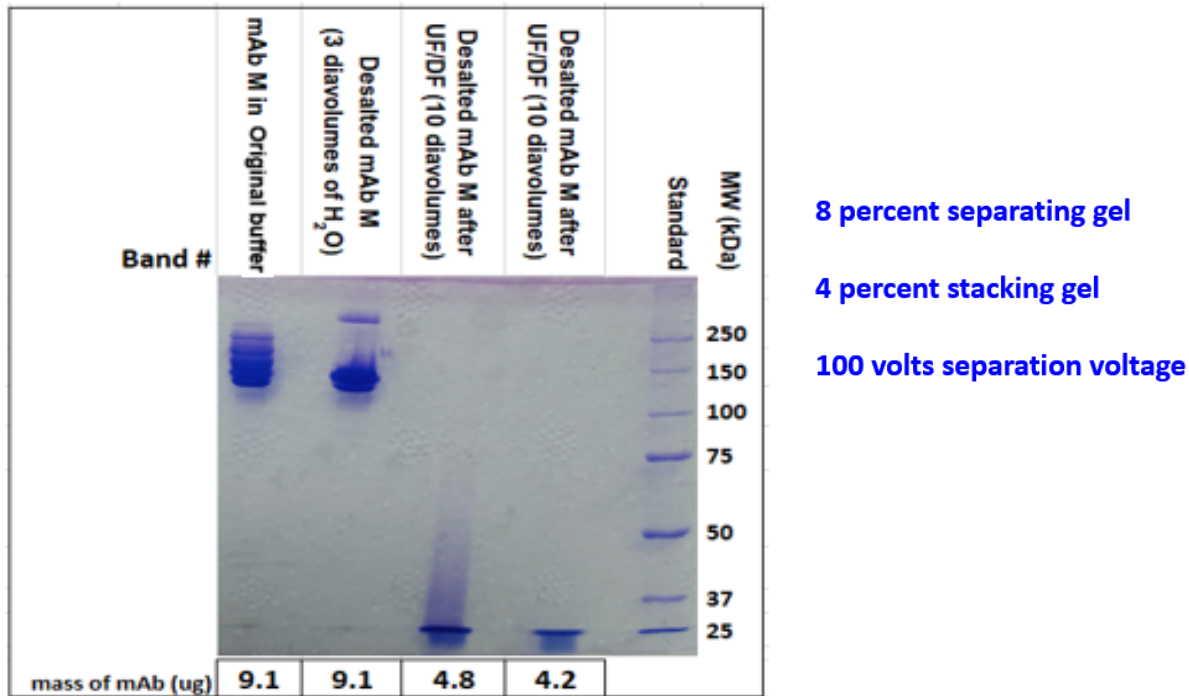
**Figure 4.25:** (A) CE SDS Electropherogram of mAb M HIC and VPro Fractions in pH 6.7, 20mM Histidine Buffer (B) CE SDS Electropherogram of mAb M IEX-S and VPro Fractions in pH 6.7, 20 mM Histidine buffer



Three main monomeric variants were observed from the CE-SDS electropherogram of mAb M HIC, IEX-S, and VPro fractions, as shown in Figure 4.25. In the feed fractions of both the HIC and IEX-S prefilters, peak C is most abundant. Peak C is the monomeric variant with the highest MW. In the permeate fractions of the HIC and IEX-S, peak C decreases, and peak B becomes most abundant. Peak C decreases even further in the VPro permeate of both Figures 4.25A and 4.25B. The variant with slightly higher molecular weight is theorized to be a glycoform with heavier glycans attached than variant B, and variant A. Eluate concentration was too low for detection. The peak at 173.2 kDa is likely an aggregate comprising a monomer (150 kDa) bound to an isolated fragment (23.5 kDa), as reported by Cao et al. [32].

#### **4.4.4 Sodium Dodecyl Sulfate (SDS) Polyacrylamide Gel Electrophoresis (PAGE) Analysis**

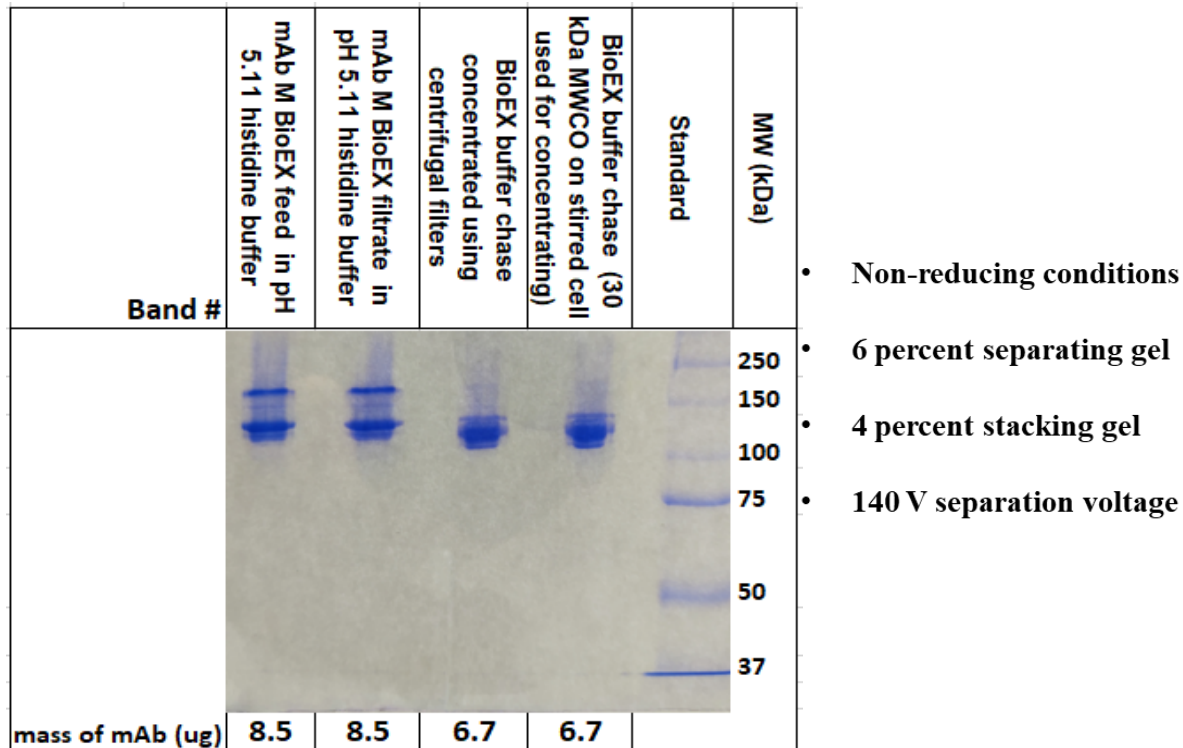
Gel electrophoresis was used to analyze the monomeric size variation of mAb M filtration fractions. The negatively charged sulfate groups impart net negative charges to all analytes in the gel such that mAb migration from cathode to anode down the gel is based on molecular weight only. Figure 4.26 below shows the SDS PAGE electrophoretogram for mAb M formulations during gradual desalting to evaluate stability.



**Figure 4.26:** SDS PAGE of mAb M Samples in Original Buffer and when in DI Water

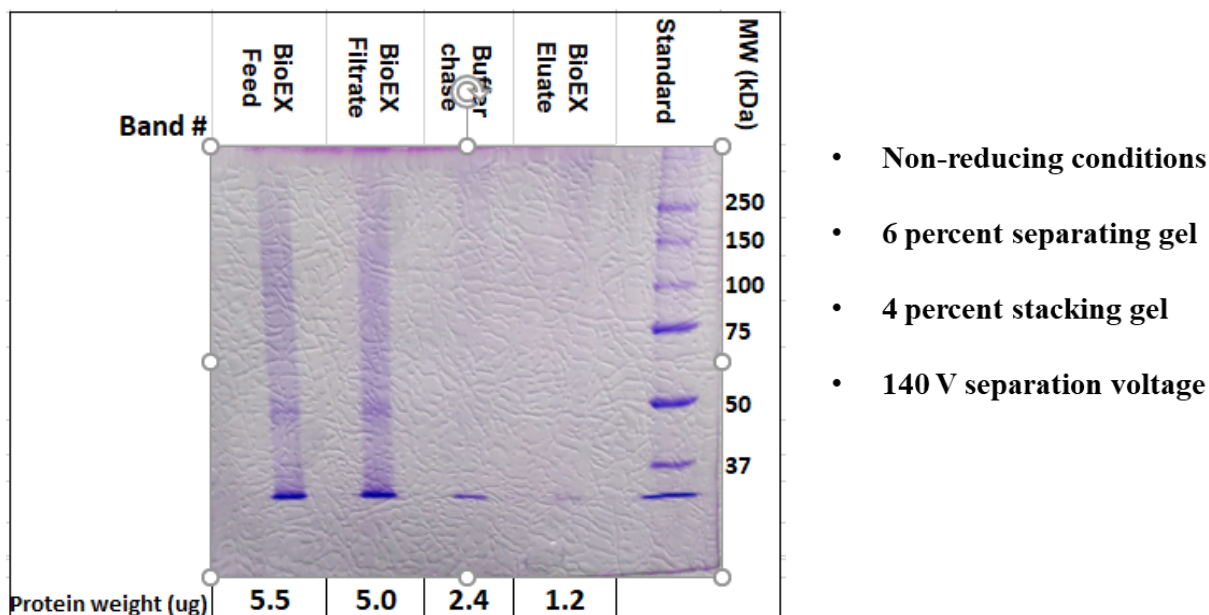
SDS PAGE was performed with non-reducing gel buffers, 8 percent polyacrylamide gel for the separating gel, and 4% for the stacking gel with a voltage of 100V. The non-reducing gel ensures that the mAb monomers do not break down into heavy (50 kDa) and light (25 kDa) chains. The mAb became unstable during the diafiltration process as the formulation buffer was replaced with DI water. The mAb showed precise bands clustered around 150 kDa in lane 1. In lane 2, some streaking of the monomeric bands occurs after buffer exchange with three diavolumes of water. A dimer band also formed in lane 2. Lanes 3 and 4 lack the monomeric bands at 150 kDa when the mAb is completely desalted by buffer exchange with 10 diavolumes of DI water. It is theorized that a significant portion of the mAb formed large irreversible aggregates in DI water.

In Figure 4.27 below, mAb M BioEX filtration fractions were characterized using SDS PAGE to observe any attribute changes between fractions.



**Figure 4.27:** SDS PAGE of mAb M Feed Titrated to Different pH Values

Figure 4.27 shows that size variants could not be resolved between the BioEX feed and the BioEX filtrate using SDS PAGE. The buffer chase appeared to have lower molecular weight bands than the feed and permeate. The type of ultrafiltration/diafiltration protocol did not significantly alter the mAb monomer bands. SDS PAGE is not a sufficiently high-resolution technique for studying microheterogeneity in therapeutic proteins. Figure 4.28 below shows the SDS PAGE spectra for BioEX filtration fractions of mAb M in 20 mM sodium acetate buffer without salt.

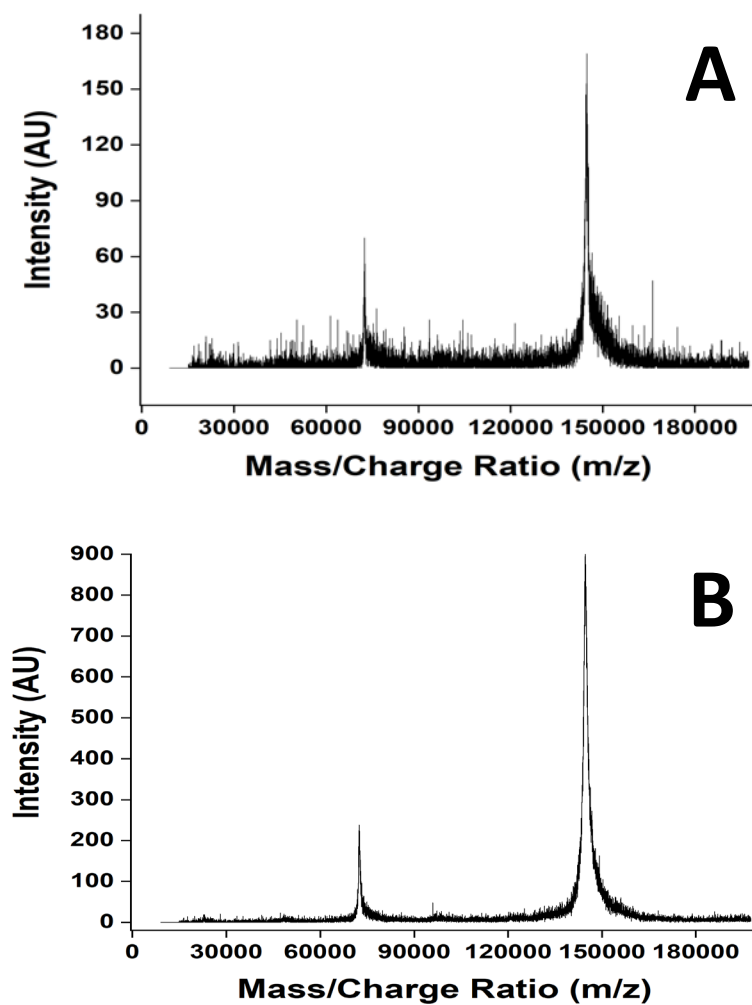


**Figure 4.28:** SDS PAGE of BioEX Fractions (No Prefiltration) for mAb M in 20 mM Sodium Acetate Buffer, No Salt

mAb M is highly unstable in low pH and low ionic strength buffers, as shown in Figure 4.28 above; the monomeric peaks were not present in this condition. It is theorized that the mAb monomers multimerize into large, irreversible aggregates. At the same time, a portion disintegrates into small, 25 kDa fragments. This phenomenon was supported by capillary electrophoresis and MALDI analysis.

#### 4.4.5. MALDI MS Characterization of mAb M Fractions

MALDI MS was performed on the various filtration fraction to evaluate the size heterogeneity of mAb monomers in the VPro feed and permeate filtration fractions, as shown in Figure 4.29 below.



**Figure 4.29:** MALDI MS Spectra for VPro Feed (A) and VPro Permeate (B) Fractions in 20 mM Histidine Buffer, pH 5.11

MALDI MS could not resolve the monomers from the higher molecular weight peaks expected at 171 kDa from CE-SDS. The double-charged ions show at 75 kDa in both instances. MALDI MS was also used to characterize desalted mAb M, and no monomeric peaks were observed at 150 kDa.

## 4.5 Conclusion

Prefiltration studies of mAb B in section 3 showed that size-exclusion-based prefilters were not effective in preventing flux decay in virus filters; hence, the focus on adsorptive prefilters in this section for mAb M. mAb M was generally a well-behaved mAb in histidine buffers pH 5.11 and pH 6.7 without salt as little fouling occurred. The use of adsorptive prefilters improved mAb M flux in the VPro and BioEX virus filters, as shown in this section, and validates earlier results obtained in section 3. However, mAb M was unstable and denatured rapidly when constituted in pH 5 acetate buffer (20 mM without salt) or when desalted in DI water.

CE-SDS characterization showed a higher molecular weight monomeric variant of mAb M decreased from the feed fraction to the BioEX filtrate fraction, as confirmed with mAb B in section 3. The presence of NaCl in very high concentrations did not significantly denature mAb M when constituted in histidine buffer thereby showing that histidine is an appropriate buffer for mAb M storage.

Virus filter fouling is mAb-specific. For mAb M, fouling is chiefly caused by soluble aggregation of mAb monomers at the virus filtration membrane's interface. As discussed in this dissertation, a host of factors can predispose a mAb to soluble aggregation. However, one of the main reasons adduced for soluble aggregation is the hydrophobicity and charge asymmetry of mAb variants and denatured monomers which self-associate during the concentration polarization that occurs at the virus filter's membrane interface. Hydrophobic patches can transiently multimerize to slow down the transport of mAbs in the narrow capillaries and cause flux decay.

mAb stability plays a considerable role in filterability with virus filters. Factors that determine the flux behavior of a mAb in virus filter mAb properties, prefilter properties, buffer excipients, and types of polishing steps used to pretreat the mAb before shipment. We have shown that arginine and histidine are suitable excipients for mAb M stability. Sodium phosphate at pH 5 is not a good formulation buffer for mAb M.

## References

1. Rogers, R.S., et al., Development of a quantitative mass spectrometry multi-attribute method for characterization, quality control testing and disposition of biologics. *MAbs*, 2015. 7(5): p. 881-90.
2. Robinson, J., D. Roush, and S. Cramer, Domain contributions to antibody retention in multimodal chromatography systems. *J Chromatogr A*, 2018. 1563: p. 89-98.
3. Roberts, C.J. and M.A. Blanco, Role of anisotropic interactions for proteins and patchy nanoparticles. *J Phys Chem B*, 2014. 118(44): p. 12599-611.
4. Nicolau, D.V., Jr., et al., Mapping hydrophobicity on the protein molecular surface at atom-level resolution. *PLoS One*, 2014. 9(12): p. e114042.
5. Masuda, Y., et al., The prevention of an anomalous chromatographic behavior and the resulting successful removal of viruses from monoclonal antibody with an asymmetric charge distribution by using a membrane adsorber in highly efficient, anion-exchange chromatography in flow-through mode. *Biotechnol Prog*, 2020. 36(3): p. e2955.
6. Regnier, F.E., The role of protein structure in chromatographic behavior. *Science*, 1987. 238(4825): p. 319-23.
7. Lesin, V. and E. Ruckenstein, Chromatographic probing of protein-sorbent interactions. *Journal of Colloid and Interface Science*, 1989. 132(2): p. 566-577.
8. Chung, W., et al., Investigation of protein binding affinity and preferred orientations in ion exchange systems using homologous protein library. *Biotechnology and bioengineering*, 2009. 102: p. 869-81.
9. Mahn, A., M.E. Lienqueo, and J. Asenjo, Effect of surface hydrophobicity distribution on protein retention in hydrophobic interaction chromatography. *Journal of Chromatography A*, 2004. 1043.

10. Jabra, M.G., et al., pH and excipient profiles during formulation of highly concentrated biotherapeutics using bufferless media. *Biotechnol Bioeng*, 2020. 117(11): p. 3390-3399.
11. Insaïdoo, F.K., et al., Targeted purification development enabled by computational biophysical modeling. *Biotechnol Prog*, 2015. 31(1): p. 154-64.
12. Coffman, J., et al., Highland games: A benchmarking exercise in predicting biophysical and drug properties of monoclonal antibodies from amino acid sequences. *Biotechnol Bioeng*, 2020. 117(7): p. 2100-2115.
13. Rogers, R.S., et al., A View on the Importance of "Multi-Attribute Method" for Measuring Purity of Biopharmaceuticals and Improving Overall Control Strategy. *AAPS J*, 2017. 20(1): p. 7.
14. Jakes, C., et al., Tracking the Behavior of Monoclonal Antibody Product Quality Attributes Using a Multi-Attribute Method Workflow. *J Am Soc Mass Spectrom*, 2021. 32(8): p. 1998-2012.
15. Carillo, S., et al., Comparing different domains of analysis for the characterisation of N-glycans on monoclonal antibodies. *J Pharm Anal*, 2020. 10(1): p. 23-34.
16. Dimer, F. and J. Hubbuch, 3D structure-based protein retention prediction for ion-exchange chromatography. *J Chromatogr A*, 2010. 1217(8): p. 1343-53.
17. Dimer, F., M. Petzold, and J. Hubbuch, Effects of ionic strength and mobile phase pH on the binding orientation of lysozyme on different ion-exchange adsorbents. *J Chromatogr A*, 2008. 1194(1): p. 11-21.
18. Fitch, C.A., et al., Arginine: Its pKa value revisited. *Protein Sci*, 2015. 24(5): p. 752-61.
19. Junter, G.A. and L. Lebrun, Cellulose-based virus-retentive filters: a review. *Rev Environ Sci Biotechnol*, 2017. 16(3): p. 455-489.
20. Billups, M., et al., Antibody retention by virus filtration membranes: Polarization and sieving effects. *Journal of Membrane Science*, 2021. 620.
21. Yadav, S., S.J. Shire, and D.S. Kalonia, Factors affecting the viscosity in high concentration solutions of different monoclonal antibodies. *J Pharm Sci*, 2010. 99(12): p. 4812-29.
22. Bieberbach, M., et al., Investigation of fouling mechanisms of virus filters during the filtration of protein solutions using a high throughput filtration screening device. *Biotechnol Prog*, 2019. 35(4): p. e2776.
23. Arakawa, T., et al., The effects of arginine on protein binding and elution in hydrophobic interaction and ion-exchange chromatography. *Protein Expr Purif*, 2007. 54(1): p. 110-6.



24. Ejima, D., et al., Arginine as an effective additive in gel permeation chromatography. *J Chromatogr A*, 2005. 1094(1-2): p. 49-55.
25. Ho, J.G., et al., The likelihood of aggregation during protein renaturation can be assessed using the second virial coefficient. *Protein Sci*, 2003. 12(4): p. 708-16.
26. Buchner, J. and R. Rudolph, Renaturation, purification and characterization of recombinant Fab-fragments produced in *Escherichia coli*. *Biotechnology (N Y)*, 1991. 9(2): p. 157-62.
27. Liu, H., et al., Characterization of recombinant monoclonal antibody charge variants using WCX chromatography, icIEF and LC-MS/MS. *Anal Biochem*, 2019. 564-565: p. 1-12.
28. Xu, Y., et al., Structure, heterogeneity and developability assessment of therapeutic antibodies. *MAbs*, 2019. 11(2): p. 239-264.
29. King, C., et al., Characterization of recombinant monoclonal antibody variants detected by hydrophobic interaction chromatography and imaged capillary isoelectric focusing electrophoresis. *J Chromatogr B Analyt Technol Biomed Life Sci*, 2018. 1085: p. 96-103.
30. Joshi, S., et al., Monitoring size and oligomeric-state distribution of therapeutic mAbs by NMR and DLS: Trastuzumab as a case study. *Journal of Pharmaceutical and Biomedical Analysis*, 2021. 195.
31. Sadavarte, R., et al., Rapid preparative separation of monoclonal antibody charge variants using laterally-fed membrane chromatography. *J Chromatogr B Analyt Technol Biomed Life Sci*, 2018. 1073: p. 27-33.
32. Cao, M., et al., Identification of a CE-SDS shoulder peak as disulfide-linked fragments from common CH<sub>2</sub> cleavages in IgGs and IgG-like bispecific antibodies. *MAbs*, 2021. 13(1): p. 1981806.

## **5.0 Ultrafiltration based fractionation of biotherapeutics**

### **5.1 Introduction**

The biopharmaceutical industry has seen a rapid transformational growth in the past few decades, culminating in the complete mapping of the entire human genome [1]. Advances in gene therapy, cell therapy, and other biologic modalities reinforce the prospect of personalized medicine. With an exponential increase in the biologics pipeline of biopharmaceutical companies, robust and cost-effective purification processes have become even more pertinent. The biopharmaceutical industry is a highly regulated industry where unit operations are mostly standardized and templated.

There has been increased research in cost-effective biologics purification processes due to intense competition between biosimilar drug manufacturers and the patent holders of the biologic reference product [2, 3]. Downstream purification typically represents a significant cost sink in the biomanufacturing industry [4]. Estimates put a 50-80 percent production cost on downstream processing compared to the cost of upstream processes [4-7]. Downstream processing starts at the bioreactor harvest step. It culminates in a purified active biopharmaceutical ingredient formulated in a stable buffer for fill-finish and delivery to the end-user. Cost optimization efforts have been focused on downstream processing to reduce costs and maximize profitability.

Fractionation of species similar in size is critical for the validation of virus clearance. There is less than a two-fold difference in size between mAb monomers and non-enveloped parvoviruses. When ultrafiltration (UF) or diafiltration (DF) is mentioned, buffer exchange and product concentration typically come to mind. Ultrafiltration membranes are typically sized

according to molecular weight cutoffs (MWCO) in kilodaltons (kDa). The steric exclusion principle ensures that proteins that are significantly larger than the UF membrane's nominal MWCO are rejected while smaller-sized proteins preferentially pass through. Zydney et al. (2010) reported that both protein charge and membrane charge play a role in the rate of protein transport through a UF membrane [8]. Separation of proteins using ultrafiltration membranes ideally requires a molecular weight ratio (MWR) of 7-10 [9].

The partitioning efficiency of ultrafiltration membranes is around  $10^2$ , which is below chromatographic separation partitioning efficiency by two orders of magnitude [9, 10]. The low resolving power of single stack ultrafiltration membranes has limited the application of UF in partitioning multi-component protein mixtures with low MWRs. When UF membranes are stacked in series, the net effect is that a membrane with specific MWCO which is not industrially available becomes available. Conversely, using multiple single UF membranes in series would require more buffer flux and offer only commercially available MWCO's.

By combining the intrinsic charge of a UF membrane with proper buffer pH and ionic strength, some measure of partitioning between bio-analytes in a two-component protein mixture can be achieved. Sirkar et al. (2004) demonstrated that a pure protein component could be obtained from a two-component mixture using multiple UF membranes in a stack (internally staged ultrafiltration) [11, 12]. It is straightforward to visualize the separation of differently sized proteins using UF membranes. However, Sirkar et al. showed that similarly sized proteins could be separated by internally staged ultrafiltration with high purity levels. Electrostatic interactions are long-range interactions that play a role in the transmission and, by extension, the partitioning of proteins on an ultrafiltration membrane [8].

Multiple stacks of UF membranes when applied in internally staged ultrafiltration amplifies the number of theoretical plates involved in a two-component separation. The intrinsic charge of these membranes ensures that similarly charged proteins are rejected by the UF membrane stack while moderately uncharged proteins pass through the UF membrane [13]. Most commonly available polymeric membranes have a net negative charge in solution due to the presence of COOH ionizable groups [14]. These negatively charged polymeric membranes include regenerated cellulose membranes and polyethersulfone (PES) membranes. Figure 5.1 shows an internally staged UF system designed to partition two monoclonal antibodies with identical molecular masses and isoelectric point differences.



**Figure 5.1:** Layout of an Internally Staged Ultrafiltration System.

Figure 5.1 above shows the layout of a three-stage ultrafiltration-based mAb fractionation system. A mixture of two mAbs can therefore be separated on the basis of differences in isoelectric point. These two similarly sized mAbs can be separated by leveraging the isoelectric point difference. The mAb with a higher pI stays negatively charged. The negatively charged membrane rejects the net negatively charged mAb while the net neutral mAb passes through the membrane. This principle can also be applied in other biologic modalities, such as charge partitioning-assisted virus clearance in UF membranes.

## **5.2 Materials and Methods**

### **5.2.1 Materials**

Ultracel regenerated cellulose UF membranes (30 kDa and 100 kDa MWCO flat sheets) were provided by MilliporeSigma (Billerica, MA). Omega mPES UF membranes (100 kDa and 300 kDa MWCO flat sheets) were provided by Pall Corporation (NY). Sulfhydryl-blocked bovine serum albumin (BSA) was purchased from Lee Biosolutions (Maryland Heights, MO). Porcine hemoglobin was purchased as a lyophilized powder from MilliporeSigma (Billerica, MA).

OmniPur sodium acetate trihydrate (molecular biology grade) and glacial acetic acid (pharma grade) were sourced from MilliporeSigma (Billerica, MA). MVM (ATCC® VR1346™) was purchased from American Type Culture Collection (Manassas, VA). Amicon stirred ultrafiltration cells were provided by MilliporeSigma (Billerica, MA). Ultrapure water with a resistivity of 18.2 MΩ was used for buffer formulation. Nalgene™ rapid-flow™ sterile single-use bottle top filters (0.2-μm and 0.1-μm) were purchased from ThermoFisher Scientific (Waltham, MA).

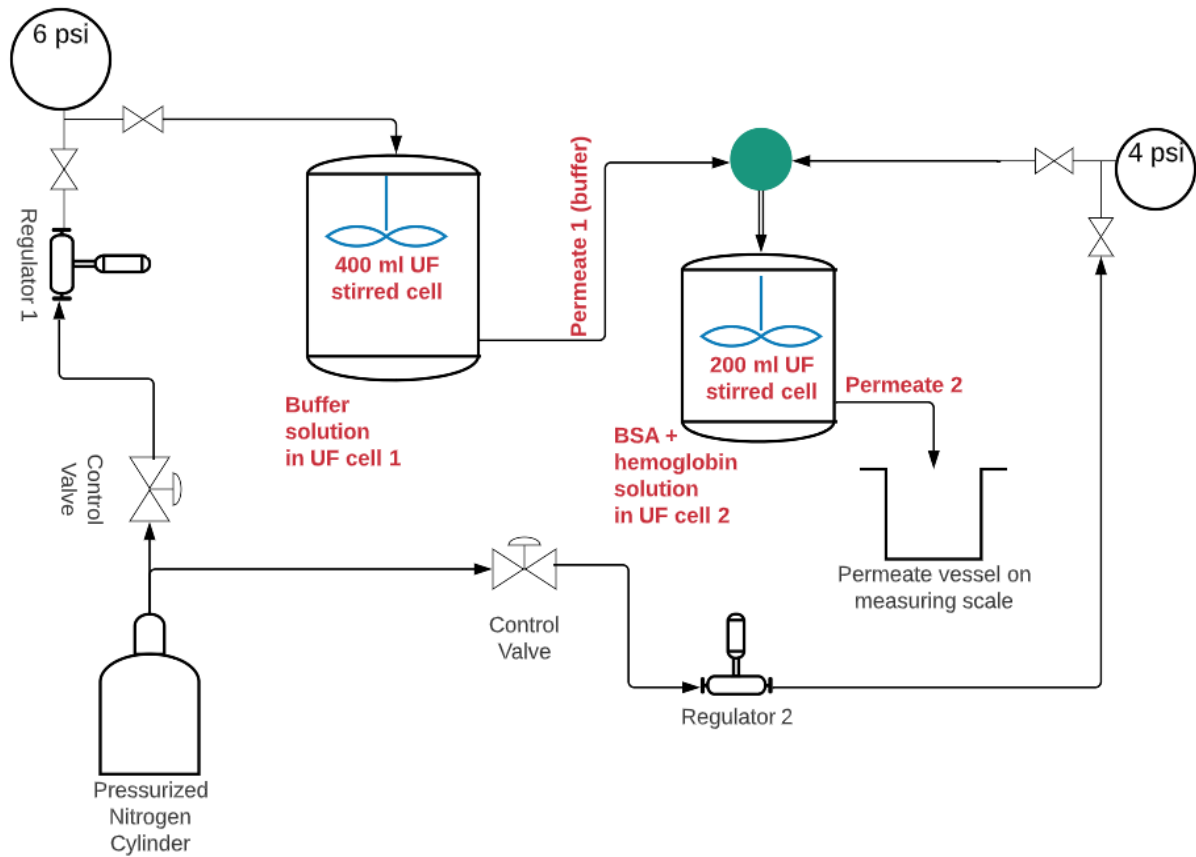
### 5.2.2 Methods

BSA and hemoglobin stock concentration was measured by UV spectrophotometric analysis at 280 nm using Genesys10 UV Scanning System (Waltham, MA) with VWR quartz spectrophotometer cell (path length 1 cm; West Chester, PA). Protein concentration was determined by measuring the absorbance at 280 nm for BSA and 407 nm for hemoglobin. Minute virus of mice (MVM) was used to perform virus clearance studies. MVM is a parvovirus referred to as the smallest virus in nature. Virus clearance studies are typically performed with parvovirus because UF membranes that provide a size cutoff of parvoviruses will ultimately reject the larger retroviruses.

Production of MVM from stock aliquot was performed by adapting a protocol from literature (U.S.A. Patent No. EP2377927A1, 2011) [15]. A9 cells (ATCC® CCL-1.4™) were used to mass-produce the MVM viruses, and the product was purified and centrifuged to desired values of virus titer. Titers of the MVM product were determined using real-time polymerase chain reaction (qPCR). The qPCR instrument was a Bio-Rad CFX Connect Real-Time System (Hercules, CA) with Bio-Rad CFX Manager software. qPCR quantifies the number of copies of viral genomes in viral samples [15]. The viral titer was calculated by plotting on a standard curve. Log reduction values of MVM between feed and permeate samples were determined by subtracting the virus titer of the permeate from that of the feed sample.

BSA, hemoglobin, and MVM solutions were constituted in 2.3 mM sodium acetate buffer, either at pH 4.8 or pH 6.8. A low conductivity buffer prevents electrostatic shielding of the negatively charged membrane's interaction with the proteins. Amicon ultrafiltration stirred cells are typically used when testing ultrafiltration membranes to prevent concentration polarization and ensure continuous homogenization of the feed or sample. Flat sheet UF

membranes are punched to the appropriate diameters and stacked at the bottom of the stirred cell reservoir before an O-ring is used to ensure a tight seal. Figure 5.2 below shows the workflow for UF cells in series experiments.



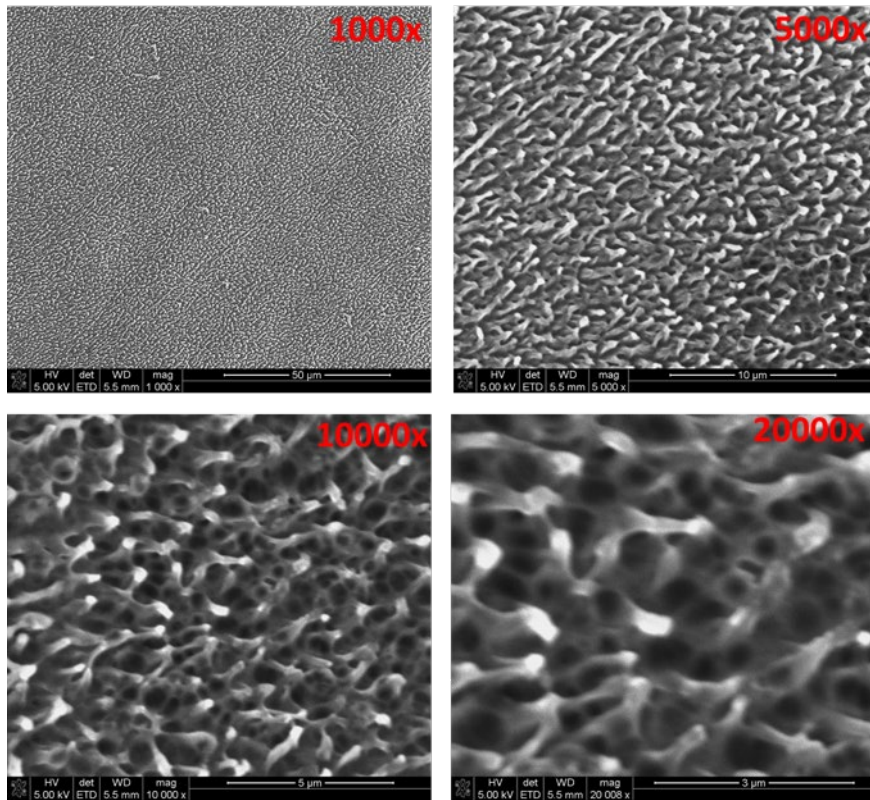
**Figure 5.2:** Workflow for an Amicon UF Cell in Series Experiment

Figure 5.2 above shows the schematic lines for performing a semi-batch fractionation of BSA and hemoglobin where the buffer in Amicon cell 1 replenishes Amicon cell 2 during internally staged ultrafiltration. A single pressurized nitrogen cylinder is used to pressurize both Amicon cells even though two pressure regulators are required. The pressure is regulated so that the downstream Amicon cell operates at a lower pressure. This prevents backpressure and enables buffer flow from Amicon cell 1 into the downstream Amicon cell.

## 5.3 Results

### 5.3.1 Partitioning of Proteins using Internally Staged Ultrafiltration (ISUF)

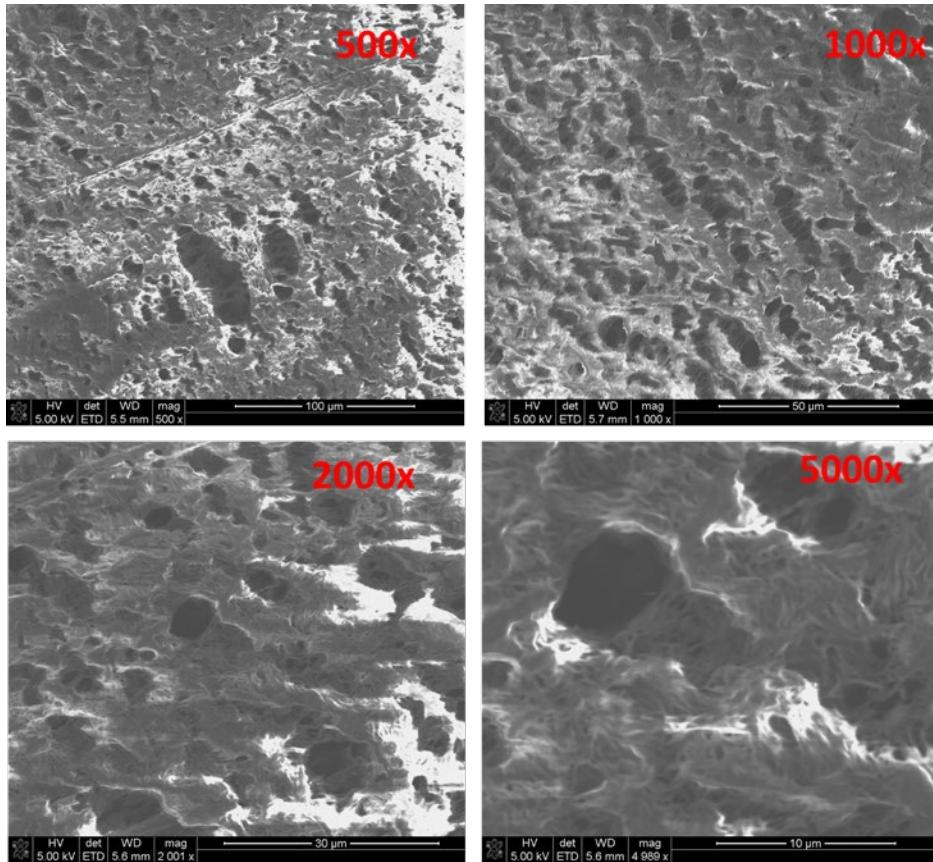
BSA and hemoglobin were selected as the proteins of interest in a two-component system. BSA has an isoelectric point of 4.7 and a molecular weight of 66 kDa. Hemoglobin has an isoelectric point of 6.8 and a molecular weight of 65 kDa. The UF membranes were previously established to be negatively charged at stated buffer conditions using zeta potential. These negatively charged membranes were then used in singles, then double stacks. Membranes were also evaluated by flipping the sides facing the feed stream from the retentive skin side to the support structure (backing side). Figure 5.3 shows the scanning electron microscopy images of the 30 kDa ultracel membrane at different magnifications.



**Figure 5.3:** SEM Images for Skin Side of 30 kDa MWCO RC Ultracel Membrane



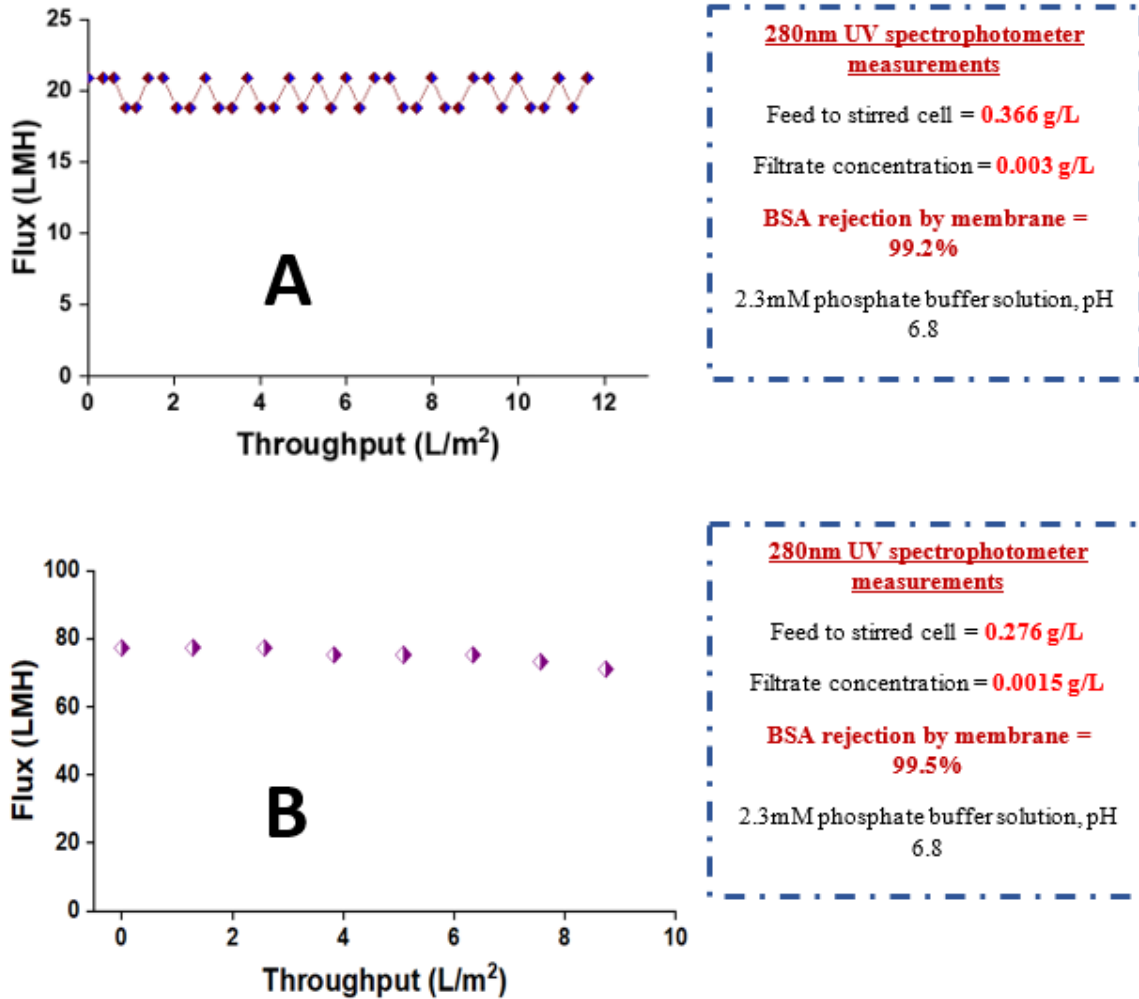
Figure 5.3 above shows that the skin side is the active separation layer. It is homogenous in pore size distribution, unlike the backing side shown in Figure 5.4 below.



**Figure 5.4:** SEM Images for the Backing Side of 30 kDa MWCO RC Ultracel Membrane

The support structure (backing) side of the UF membrane provides structural rigidity and mechanical integrity to the separation-active layer. Ultrafiltration membranes typically have more open pores and pore size asymmetry on the backing side. The fouling propensity is typically different with the skin side facing the feed than when the backing side faces the feed.

Flux experiments were performed initially with just BSA to determine the sealing integrity of the Amicon cell with an Ultracel 30 kDa MWCO membrane, as shown in Figure 5.5 below.

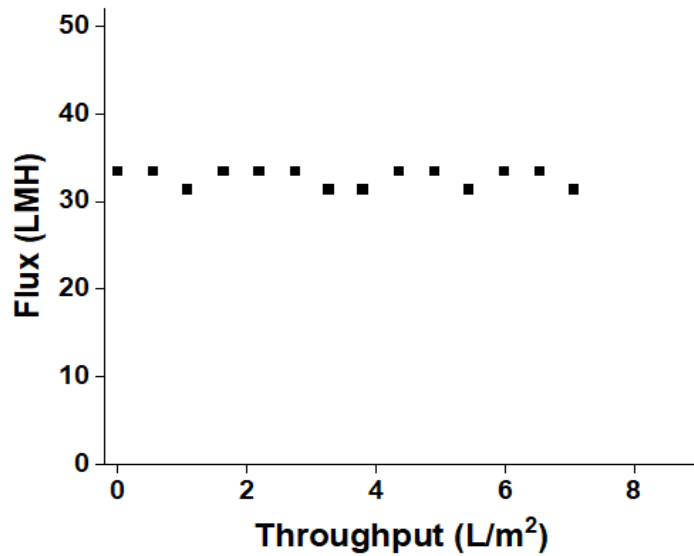


**Figure 5.5:** Ultrafiltration using a Single 30 kDa Ultracel RC Membrane to Evaluate BSA Rejection with (A) Skin Side as Feed-Facing. (B) Backing Side as Feed-Facing.

The BSA and hemoglobin separation experiments typically attain high separation into single-component systems over long hours of continuous filtration and continuous dilution of feed in the Amicon cell. If filtration occurs in an Amicon cell without continuous dilution, the concentration of biomolecules in the Amicon cell goes up. This increases the passage of undesirable components into the permeate and hinders separation. The absence of a selector valve connected to a buffer reservoir hinders high purity separation using the ISUF technique.

### 5.3.2 MVM Clearance using Internally Staged Ultrafiltration

These experiments were designed to separate MVM from a spiked solution in different combinations of stacked ultrafiltration membranes. Permeate fractions were collected while MVM titer was determined with qPCR, as shown in Figure 5.6 below.



Filtration fraction	qPCR titer (logs/ml)
Feed	8.80 ± 0.117
Permeate	3.83 ± 0.455

- qPCR Logarithmic reduction value (LRV) = 4.97 logs/mL
- 20 mM sodium acetate buffer, pH 4.8
- Pall omega 300 kDa + 100 kDa MWCO mPES membranes
- Initial virus titer spiked = 8.80 logs
- Backing side of membranes were feed-facing
- 3 psi operating pressure

**Figure 5.6:** Ultrafiltration of MVM-spiked, pH 4.8 Acetate Buffer using Double Pall Omega 300 kDa + Pall Omega 100 kDa MWCO Membranes at 3 psi (Backing Sides were Feed-Facing).

The objective of stacking double ultrafiltration membranes was to evaluate the increment in virus clearance between one UF membrane and stacked UF membranes. Figure 5.6 is one example of the virus clearance experiments that were conducted. The rest of the virus clearance experiments with different membrane stack combinations are shown in Table 5.1.

**Table 5.1:** Summary of Virus Clearance Experiments for Multiple Configurations of UF Membranes in Ultrafiltration Stirred Cells.

Membrane(s)	No. of membranes	Skin side or backing	Operating pressure	BSA rejection	MVM rejection (qPCR)	BSA feed concentration and buffer pH
Millipore Ultracel 30 kDa	1	Skin	2 psi	99.30%	4.35 logs	10 g/L, pH 6.8
Millipore Ultracel 30 kDa	1	Backing	35 psi	92.10%	3.73 logs	10 g/L, pH 6.8
Millipore Ultracel 100 kDa	1	Skin	2 psi	6.70%	3.61 logs	0.6 g/L, pH 4.8
Millipore Ultracel 100 kDa	1	Backing	2 psi	3.20%	4.17 logs	0.6 g/L, pH 4.8
Pall Omega 100 kDa	1	Skin	2 psi	21.20%	3.58 logs	0.6 g/L, pH 4.8
Pall Omega 100 kDa	1	Backing	2 psi	11%	3.58 logs	0.6 g/L, pH 4.8
Pall Omega 300 kDa	1	Skin	2 psi	No BSA	3.45 logs	pH 4.8
Pall Omega 300 kDa	1	Backing	2 psi	No BSA	4.18 logs	pH 4.8
Millipore Ultracel 100 kDa	2	Skin-Backing	3 psi	No BSA	4.57 logs	pH 4.8
Pall Omega 300 kDa	2	Skin-Backing	3 psi	No BSA	4.33 logs	pH 4.8
Millipore Ultracel 100 kDa + Millipore ultracel 30 kDa	2	Skin-Skin	3 psi	No BSA	5.09 logs	pH 4.8
Pall omega 300 kDa + Pall omega 100 kDa	2	Skin-Skin	3 psi	No BSA	5.49 logs	pH 4.8
Pall omega 300 kDa + Pall omega 100 kDa	2	Backing-Backing	3 psi	No BSA	4.97 logs	pH 4.8
Millipore Ultracel 100 kDa + Millipore ultracel 30 kDa	2	Backing-Backing	3 psi	No BSA	4.28 logs	pH 4.8
Pall Omega 300 kDa + Millipore ultracel 30 kDa	2	Skin-Skin	3 psi	No BSA	4.76 logs	pH 4.8

Table 5.1 shows an increase in the number of membranes per stack and virus clearance. The backing side of these UF membranes tended to foul in the presence of BSA more than the skin

side. The backing side often required higher pressure to maintain flow, as shown in row 2 with the Millipore ultracel 30 kDa backing side (35 psi). The increased pressure potentially resulted in a loss of amicon cell sealing integrity, leading to increased MVM titer in the permeate and reduced LRV. All other experiments were conducted at 2 psi for single membranes and 3 psi for double membranes. A target value of 8 logs feed virus titer was used across experiments involving single membranes. In comparison, a target of 9 logs feed virus titer was used for the double membranes. Nine logs represent  $10^9$  virus particles, while eight logs represent  $10^8$  virus particles. The increase in feed virus titer for double membranes by 1 log enabled better permeate virus titer evaluation by qPCR. LRVs were the difference between feed and permeate MVM titers.

## **Conclusion**

Multi-component systems may be challenging to separate with single UF devices having a unit molecular weight cutoff. ISUF proffers an alternative option by changing the skin and backing sides of UF membranes in a stack, thereby attaining unique MWCOs. The pore size of UF membranes, biomolecular size, and membrane charge are parameters that can be optimized to obtain effective ISUF systems. Using the ISUF technique, ultrafiltration-based fractionation can lead to cost-effective purification of industrial pools of biomolecules requiring separation. Food items such as milk can be made lactose-free in a cost-effective way using UF membranes to remove lactose in the permeate. Staging the membranes could potentially achieve better results.

The ISUF technique was used to study MVM (parvovirus) rejection in multi-stack membranes with multiple configurations, such as Omega PES 300 kDa skin-backing versus backing skin. The addition of UF membranes to a filtration stack increased the rejection of MVM

as measured with qPCR, especially when the feed-facing layer was on the skin side of the membrane. Combining the Omega PES 300 kDa with the Omega PES 100 kDa membrane (skin-skin) resulted in 5.5 logs rejection of MVM at pH 4.8. 5.5 logs LRV implies the difference in the number of virus particles from the feed to the permeate was  $10^{5.5}$  virus particles.

## References

1. Nagappa, A.N. and S. Bhatt, *Biotherapeutics: Monoclonal Antibodies, Biologicals, Biogenerics, Biosimilar, and Biobetters*, in *Perspectives in Pharmacy Practice: Trends in Pharmaceutical Care*, A.N. Nagappa, et al., Editors. 2022, Springer Singapore: Singapore. p. 255-262.
2. Isu, S., et al., *Process- and Product-Related Foulants in Virus Filtration*. *Bioengineering*, 2022. 9(4).
3. Udpa, N. and R.P. Million, *Monoclonal antibody biosimilars*. *Nature Reviews Drug Discovery*, 2016. 15(1): p. 13-14.
4. Farid, S.S., *Process economics of industrial monoclonal antibody manufacture*. *J Chromatogr B Analyt Technol Biomed Life Sci*, 2007. 848(1): p. 8-18.
5. Gavara, P., et al., *Chromatographic Characterization and Process Performance of Column-Packed Anion Exchange Fibrous Adsorbents for High Throughput and High Capacity Bioseparations*. *Processes*, 2015. 3(1): p. 204-221.
6. Low, D., R. O'Leary, and N.S. Pujar, *Future of antibody purification*. *J Chromatogr B Analyt Technol Biomed Life Sci*, 2007. 848(1): p. 48-63.
7. Gottschalk, U. *Overview of Downstream Processing in the Biomanufacturing Industry*. 2011.
8. Rohani, M.M. and A.L. Zydney, *Role of electrostatic interactions during protein ultrafiltration*. *Adv Colloid Interface Sci*, 2010. 160(1-2): p. 40-8.
9. Cherkasov, A.N. and A.E. Polotsky, *The resolving power of ultrafiltration*. *Journal of Membrane Science*, 1996. 110(1): p. 79-82.
10. Polotskii, A.E. and A.N. Cherkasov, *Efficiency of membrane filtration in separation processes*. *Kolloidn. Z.*, 1988. 50: p. 287-292.
11. Feins, M. and K.K. Sirkar, *Highly selective membranes in protein ultrafiltration*. *Biotechnol Bioeng*, 2004. 86(6): p. 603-11.

12. Feins, M. and K.K. Sirkar, Novel internally staged ultrafiltration for protein purification. *Journal of Membrane Science*, 2005. 248(1-2): p. 137-148.
13. van Reis, R. and A. Zydney, Bioprocess membrane technology. *Journal of Membrane Science*, 2007. 297(1-2): p. 16-50.
14. Zydney, A., Charged Ultrafiltration Membrane, in *Encyclopedia of Membranes*, E. Drioli and L. Giorno, Editors. 2015, Springer Berlin Heidelberg: Berlin, Heidelberg. p. 1-2.
15. Namila, N., The Effects of Solution Condition on Virus Filtration Performance. 2020, University of Arkansas at Fayetteville: ProQuest LLC, Ann Arbor. p. 62.

## 6.0 Conclusion and Future Directions

A primary goal of this project is to address the high processing costs associated with mAb production through improvements in mAb prefiltration and virus filtration. This project was nominated by the industry advisory board and addressed an essential need in the biopharmaceutical space. This research correlates molecular properties of mAbs in different buffer conditions to fouling behavior in virus filters and guides prefilter selection criteria.

Some mAb variants with post-translational modifications have micro heterogeneous attributes that could increase fouling propensity, including loss of native-state conformations, charge variation, and hydrophobicity variation. mAb monomeric variants could foul virus filters through adsorptive cake formation or by forming reversible multimers that plug the virus filter pores.

Principally fouling mAb variants can be captured by optimizing the prefiltration process before virus filtration. The capture of principally fouling mAb variants enables longer runtimes for virus filter banks with seamless operations and fewer process downtimes, thereby reducing cost. Hydrophobic interaction chromatography membrane adsorbers were found to be very robust for mAb prefiltration in the buffer conditions evaluated for mAb B and M, including acetate buffers of pH 5, 7.5, and 8.6, as well as histidine only buffer of pH 5.1 and pH 6.7.

Future work could evaluate multiple mAb products from more biopharmaceutical companies to increase the data set for a machine learning model. Emphasis can be placed on mAb variant partitioning and characterization to identify mAb variants with high fouling index and create a guideline for prefilter selection. More work should be performed using virus filters



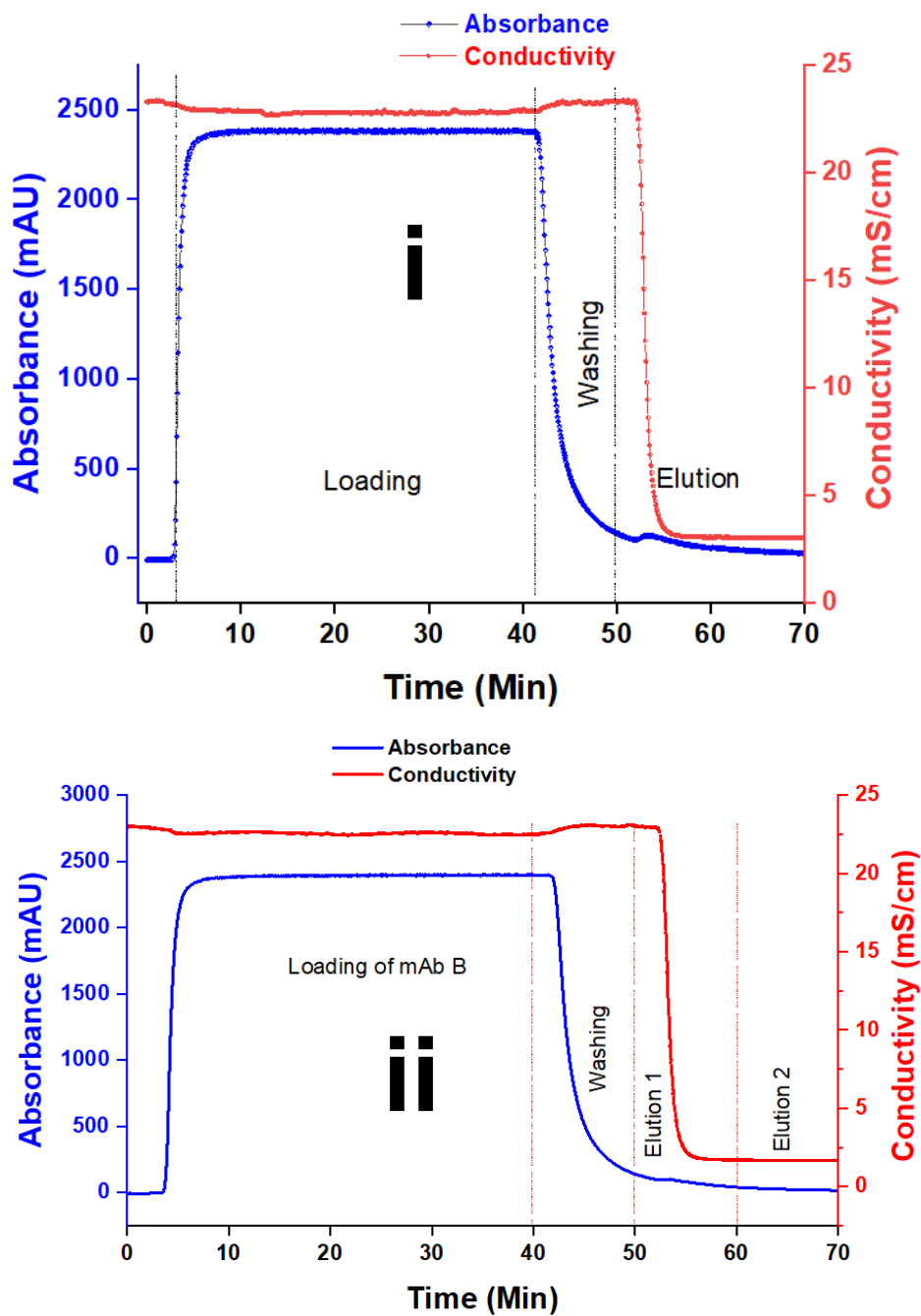
and prefilters from multiple manufacturers. Efforts should be made toward the assessment of multimodal prefilters and their impact on mitigating virus filter flux decay.

Further studies should try to identify mAb PTMs which promote rapid flux decay during virus filtration while critically examining the impact of mAb glycosylation on mAb filterability and stability. A filterability index for mAb products using experimental data would be the outcome of this expected database. A machine learning model could match mAb sequence, native conformation, PTMs, hydrophobicity, and solution conditions to filterability in different prefilter and virus filter types. The machine learning model would be a template for biopharmaceutical companies in process development for mAb production trains.

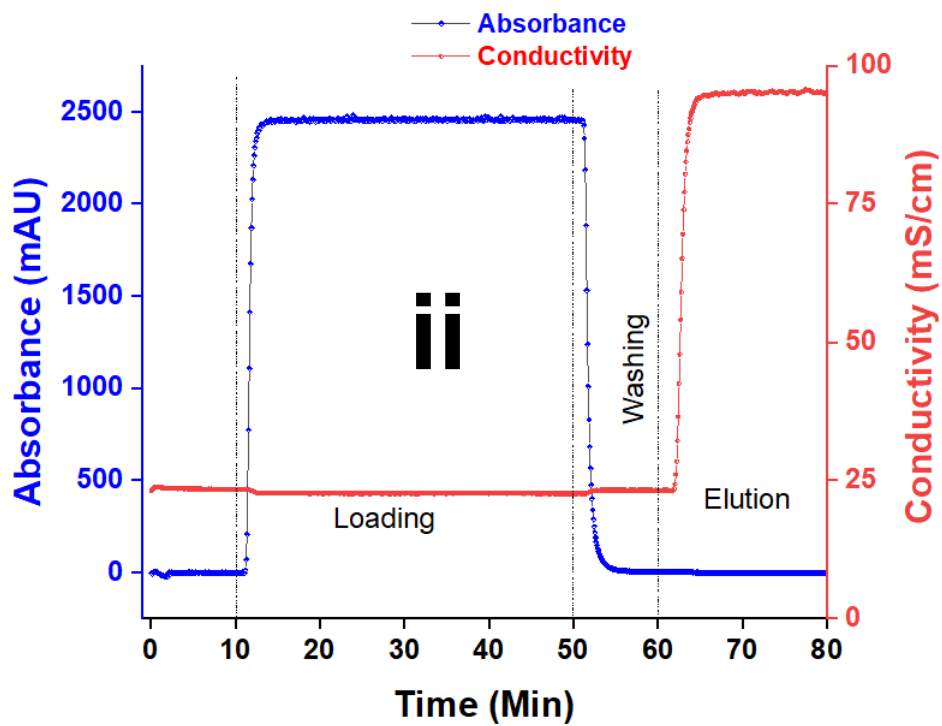
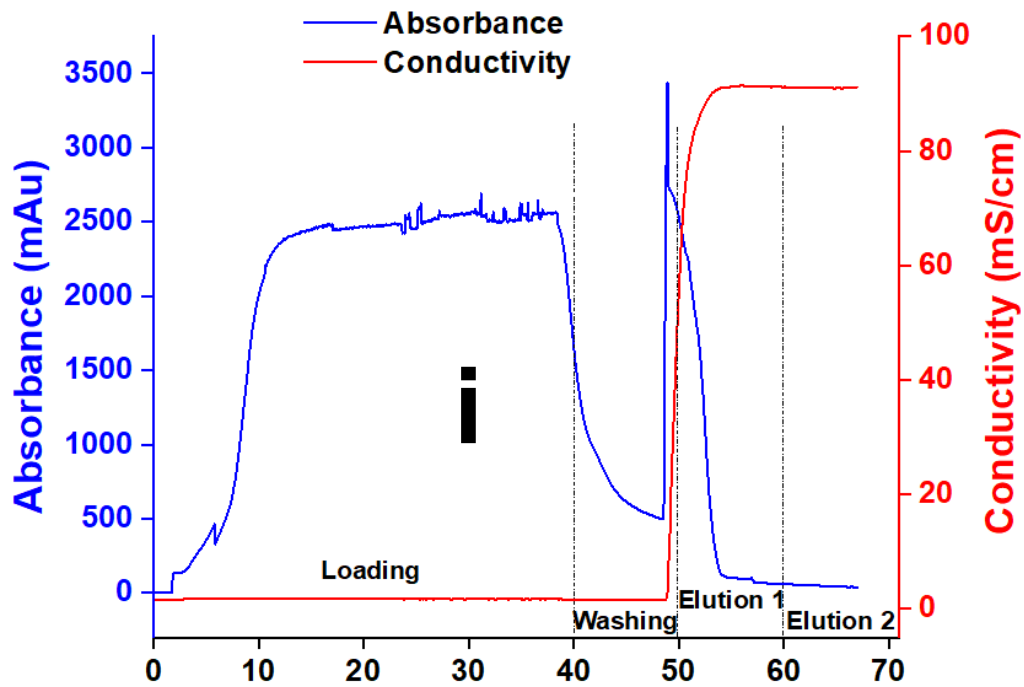
Optimizing the mAb formulation buffer during prefiltration will provide biopharmaceutical companies with a robust template for process development, maximize the performance of the virus filter and reduce drug end-user costs. Insights into the nature and characteristics of principal foulants can also help virus filter manufacturers to improve the design of virus filters for increased utility and safety. The intravenous mode of administering monoclonal antibodies to patients justifies investment in this research to improve mAb product safety and reduce the cost of mAb manufacture.

Based on the general scientific view that soluble aggregation causes virus filter fouling, as seen in multiple peer-reviewed publications and not disproved by our work, virus filter manufacturers can perform more flow field studies to design virus filtration membranes with better pore geometry that could mitigate plugging.

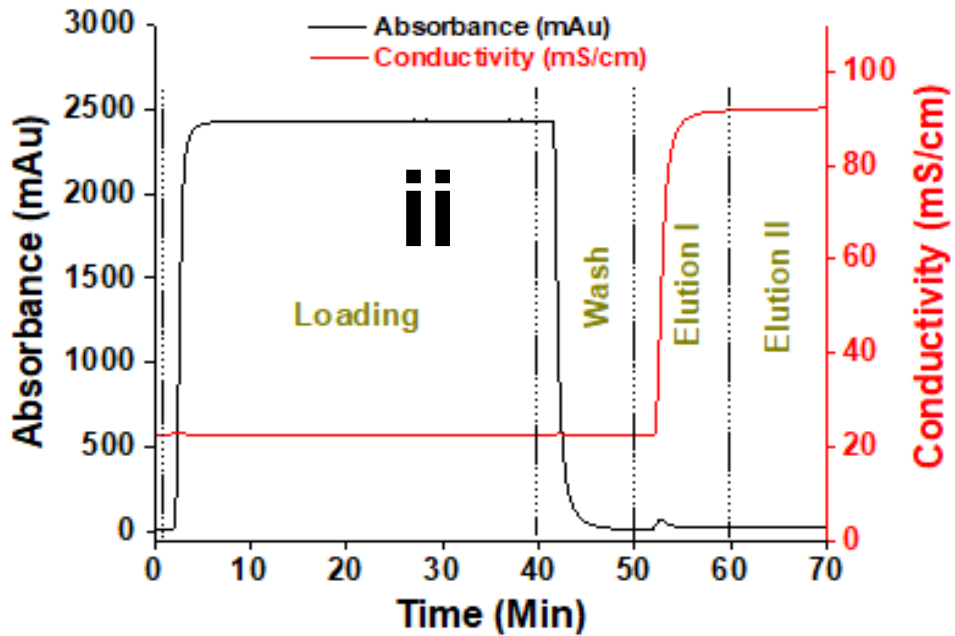
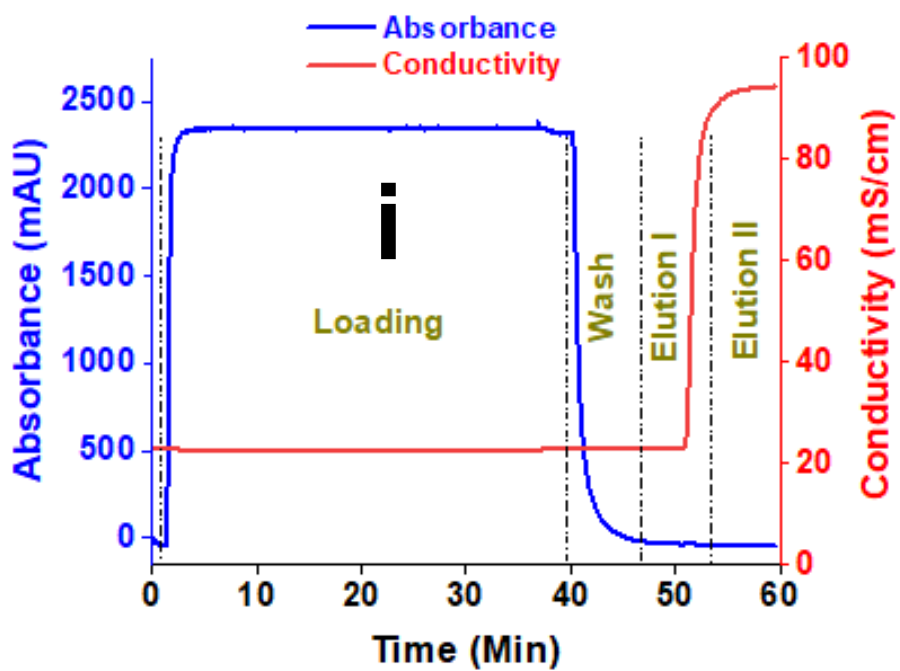
## Appendix A: Supplementary Chromatograms for Adsorptive Prefiltration of mAb B



**Figure A1:** Chromatograms for HIC Prefiltration of mAb B in 20 mM Sodium Acetate Buffer at (i) pH 7.5 with 200 mM NaCl. (ii) pH 8.6 with 200 mM NaCl.

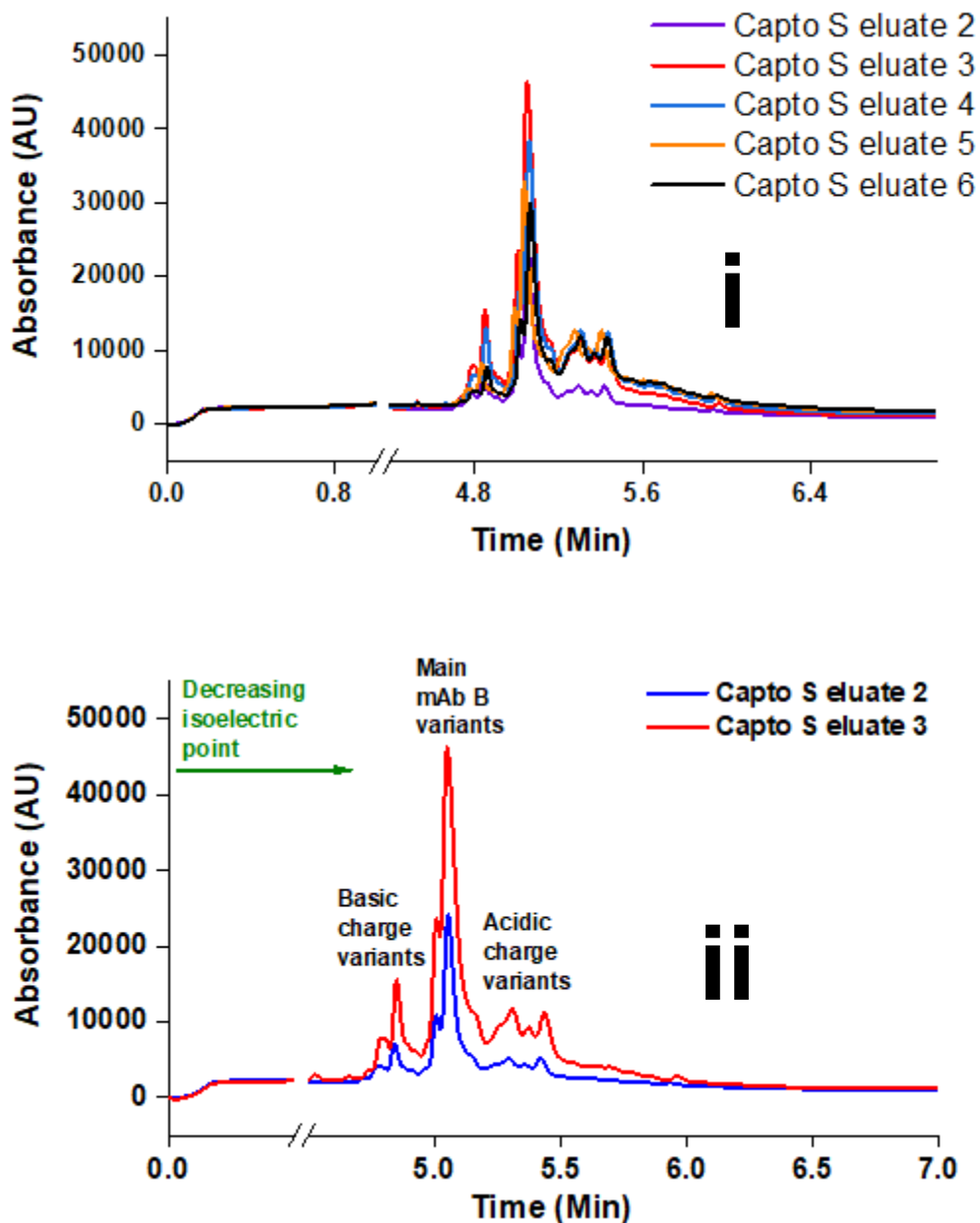


**Figure A2:** Chromatograms for IEX-S Prefiltration of mAb B in 20 mM Sodium Acetate Buffer at (i) pH 7.5 without Salt. (ii) pH 8.6 with 200 mM NaCl.



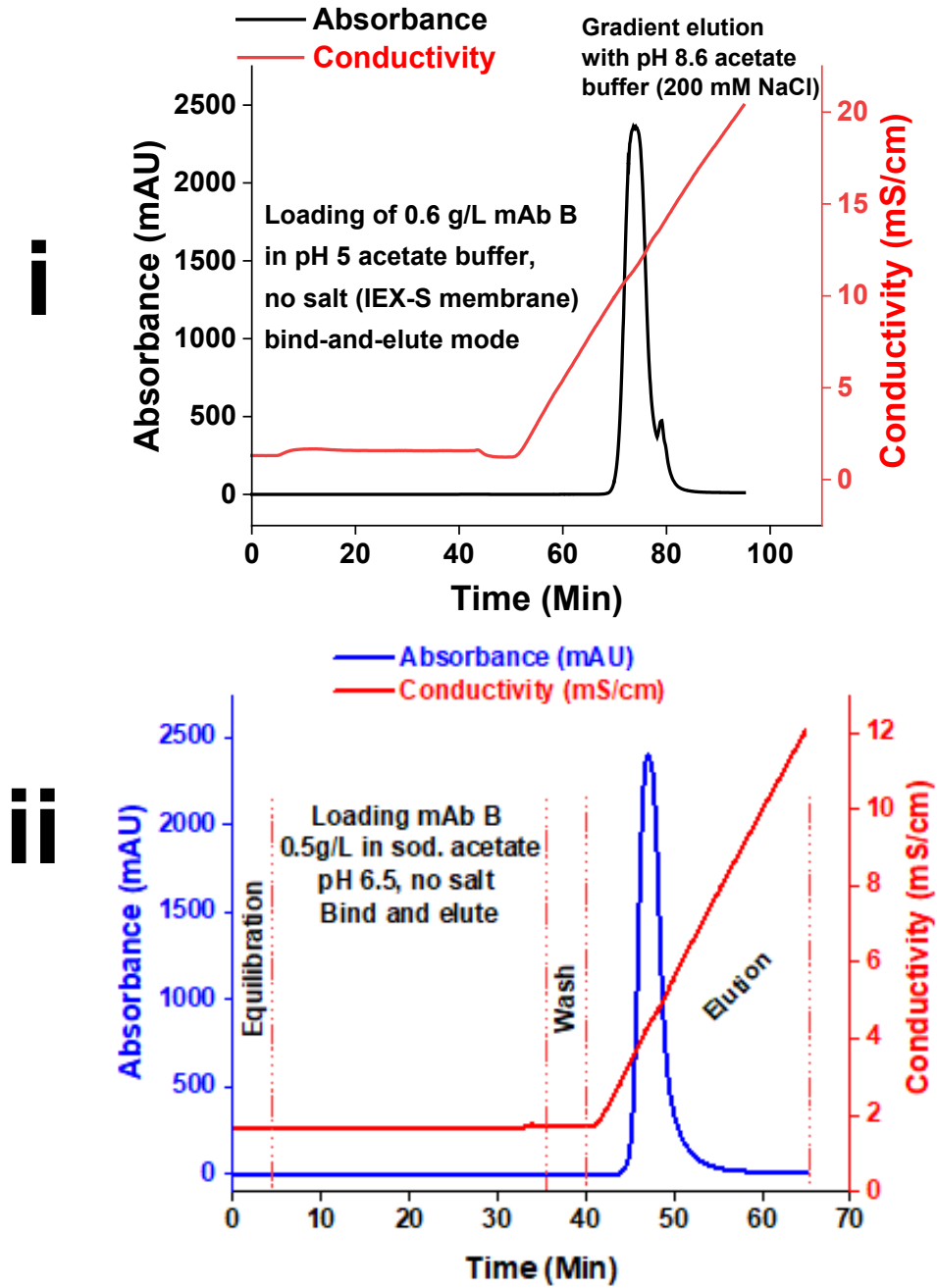
**Figure A3:** Chromatograms for IEX-Q Prefiltration of mAb B in 20 mM Sodium Acetate Buffer at (i) pH 5 with 200 mM NaCl. (ii) pH 8.6 with 200 mM NaCl.

## Appendix B: Supplementary Characterization for mAb B Bind-and-Elute Fractionation

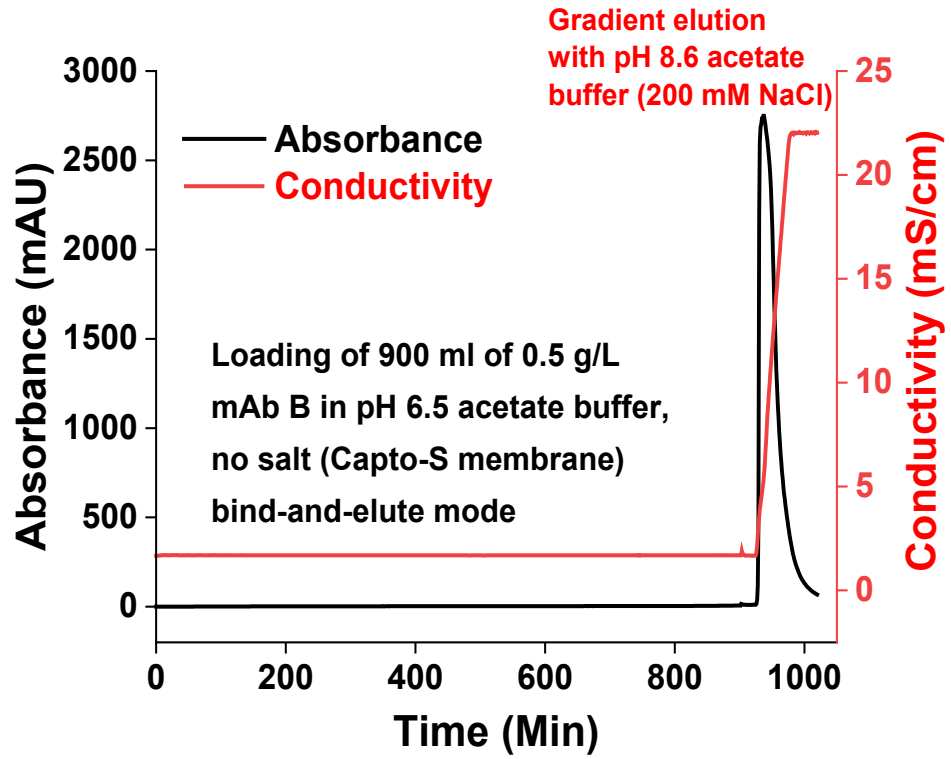


**Figure B1:** Capillary Zone Electrophoresis of mAb B Fractionated by Gradient Elution using a Capto S Cation Exchange Column after Bind-and-Elute (Buffer A: 20 mM Sodium Acetate, pH 6.5, No Salt. Buffer B: pH 8.6, 20 mM Sodium Acetate with 200 mM NaCl). (i) Composite Plot for Fractions 2 - 6. (ii) Plot of Capto S Eluate Fractions 2 and 3 Only.

Appendix C: mAb B partitioning using cation exchange columns in bind-and-elute mode

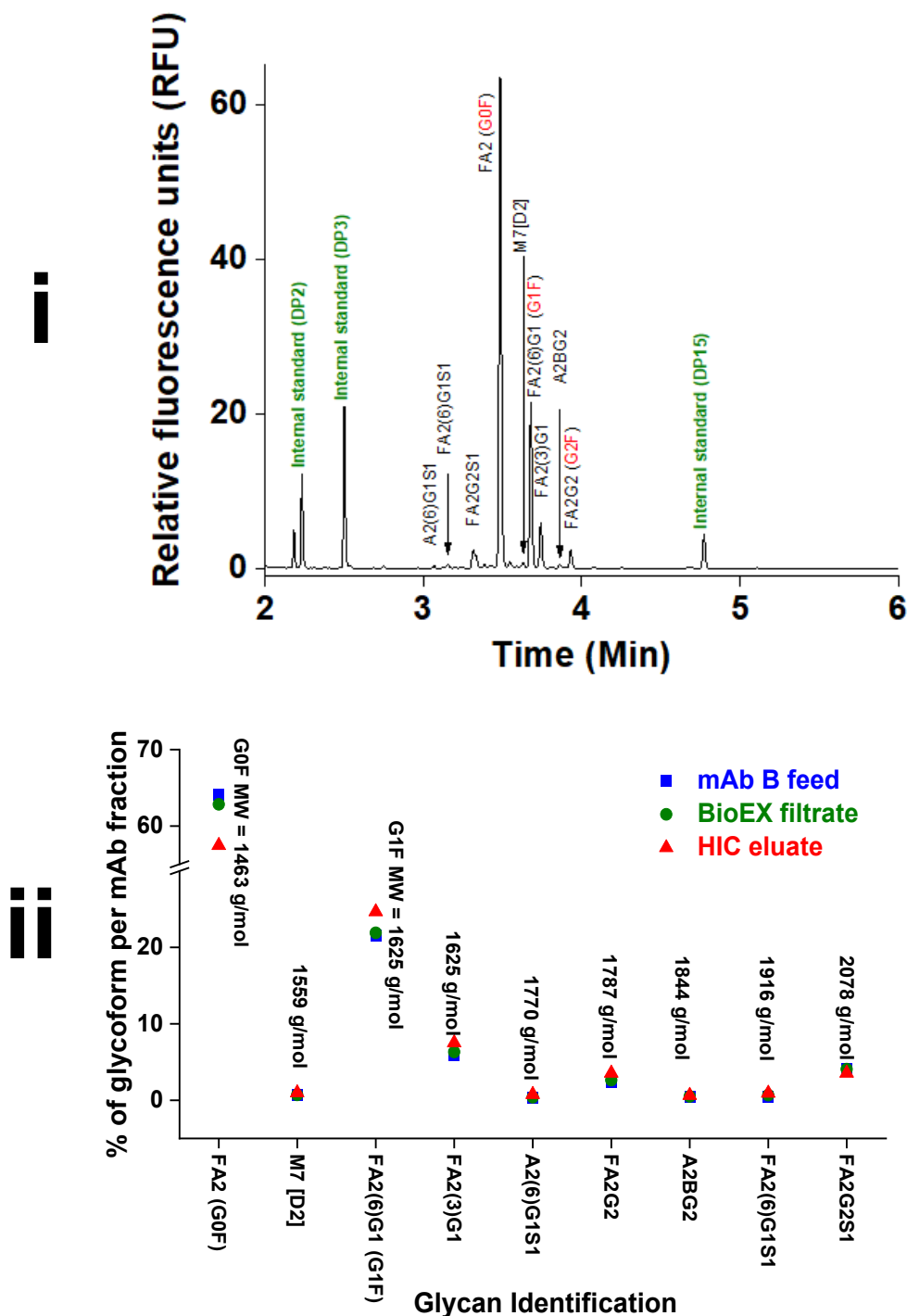


**Figure C1:** IEX-S Bind-and-Elute Chromatograms for Charge Variant Partitioning of mAb B in 20 mM Sodium Acetate Buffer (i) pH 5 without Salt. (ii) pH 6.5 without Salt.



**Figure C2:** Capto-S Bind-and-Elute Chromatograms for Charge Variant Partitioning of 0.5 g/L mAb B in 20 mM Sodium Acetate Buffer at pH 6.5 without Salt.

## Appendix D: Glycan Profiles of mAb B Determined using Capillary Electrophoresis

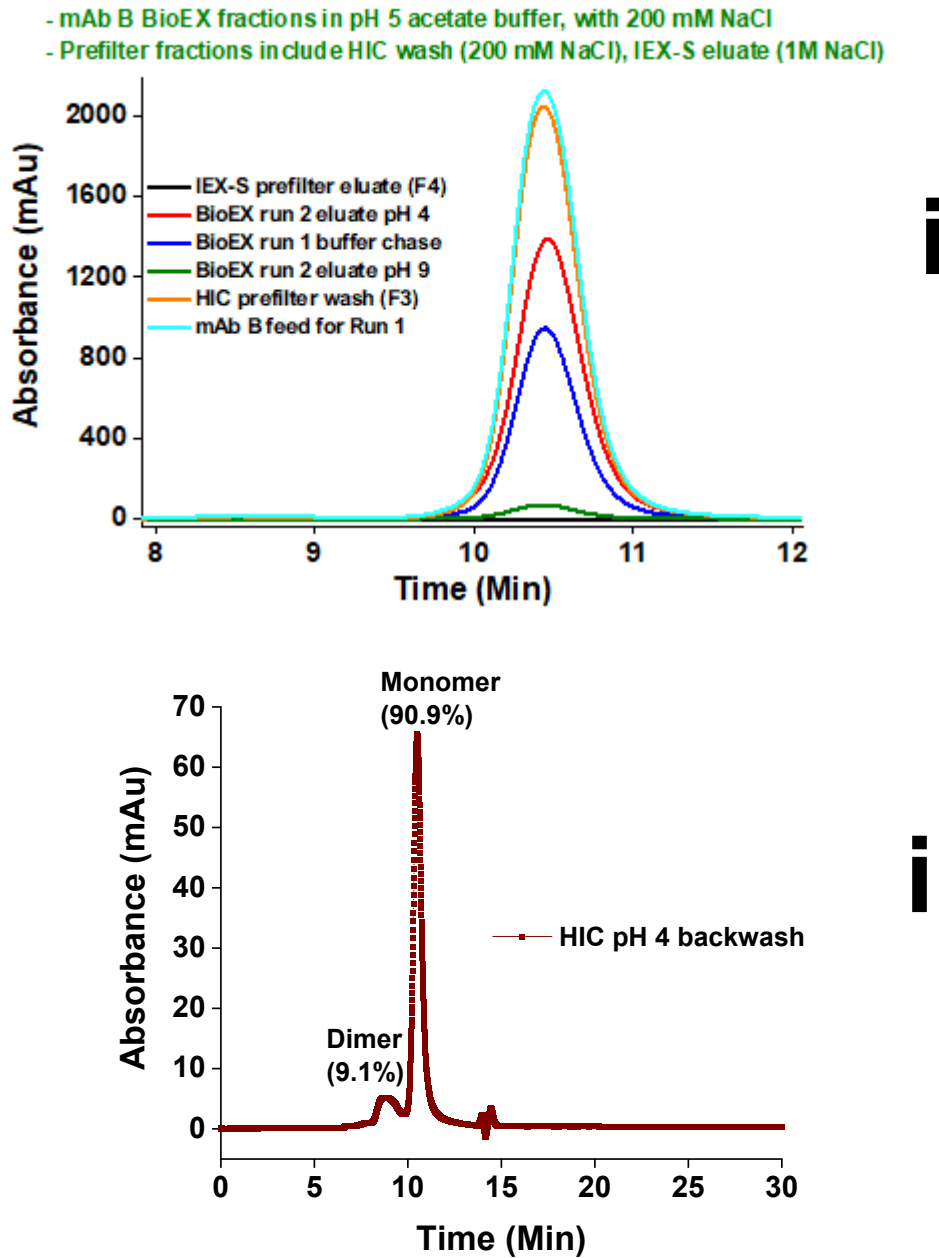


**Figure D1:** Fast Glycan Analysis Characterization of mAb B BioEX Filtration fractions in DI Water after PNGase Deglycosylation and Glycan Purification by Solid-Phase Extraction.



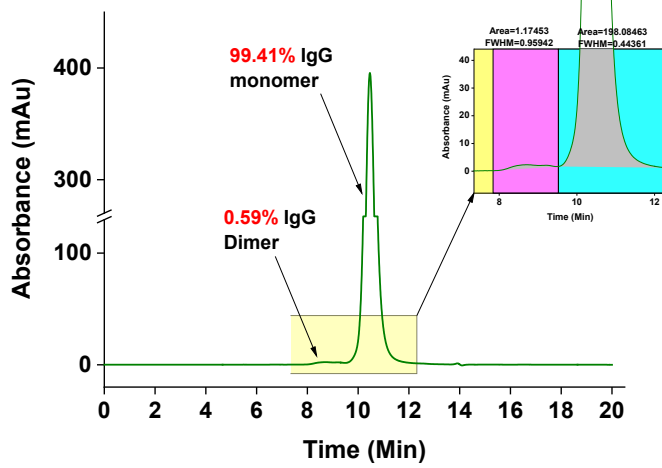
(i) Fast Glycan Electropherogram for mAb B Feed Desalted and Reconstituted in DI Water before Deglycosylation. (ii) Peak Integration Derived Quantification of Relative Percentages of Glycan Types in mAb B Feed, BioEX Filtrate, and HIC Eluate. MW of Each Glycan Category is included for Clarity.

## Appendix E: SEC data for mAb B prefiltration and virus filtration fractions

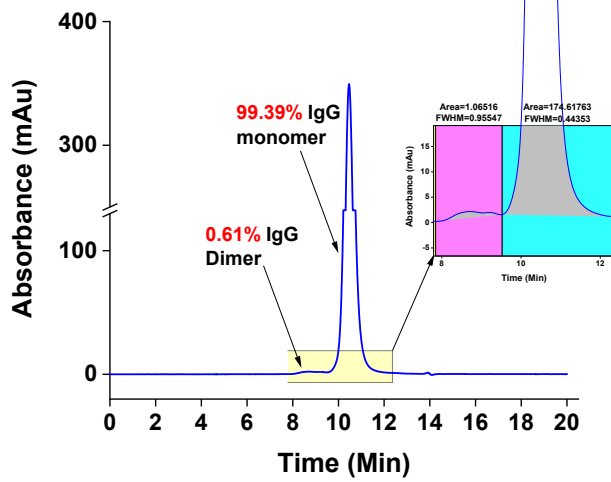


**Figure E1:** 220 nm Absorbance Spectra for TSKgel HPLC SEC Characterization of (i) mAb B Feed in 20 mM Sodium Acetate Buffer (pH 5 with 200 mM NaCl), BioEX Buffer Chase (pH 5 with 200 mM NaCl), BioEX Eluate Fractions (pH 4 and pH 9 without Salt), HIC Wash (pH 5 with 200 mM NaCl), and IEX-S Eluate Fraction (pH 5 with 1 M NaCl). (ii) HIC pH 4 Backwash.

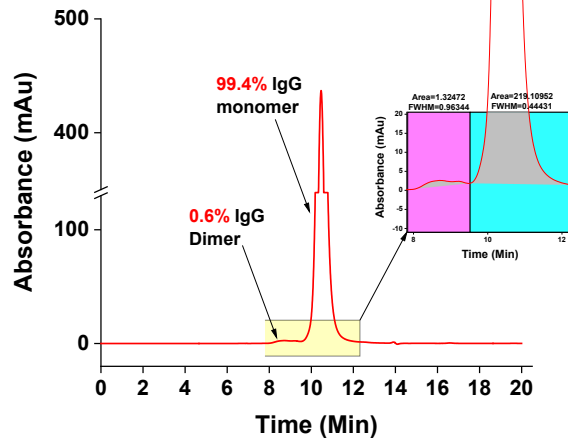
**Fresh mAb B feed before 0.2- $\mu$ m filter (no prefiltration)**



**BioEX filtrate (mAb B, pH 7.5, no salt, no prefiltration)**



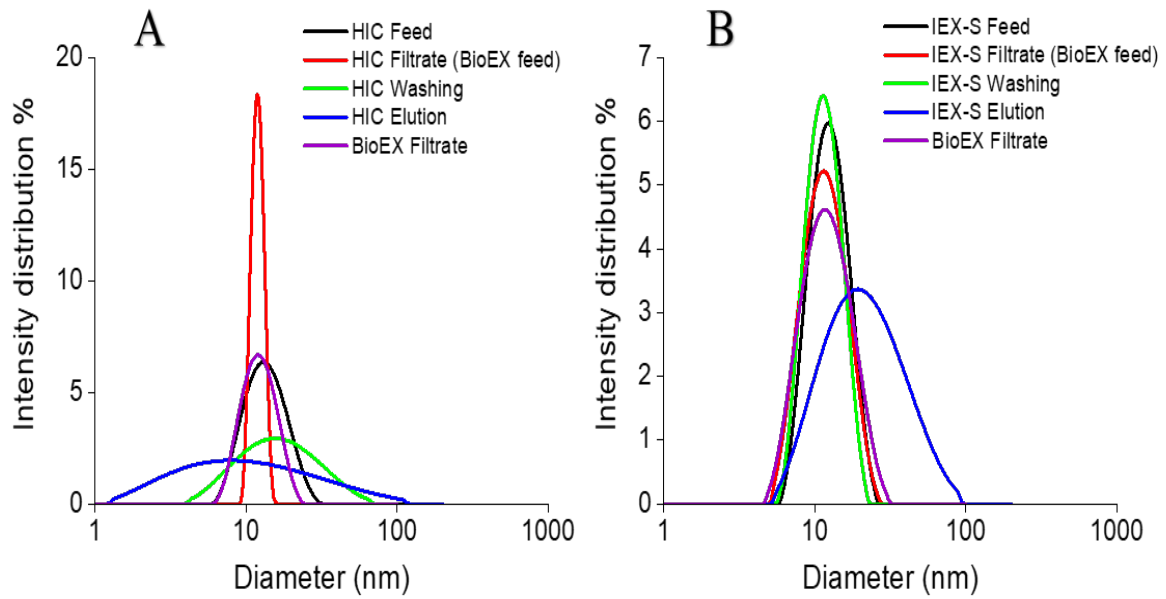
**BioEX buffer chase (pH 7.5, no salt)**



**Figure E2:** Dimer Quantitation from TSKgel HPLC SEC Characterization of mAb B BioEX

Feed, Permeate and Buffer Chase in 20 mM Sodium Acetate Buffer without Salt, pH 7.5.

**Appendix F: DLS data for mAb B prefiltration and virus filtration fractions**



**Figure F1:** DLS Spectra of mAb B HIC, IEX-S, and BioEX Filtration Fractions